

Crewed Missions to Mars: Modeling the Impact of Astrophysical Charged Particles on Astronauts and Assessing Health Effects

Dimitra Atri¹

Center for Space Science, New York University Abu Dhabi, Saadiyat Island, PO Box 129188, Abu Dhabi, UAE

Blue Marble Space Institute of Science, 600 1st Avenue, Seattle, WA 98104, USA

Caitlin MacArthur

Pathology and Molecular Medicine, University of Otago, Wellington, 23A Mein Street, Newtown, Wellington 6242, New Zealand

Sriram Devata

International Institute of Information Technology, Gachibowli, Hyderabad, Telangana 500032, India

Shireen Mathur

Blue Marble Space Institute of Science, Seattle, WA 98154, USA

Giulia Carla Bassani

Polytechnic University of Turin, 10129 Torino (TO), Italy

Roberto Parisi

Department of Medicine and Surgery, Università degli Studi di Salerno, Fisciano, Salerno 84084, Italy

Dionysios Gakis

Department of Physics, University of Patras, Patras, 26504, Greece

Konstantin Herbst

Institut für Experimentelle und Angewandte Physik, Christian-Albrechts Universität zu Kiel, Leibnizstraße 11, D-24118 Kiel, Germany

Azza Al Bakr

National Space Science and Technology Centre, Al Ain, UAE

Tammy Witzens

Ira A. Fulton Schools of Engineering, Arizona State University, PO Box 879309, Tempe, AZ 85287, USA

Abstract

The impact of exposure to astrophysical ionizing radiation on astronaut health is one of the main concerns in

¹Corresponding author: atri@nyu.edu

planning crewed missions to Mars. Astronauts will be exposed to energetic charged particles from Galactic and Solar origin for a prolonged period with little protection from a thin spacecraft shield in transit and from the rarefied Martian atmosphere when on the surface. Adverse impacts on astronaut health include, for example, Acute Radiation Syndrome, damage to the nervous system, and increased cancer risk. Using a combination of radiation measurements and numerical modeling with the GEANT4 package, we calculate the distribution of radiation dose in various organs of the human body for various expected scenarios simulated with a model human phantom. We rely on medical studies to assess the impact of enhanced levels of radiation dose on various physiological systems and on the overall health of astronauts. We suggest mitigation strategies such as improved ways of shielding and dietary supplements, and make recommendations for the safety of astronauts in future crewed missions to Mars.

Keywords: cosmic rays, solar energetic particles, Mars, radiobiology, human spaceflight

Contents

1	Introduction	3
2	Astrophysical Ionizing Radiation Environments	5
2.1	Measurements in LEO and from Lunar missions	5
2.2	Measurements from deep space and the Martian Surface	7
3	Numerical Modeling	8
4	Impact of Ionizing Radiation on Astronaut Health	21
4.1	The Impact of Ionizing Radiation on the Physiological Systems	21
4.1.1	Acute Radiation Syndrome	21
4.1.2	The Nervous System	22
4.1.3	Behavioral Effects	24
4.1.4	The Ocular System	26
4.1.5	The Thyroid Gland	28
4.1.6	The Skeletal System	29
4.1.7	The Immune System	31
4.1.8	The Cardiovascular System	33
4.1.9	The Pulmonary System	35

4.1.10	The Integumentary System	37
4.1.11	The Reproductive System	39
4.1.12	The Digestive System	40
4.2	The Impact of Ionizing Radiation on the Genetic Material	43
4.2.1	Reactive Oxygen Species	43
4.2.2	DNA Damage	45
4.3	The Impact of Ionizing Radiation on Cancer Risk	48
5	Radiation Mitigation Strategies	50
5.1	Radiation Environment Tracking	50
5.2	Medicine and Dietary Strategies	51
5.2.1	Probiotics	51
5.2.2	Antioxidants and Vitamins	52
5.3	Mitigation Hardware	54
5.3.1	Active Shielding	54
5.3.2	Passive Shielding	58
5.3.3	Martian Habitats	61
6	Discussion and Conclusions	64

1. Introduction

Since the first crewed spaceflight in 1961 and the first human mission to the Moon in 1969, several crewed missions and long-term visits to the International Space Station (ISS) have been carried out. With new deep space missions planned for the near future, astronauts will further explore our Solar System and thus be exposed to different environment of interplanetary space and the Martian atmosphere and surface within the coming decades. Of utmost importance thereby are radiation environmental factors like galactic and solar cosmic rays, the atmospheric secondary particle environment produced by the interaction of the cosmic rays with the atmospheric components, the reduced planetary gravity (3.72 m/s^2 at the Martian surface) after months of traveling in microgravity, and their impact on the human body.

Interstellar space is dominated by (E)UV, soft and hard X-rays, and energetic cosmic rays of galactic and solar origin, that can adversely affect human health. In particular, solar energetic particles (SEPs) accelerated,

for example, in solar flares, coronal mass ejections (CMEs), or at interplanetary shocks [1] are predominantly composed of 89% protons, 10% helium, and about 1% of electrons and can have energies between several keV and hundreds of MeV. In the case of rather strong SEP events, known as ground-level enhancement (GLE) events, SEPs with energies up to a few GeV can be found. The strongest event ever measured is GLE05 (18 February 1956). However, cosmogenic radionuclide records showed strong increases (about 15%) in the production rates around AD774/775 [e.g., 2] associated with a solar superevent about 30 to 70 times stronger than GLE05 [3, 4]. Most recently, however, [5] found two even stronger events in tree ring records around 5259 BC and 7176 BC with an increase of about 19%.

While being about four orders of magnitude lower than the SEP flux in the keV range, the differential particle flux of Galactic Cosmic Rays (GCRs), accelerated at supernova remnants [6, 7], extends over more than 15 orders of magnitudes, up to more than 10^{15} MeV. Because the solar magnetic field is frozen into the solar wind and carried outwards into the interplanetary medium, the heliospheric magnetic field is formed and extended into interplanetary space. Therefore, the low-energetic part of the GCR spectrum is modulated with changing solar activity, reflecting in an 11-year solar and 22-year magnetic activity cycle variation. GCRs are known to consist of mostly hadrons, consisting of approximately 87% protons, 12% helium nuclei (He), and a small fraction of 1% heavier elements up to iron [e.g., 8].

While being exposed to photons in interplanetary space can be easily be prevented by adding a thin shield, charged particles can penetrate deeper into spacecraft. They may lead to the production of secondary particles capable of penetrating through even thick shielding, limited to weight restrictions on spaceflights. In particular, strong solar events and potential superevents can cause tremendous radiation hazard and risk for crewed space missions, and can cause direct damage by ionization or can produce harmful radicals in the body leading to secondary effects.

Besides, once charged particles enter planetary atmospheres, they are the primary drivers of the planetary altitude-dependent atmospheric ionization. While the low energy cosmic rays (CRs) lose most of their energy due to elastic collisions with atmospheric neutrals, CRs with energies above ~ 1 GeV can induce extensive secondary particle cascades. Thereby, secondary mesons (π^\pm and κ^\pm), nucleons, gamma particles, and nuclear fragments are created, which may interact further. Thus, the cosmic ray cascade evolves with increasing atmospheric depth, and the secondary particle flux continues to rise.

An astronaut's health is the number one priority for any space mission. When sending humans into space, they are constantly bombarded with ionizing radiation that could lead to severe health problems or permanent biological mutations. Before identifying the right shielding thickness and material to protect

astronauts, a radiation dose estimate needs to be determined with the corresponding biological effect. In order to make these dose estimates, we utilize the model spectra of GCRs and historical SEPs to estimate the radiation environment in deep space and on the surface of Mars. We then use the GEANT4 numerical model to calculate the propagation of charged particles in various scenarios, namely (1) deep space, (2) surface of Mars, (3) deep space with shielding, and (4) surface of Mars with shielding. A standard human phantom was used to calculate radiation absorbed by various organs of the human body. GEANT4 being an open source code, is well-known in the community and is validated with a variety of experiments around the globe. Our approach is therefore advantageous over other studies using proprietary software which cannot be validated by the community.

In this paper, our purpose is to assess the impact of astrophysical radiation during long-duration mission to Mars on the health of astronauts. At first, we evaluate shortly the radiation environments astronauts will encounter on their way to Mars (Section 2). We proceed with describing our numerical model to estimate radiation exposure (Section 3) and present our results after compiling data available from past and current operating missions in Section 3. A thorough review of the effects of ionizing radiation on the physiological systems, the genetic material and the cancer risks is provided in Section 4. Section 5 outlines the main radiation mitigation strategies. We conclude with a summary of this work in Section 6.

2. Astrophysical Ionizing Radiation Environments

2.1. Measurements in LEO and from Lunar missions

There are three main sources of primary ionizing radiation found in low Earth orbit (LEO), namely: Galactic cosmic rays (GCRs), Earth's radiation belts (ERBs), and Solar particle events (SPEs). GCRs are charged particles originating from outer space and range from several tens to 10¹² MeV and peak around 1 GeV. The GCR consists of 85% hydrogen nuclei, 14% helium nuclei, and 1% heavy ions called HZE (high charge and energy). On the surface of Earth, the atmosphere and magnetic field protect us from harmful GCR radiation, while GCRs are a dominant source in space and can be extremely hazardous [9][10].

The ERBs, also known as the Van Allen radiation belts, consist of high-energy electrons and ions, primarily protons, trapped in the geomagnetic field, forming two belts in the inner magnetosphere of the Earth, where the geomagnetic field resembles a magnetic dipole [e.g. 11]. While the inner belt extends from 1,000 to 12,000 km and is composed of electrons of energies less than 5 MeV, in the outer belt (13,000 to 60,000 km), electrons with energies around 7 MeV are trapped [9]. For an interplanetary mission, the

spacecraft passes through this zone for a short amount of time. Hence, it does not affect the crew and can be stopped by the spacecraft's shielding.

Another major source of radiation is the Sun, emitting high-energy particles in the form of X-rays, gamma rays, and the solar wind, a constant stream of protons and electrons. During times of higher solar activity, particles can be accelerated in solar flares and at the shock fronts of CME, detectable in interplanetary space as SPEs. Solar flares last for a short amount of time, in the order of hours, and are restricted to a 30 – 45 degrees angle in solar longitude, while CMEs can last for days and extend on a larger angle of 60 to 180 degrees [9]. Each of the three primary sources varies depending on altitude, the inclination of the spacecraft's orbit, and the phase of the solar cycle.

The International Space Station (ISS) orbiting the Earth in LEO at around 400 km, is an active space laboratory with much research being conducted. In one study, astronaut Scott Kelly was sent to the ISS for a year to study the impact of long-duration spaceflight on the human body. Results showed that changes were no more significant than that observed on his twin brother Mark Kelly who stayed on Earth [12]. Also, 91.3% of Scott's gene expression levels returned to normal a few months after returning to Earth, suggesting that health can be sustained during this time in space. Although some biological mutations were observed in Scott, they were not fully understood due to the fact that Scott was the only astronaut that went through this experiment. Thus, more research needs to be done on a larger number of astronauts.

The Apollo program is one of the most complex and most extensive scientific exploration programs in the history of humankind and the farthest point traveled by humans beyond low Earth orbit. Although Moon does not belong in the current plans for the human transfer to Mars, collective data from the Apollo missions are presented in this section to understand better the radiation dose and its effect on astronauts, which is crucial for developing and planning for future deep-space missions. Six out of seven missions planned for lunar landing were successful. This includes Apollo 11, 12, 14, 15, 16, and 17, putting twelve astronauts on the moon's surface. Table 1 presents the dosimetry data from Apollo missions, retrieved from [13].

Table 1 shows the mean dose rate per day as a function of the mission duration. The dose rate varies depending on the lunar surface activity, intra-vehicular Command and Lunar Module activity, and the changes due to cosmic ray modulation and solar activity. According to a NASA report, the doses received by the Apollo crew were small and had no harmful impact on their health [14]. This, however, comes to no surprise since, luckily, no major SPE occurred throughout the missions [2]. However, some significant biological observations were reported in [13], including vestibular disturbances, inflight cardiac arrhythmia, reduced postflight orthostatic tolerance, reduced postflight exercise tolerance, postflight dehydration, and weight loss.

Mission	Time (days)	Absorbed dose (mGy)	Mean dose rate ($\mu\text{Gy}/\text{day}$)
Apollo 11	8	1.8	220
Apollo 12	10	5.8	570
Apollo 14	9	11.4	1270
Apollo 15	10	3	240
Apollo 16	11	5.1	460
Apollo 17	12	5.5	440

Table 1: Dosimetry data from Apollo missions [13]

Several causes have been suspected. Although the flight diet was adequate, the food consumption was suboptimal, in the end, it led to a decrease in the red cell mass and the plasma volume, and a negative inflight balance trend for nitrogen, calcium, and other electrolytes. In addition, increased inflight adrenal hormone secretion has been reported.

2.2. Measurements from deep space and the Martian Surface

One of the main challenges for sending humans to Mars is the exposure to high ionizing radiation over a long period. The journey to Mars takes up around six to eight months. While coming back to Earth will need another launch window, spending around 500 days on the Martian surface, and another six to eight months journey back to Earth, making the total duration of a roundtrip around two - three years. However, since the martian atmosphere is much thinner than that of the Earth, the radiation exposure on Mars is much higher.

In 2012, NASA successfully landed the Curiosity rover on the Martian surface in Gale Crater. Since then, Curiosity's Radiation Assessment Detector (RAD) has been measuring the energetic particle radiation environment, e.g., in the form of charged particle and neutral particle radiation, giving the total dose rate and particle spectra from 10 to >100 MeV/u [15, 16, 17]. The radiation dose rate can be seen to vary between 180 and 225 $\mu\text{Gy}/\text{day}$. It was also found that the average GCR dose rate at Gale Crater varied between 0.210 ± 0.040 mGy/day, while the Mars Science Laboratory (MSL) spacecraft carrying Curiosity measured a dose rate of 0.48 ± 0.08 mGy/day during cruise [18]. Accordingly, the quality factor Q characterizing the severeness of a radiation environment, was found 3.05 ± 0.3 on the Martian surface, much lower than the value of 3.82 ± 0.3 in deep space. This difference is also driven by the heliospheric conditions, which reduced the dose rate by a factor of two in comparison to the cruise phase.

There are two scenarios examined for the human journeys to Mars, the conjunction-class and the opposition-class mission [19]. The first type of mission involves a longer stay on Mars than the second [20] and seems as the preferable choice in order to maximize the stay on Mars because of the lower doses there. Based on the measurements and calculations for the conjunction-class mission, the total mission dose for an entire round trip has been estimated to be around 1.01 Sv, but this value may differ according to the specific mission characteristics and the solar conditions.

Evidently, any decisions concerning the shielding strategies on the surface of Mars must be taken in alignment with the type of journey chosen, and vice versa [21]. For example, during very short stays additional shielding might be unnecessary as exposure levels would be much lower than acceptable limits. Likewise, if adequate shielding is ensured on the surface of the planet, we could increase the duration of the human presence there.

3. Numerical Modeling

We calculate radiation exposure in two situations, (1) during transit in interplanetary space, when the spacecraft is in cruise phase, and (2) on the surface of Mars where some shielding is provided by the thin atmosphere. In each of the two cases, we calculate direct radiation exposure to astronauts with no shielding, as well as from 5 g cm^{-2} of aluminum shielding, which is commonly used in spacecrafts. Charged particle interactions with the human body (and the shield in some cases) are simulated using the GEANT4 package [22]. GEANT4 is a Monte Carlo package which is widely used to model the propagation of charged particles through matter. Since the code is used widely in fields such as high-energy physics, planetary science and space medicine, it is calibrated with a wide variety of experimental results. In order to compute the dose deposition in various organs of the human body, we use the MIRD (Committee on Medical Internal Radiation Dose) human phantom available as a part of the package, originally developed by [23]. Although some organs were not implemented in the original package, we modified the code to incorporate the missing organs. In further processing, the organ masses for these missing organs were based on specifications from ICRP-89 [24]. We also imported appropriate physics models into the human phantom model to simulate high-energy charged particle interactions.

In order to estimate the radiation exposure to astronauts, we need both the energy spectra of GCRs to calculate background radiation exposure and the spectra of major SPEs to calculate dose from episodic events. We use the Badhwar O'Neill (BON10) model [25] to calculate the GCR spectra in outer space. Since the GCR spectrum varies considerably depending on solar modulation, we calculate the spectra for both

solar minimum and maximum conditions, to account for the two extremes. Heliospheric modulation changes with the distance from the Sun but that effect is minor and can be ignored, so we make the assumption that the GCR flux remains the same between 1 and 1.5 AU. GCR spectrum consists primarily of hydrogen and helium nuclei, which we have modeled in this paper and ignored the minor heavier species to simplify our calculations and save computing time. In order to simulate the impact of Solar Particle Events, we used two databases from where we obtained the energy spectra of various events (citation)[26]. The GCR spectra from BON10 model along with the SPEs (2 cases) are shown in Figure 1 and Figure 2 respectively. The human phantom was exposed to isotropic radiation to simulate deep-space conditions.

The code models the propagation of charged particles through the phantom and calculates energy deposition in each organ. The QGSP physics list was used to model all physical interactions, which is also recommended for incorporating neutron interactions better [27]. An outer layer of 5 g cm^{-2} aluminum shield was added and the simulations were repeated to estimate the radiation dose on astronauts inside the spacecraft.

For the dose calculation on the Martian surface, incident particles first interact with the Martian atmosphere and undergo hadronic and electromagnetic interactions. These interactions were modeled with GEANT4 using the method described in [26] in more detail. The Mars Climate Database (MCD) [28] was used to model the atmosphere of Mars. The simulations were set up in a way that the incident radiation first interacted with the atmosphere, propagating down to the surface and then interacted with the human phantom. In order to validate our method, we compare our calculations with measurements of the Radiation Assessment Detector (RAD) instrument on board the Curiosity rover (NASA's Mars Science Laboratory) deployed at Gale crater, Mars. The radiation dose deposited in a standard ICRU (International Commission on Radiation Units and Measurements) sphere from our simulations was 0.59 mSv/day , which is consistent with the RAD instrument measurement at $0.64 \pm 0.12 \text{ mSv/day}$ [18] within instrumental uncertainties. The radiation dose calculated by this method was found to be consistent with measurements made by the RAD instrument on board MSL within a few percentage.

Overall, we simulate the impact of radiation from GCRs in both solar maxima and minima conditions, and from two databases of SPEs. All simulations were carried out in the following four scenarios: (1) Cruise phase with no shielding, (2) Cruise phase with 5 g cm^{-2} Al shielding, (3) Surface with no shielding, (4) Surface with 5 g cm^{-2} Al shielding.

Here, we present the results of radiation dose deposition in various organs of the human body. Specifically, Tables 2 and 3 show the GCR-induced dose in various organs for male and female astronauts, in solar and

maximum conditions, separated by proton primaries, alpha particles and heavier nuclei, during cruise phase with no shielding and behind 5 g cm^{-2} aluminum shielding, respectively. Likewise, Tables 4 and 5 show the respective situations in the Martian environment. The dose depositions in human organs by 60 different solar events are presented in Tables 6-11.

In the case of GCRs, there is a significant difference between the dose in the cruise phase and on the surface. The dose is reduced by a factor of about 2.5 on the surface. The aluminum shield provides some reduction in dose, although not much as expected given the high-energy of incident charged particles. In the case of SEPs, just like in the case of GCRs, there is a significant difference between dose rates during the cruise phase and on the ground. However, the effect of shielding is much greater as compared to GCRs because the energy of particles is much lower. Also, organ-to-organ variation in dose rates is much higher in the case of SEPs because of the lower energy particles, whereas in GCRs, it is more uniform due to higher energy particles.

Organ	Male Phantom						Female Phantom					
	Hydrogen		Helium		Heavy		Hydrogen		Helium		Heavy	
	Solar Min.	Solar Max.	Solar Min.	Solar Max.	Solar Min.	Solar Max.	Solar Min.	Solar Max.	Solar Min.	Solar Max.	Solar Min.	Solar Max.
Brain	2.46E+02	1.76E+02	1.87E+02	1.45E+02	3.67E+02	2.63E+02	2.28E+02	1.65E+02	1.74E+02	1.36E+02	3.40E+02	2.45E+02
Head	1.36E+02	9.78E+01	1.33E+02	1.01E+02	2.03E+02	1.46E+02	1.30E+02	9.26E+01	1.27E+02	9.56E+01	1.94E+02	1.38E+02
Heart	1.65E+02	1.20E+02	1.40E+02	1.11E+02	2.45E+02	1.79E+02	1.43E+02	1.05E+02	1.21E+02	9.62E+01	2.13E+02	1.56E+02
LeftAdrenal	1.88E+02	1.36E+02	1.54E+02	1.20E+02	2.80E+02	2.03E+02	2.32E+02	1.69E+02	1.68E+02	1.32E+02	3.46E+02	2.52E+02
LeftArmBone	2.70E+02	1.92E+02	2.00E+02	1.53E+02	4.02E+02	2.87E+02	2.66E+02	1.90E+02	1.96E+02	1.50E+02	3.96E+02	2.83E+02
LeftBreast	0.00E+00	0.00E+00	0.00E+00	0.00E+00	0.00E+00	0.00E+00	3.48E+02	2.48E+02	3.18E+02	2.38E+02	5.19E+02	3.70E+02
LeftClavicle	2.40E+02	1.73E+02	1.76E+02	1.37E+02	3.58E+02	2.57E+02	2.28E+02	1.65E+02	1.79E+02	1.40E+02	3.40E+02	2.45E+02
LeftKidney	1.98E+02	1.43E+02	1.45E+02	1.15E+02	2.94E+02	2.13E+02	1.95E+02	1.41E+02	1.43E+02	1.12E+02	2.90E+02	2.10E+02
LeftLeg	2.40E+02	1.71E+02	2.06E+02	1.57E+02	3.58E+02	2.55E+02	2.38E+02	1.70E+02	2.06E+02	1.56E+02	3.55E+02	2.54E+02
LeftLegBone	1.75E+02	1.27E+02	1.46E+02	1.15E+02	2.60E+02	1.90E+02	1.71E+02	1.25E+02	1.42E+02	1.12E+02	2.55E+02	1.86E+02
LeftLung	1.99E+02	1.44E+02	1.56E+02	1.23E+02	2.97E+02	2.15E+02	1.95E+02	1.42E+02	1.56E+02	1.23E+02	2.91E+02	2.11E+02
LeftOvary	0.00E+00	0.00E+00	0.00E+00	0.00E+00	0.00E+00	0.00E+00	2.10E+02	1.55E+02	1.90E+02	1.51E+02	3.13E+02	2.31E+02
LeftScapula	2.52E+02	1.81E+02	1.87E+02	1.43E+02	3.75E+02	2.69E+02	2.86E+02	2.04E+02	2.10E+02	1.61E+02	4.26E+02	3.04E+02
LeftTeste	2.64E+02	1.90E+02	1.73E+02	1.33E+02	3.93E+02	2.83E+02	0.00E+00	0.00E+00	0.00E+00	0.00E+00	0.00E+00	0.00E+00
LowerLargeIntestine	1.37E+02	1.01E+02	1.15E+02	9.18E+01	2.05E+02	1.50E+02	1.67E+02	1.22E+02	1.38E+02	1.09E+02	2.49E+02	1.82E+02
MaleGenitalia	2.30E+02	1.65E+02	2.28E+02	1.71E+02	3.43E+02	2.46E+02	0.00E+00	0.00E+00	0.00E+00	0.00E+00	0.00E+00	0.00E+00
MiddleLowerSpine	1.55E+02	1.13E+02	1.23E+02	9.70E+01	2.31E+02	1.69E+02	1.53E+02	1.12E+02	1.22E+02	9.62E+01	2.28E+02	1.66E+02
Pancreas	1.17E+02	8.60E+01	9.84E+01	7.86E+01	1.74E+02	1.28E+02	1.36E+02	1.00E+02	1.20E+02	9.56E+01	2.03E+02	1.49E+02
Pelvis	1.60E+02	1.17E+02	1.25E+02	9.92E+01	2.39E+02	1.74E+02	1.57E+02	1.15E+02	1.22E+02	9.62E+01	2.34E+02	1.71E+02
RibCage	2.70E+02	1.93E+02	2.08E+02	1.59E+02	4.02E+02	2.88E+02	2.58E+02	1.85E+02	1.98E+02	1.51E+02	3.84E+02	2.76E+02
RightAdrenal	2.14E+02	1.54E+02	1.45E+02	1.14E+02	3.19E+02	2.30E+02	2.08E+02	1.51E+02	1.52E+02	1.20E+02	3.10E+02	2.26E+02
RightArmBone	2.78E+02	1.99E+02	2.06E+02	1.57E+02	4.14E+02	2.97E+02	2.66E+02	1.91E+02	1.98E+02	1.52E+02	3.96E+02	2.85E+02
RightBreast	0.00E+00	0.00E+00	0.00E+00	0.00E+00	0.00E+00	0.00E+00	3.74E+02	2.66E+02	3.36E+02	2.52E+02	5.57E+02	3.96E+02
RightClavicle	2.16E+02	1.56E+02	1.59E+02	1.25E+02	3.22E+02	2.32E+02	2.44E+02	1.75E+02	1.76E+02	1.37E+02	3.64E+02	2.60E+02
RightKidney	1.90E+02	1.38E+02	1.39E+02	1.09E+02	2.83E+02	2.06E+02	1.81E+02	1.32E+02	1.32E+02	1.03E+02	2.70E+02	1.96E+02
RightLeg	2.38E+02	1.70E+02	2.06E+02	1.56E+02	3.55E+02	2.54E+02	2.46E+02	1.76E+02	2.12E+02	1.61E+02	3.67E+02	2.62E+02
RightLegBone	1.67E+02	1.21E+02	1.37E+02	1.08E+02	2.49E+02	1.81E+02	1.76E+02	1.28E+02	1.45E+02	1.14E+02	2.63E+02	1.90E+02
RightLung	1.95E+02	1.41E+02	1.53E+02	1.20E+02	2.90E+02	2.10E+02	1.95E+02	1.41E+02	1.57E+02	1.23E+02	2.91E+02	2.10E+02
RightOvary	0.00E+00	0.00E+00	0.00E+00	0.00E+00	0.00E+00	0.00E+00	1.28E+02	9.34E+01	1.00E+02	7.94E+01	1.90E+02	1.39E+02
RightScapula	2.60E+02	1.87E+02	1.95E+02	1.48E+02	3.87E+02	2.78E+02	2.64E+02	1.88E+02	1.94E+02	1.48E+02	3.93E+02	2.80E+02
RightTeste	1.98E+02	1.43E+02	1.37E+02	1.07E+02	2.96E+02	2.13E+02	0.00E+00	0.00E+00	0.00E+00	0.00E+00	0.00E+00	0.00E+00
Skull	2.64E+02	1.90E+02	2.20E+02	1.68E+02	3.93E+02	2.83E+02	2.58E+02	1.84E+02	2.14E+02	1.63E+02	3.84E+02	2.75E+02
SmallIntestine	1.34E+02	9.84E+01	1.12E+02	8.88E+01	2.00E+02	1.47E+02	1.43E+02	1.05E+02	1.18E+02	9.40E+01	2.13E+02	1.56E+02
Spleen	1.68E+02	1.23E+02	1.34E+02	1.06E+02	2.51E+02	1.83E+02	1.59E+02	1.15E+02	1.31E+02	1.04E+02	2.36E+02	1.72E+02
Stomach	1.61E+02	1.18E+02	1.26E+02	1.00E+02	2.40E+02	1.75E+02	1.63E+02	1.19E+02	1.27E+02	1.01E+02	2.43E+02	1.77E+02
Thymus	1.56E+02	1.14E+02	1.24E+02	9.78E+01	2.33E+02	1.70E+02	1.54E+02	1.12E+02	1.23E+02	9.70E+01	2.30E+02	1.66E+02
Thyroid	1.74E+02	1.27E+02	1.42E+02	1.12E+02	2.60E+02	1.90E+02	1.61E+02	1.17E+02	1.21E+02	9.56E+01	2.40E+02	1.74E+02
Trunk	1.63E+02	1.18E+02	1.42E+02	1.09E+02	2.43E+02	1.75E+02	1.63E+02	1.18E+02	1.41E+02	1.08E+02	2.43E+02	1.75E+02
UpperLargeIntestine	1.38E+02	1.01E+02	1.15E+02	9.18E+01	2.06E+02	1.51E+02	1.48E+02	1.08E+02	1.23E+02	9.84E+01	2.20E+02	1.61E+02
UpperSpine	1.98E+02	1.43E+02	1.52E+02	1.20E+02	2.94E+02	2.13E+02	1.75E+02	1.27E+02	1.39E+02	1.09E+02	2.60E+02	1.90E+02
UrinaryBladder	1.62E+02	1.18E+02	1.26E+02	9.92E+01	2.41E+02	1.76E+02	1.75E+02	1.27E+02	1.34E+02	1.07E+02	2.60E+02	1.90E+02
Uterus	0.00E+00	0.00E+00	0.00E+00	0.00E+00	0.00E+00	0.00E+00	1.38E+02	1.01E+02	1.12E+02	8.96E+01	2.06E+02	1.51E+02

Table 2: Effective dose (mSv) during cruise phase in different organs

Organ	Male Phantom						Female Phantom					
	Hydrogen		Helium		Heavy		Hydrogen		Helium		Heavy	
	Solar Min.	Solar Max.	Solar Min.	Solar Max.	Solar Min.	Solar Max.	Solar Min.	Solar Max.	Solar Min.	Solar Max.	Solar Min.	Solar Max.
Brain	2.21E+02	1.59E+02	1.69E+02	1.31E+02	3.30E+02	2.37E+02	2.05E+02	1.48E+02	1.57E+02	1.22E+02	3.06E+02	2.21E+02
Head	1.22E+02	8.80E+01	1.20E+02	9.05E+01	1.82E+02	1.31E+02	1.17E+02	8.33E+01	1.14E+02	8.60E+01	1.74E+02	1.24E+02
Heart	1.48E+02	1.08E+02	1.26E+02	9.99E+01	2.21E+02	1.61E+02	1.29E+02	9.45E+01	1.09E+02	8.66E+01	1.92E+02	1.41E+02
LeftAdrenal	1.69E+02	1.22E+02	1.38E+02	1.08E+02	2.52E+02	1.82E+02	2.09E+02	1.52E+02	1.51E+02	1.18E+02	3.11E+02	2.27E+02
LeftArmBone	2.43E+02	1.73E+02	1.80E+02	1.38E+02	3.62E+02	2.58E+02	2.39E+02	1.71E+02	1.77E+02	1.35E+02	3.57E+02	2.54E+02
LeftBreast	0.00E+00	0.00E+00	0.00E+00	0.00E+00	0.00E+00	0.00E+00	3.13E+02	2.23E+02	2.86E+02	2.14E+02	4.67E+02	3.33E+02
LeftClavicle	2.16E+02	1.55E+02	1.58E+02	1.23E+02	3.22E+02	2.31E+02	2.05E+02	1.48E+02	1.61E+02	1.26E+02	3.06E+02	2.21E+02
LeftKidney	1.78E+02	1.29E+02	1.31E+02	1.03E+02	2.65E+02	1.92E+02	1.75E+02	1.27E+02	1.28E+02	1.00E+02	2.61E+02	1.89E+02
LeftLeg	2.16E+02	1.54E+02	1.85E+02	1.41E+02	3.22E+02	2.30E+02	2.14E+02	1.53E+02	1.85E+02	1.41E+02	3.19E+02	2.29E+02
LeftLegBone	1.57E+02	1.14E+02	1.32E+02	1.03E+02	2.34E+02	1.71E+02	1.54E+02	1.12E+02	1.28E+02	1.00E+02	2.30E+02	1.67E+02
LeftLung	1.79E+02	1.30E+02	1.41E+02	1.10E+02	2.67E+02	1.93E+02	1.76E+02	1.28E+02	1.41E+02	1.10E+02	2.62E+02	1.90E+02
LeftOvary	0.00E+00	0.00E+00	0.00E+00	0.00E+00	0.00E+00	0.00E+00	1.89E+02	1.40E+02	1.71E+02	1.36E+02	2.82E+02	2.08E+02
LeftScapula	2.27E+02	1.63E+02	1.68E+02	1.28E+02	3.38E+02	2.42E+02	2.57E+02	1.84E+02	1.89E+02	1.45E+02	3.84E+02	2.74E+02
LeftTeste	2.38E+02	1.71E+02	1.55E+02	1.20E+02	3.54E+02	2.54E+02	0.00E+00	0.00E+00	0.00E+00	0.00E+00	0.00E+00	0.00E+00
LowerLargeIntestine	1.24E+02	9.05E+01	1.04E+02	8.26E+01	1.84E+02	1.35E+02	1.50E+02	1.10E+02	1.24E+02	9.85E+01	2.24E+02	1.64E+02
MaleGenitalia	2.07E+02	1.49E+02	2.05E+02	1.54E+02	3.08E+02	2.22E+02	0.00E+00	0.00E+00	0.00E+00	0.00E+00	0.00E+00	0.00E+00
MiddleLowerSpine	1.40E+02	1.02E+02	1.10E+02	8.73E+01	2.08E+02	1.52E+02	1.38E+02	1.00E+02	1.10E+02	8.66E+01	2.05E+02	1.50E+02
Pancreas	1.05E+02	7.74E+01	8.86E+01	7.07E+01	1.57E+02	1.15E+02	1.22E+02	9.00E+01	1.08E+02	8.60E+01	1.82E+02	1.34E+02
Pelvis	1.44E+02	1.05E+02	1.12E+02	8.93E+01	2.15E+02	1.57E+02	1.41E+02	1.03E+02	1.10E+02	8.66E+01	2.11E+02	1.54E+02
RibCage	2.43E+02	1.74E+02	1.87E+02	1.43E+02	3.62E+02	2.59E+02	2.32E+02	1.67E+02	1.79E+02	1.36E+02	3.46E+02	2.48E+02
RightAdrenal	1.93E+02	1.39E+02	1.30E+02	1.02E+02	2.87E+02	2.07E+02	1.87E+02	1.36E+02	1.37E+02	1.08E+02	2.79E+02	2.03E+02
RightArmBone	2.50E+02	1.79E+02	1.85E+02	1.41E+02	3.73E+02	2.67E+02	2.39E+02	1.72E+02	1.79E+02	1.37E+02	3.57E+02	2.56E+02
RightBreast	0.00E+00	0.00E+00	0.00E+00	0.00E+00	0.00E+00	0.00E+00	3.37E+02	2.39E+02	3.02E+02	2.27E+02	5.02E+02	3.57E+02
RightClavicle	1.94E+02	1.40E+02	1.43E+02	1.12E+02	2.90E+02	2.09E+02	2.20E+02	1.57E+02	1.59E+02	1.24E+02	3.27E+02	2.34E+02
RightKidney	1.71E+02	1.24E+02	1.25E+02	9.85E+01	2.55E+02	1.85E+02	1.63E+02	1.18E+02	1.18E+02	9.25E+01	2.43E+02	1.76E+02
RightLeg	2.14E+02	1.53E+02	1.85E+02	1.41E+02	3.19E+02	2.29E+02	2.21E+02	1.58E+02	1.91E+02	1.45E+02	3.30E+02	2.35E+02
RightLegBone	1.50E+02	1.09E+02	1.24E+02	9.72E+01	2.24E+02	1.63E+02	1.59E+02	1.15E+02	1.31E+02	1.02E+02	2.37E+02	1.71E+02
RightLung	1.75E+02	1.27E+02	1.38E+02	1.08E+02	2.61E+02	1.89E+02	1.76E+02	1.27E+02	1.41E+02	1.11E+02	2.62E+02	1.89E+02
RightOvary	0.00E+00	0.00E+00	0.00E+00	0.00E+00	0.00E+00	0.00E+00	1.15E+02	8.41E+01	9.00E+01	7.15E+01	1.71E+02	1.25E+02
RightScapula	2.34E+02	1.68E+02	1.75E+02	1.34E+02	3.49E+02	2.50E+02	2.38E+02	1.69E+02	1.75E+02	1.33E+02	3.54E+02	2.52E+02
RightTeste	1.79E+02	1.29E+02	1.23E+02	9.59E+01	2.66E+02	1.92E+02	0.00E+00	0.00E+00	0.00E+00	0.00E+00	0.00E+00	0.00E+00
Skull	2.38E+02	1.71E+02	1.98E+02	1.51E+02	3.54E+02	2.54E+02	2.32E+02	1.66E+02	1.93E+02	1.47E+02	3.46E+02	2.47E+02
SmallIntestine	1.21E+02	8.86E+01	1.00E+02	7.99E+01	1.80E+02	1.32E+02	1.29E+02	9.45E+01	1.06E+02	8.46E+01	1.92E+02	1.41E+02
Spleen	1.51E+02	1.10E+02	1.21E+02	9.52E+01	2.26E+02	1.64E+02	1.43E+02	1.04E+02	1.18E+02	9.32E+01	2.13E+02	1.55E+02
Stomach	1.45E+02	1.06E+02	1.14E+02	9.00E+01	2.16E+02	1.58E+02	1.47E+02	1.07E+02	1.14E+02	9.05E+01	2.19E+02	1.60E+02
Thymus	1.41E+02	1.02E+02	1.12E+02	8.80E+01	2.10E+02	1.53E+02	1.39E+02	1.00E+02	1.10E+02	8.73E+01	2.07E+02	1.50E+02
Thyroid	1.57E+02	1.14E+02	1.28E+02	1.01E+02	2.34E+02	1.71E+02	1.45E+02	1.05E+02	1.09E+02	8.60E+01	2.16E+02	1.57E+02
Trunk	1.47E+02	1.06E+02	1.28E+02	9.79E+01	2.19E+02	1.58E+02	1.47E+02	1.06E+02	1.27E+02	9.72E+01	2.19E+02	1.58E+02
UpperLargeIntestine	1.24E+02	9.13E+01	1.04E+02	8.26E+01	1.85E+02	1.36E+02	1.33E+02	9.72E+01	1.11E+02	8.86E+01	1.98E+02	1.45E+02
UpperSpine	1.78E+02	1.29E+02	1.37E+02	1.08E+02	2.65E+02	1.92E+02	1.57E+02	1.14E+02	1.25E+02	9.79E+01	2.34E+02	1.71E+02
UrinaryBladder	1.45E+02	1.06E+02	1.13E+02	8.93E+01	2.17E+02	1.59E+02	1.57E+02	1.14E+02	1.21E+02	9.59E+01	2.34E+02	1.71E+02
Uterus	0.00E+00	0.00E+00	0.00E+00	0.00E+00	0.00E+00	0.00E+00	1.24E+02	9.13E+01	1.00E+02	8.06E+01	1.85E+02	1.36E+02

Table 3: Effective dose (mSv) during cruise phase with 5 g cm⁻² Al shielding in different organs

Organ	Male Phantom						Female Phantom					
	Hydrogen		Helium		Heavy		Hydrogen		Helium		Heavy	
	Solar Min.	Solar Max.	Solar Min.	Solar Max.	Solar Min.	Solar Max.	Solar Min.	Solar Max.	Solar Min.	Solar Max.	Solar Min.	Solar Max.
Brain	1.72E+02	1.23E+02	1.31E+02	1.02E+02	8.43E+01	6.05E+01	1.60E+02	1.15E+02	1.22E+02	9.52E+01	7.81E+01	5.64E+01
Head	9.52E+01	6.85E+01	9.31E+01	7.04E+01	4.66E+01	3.35E+01	9.10E+01	6.48E+01	8.90E+01	6.69E+01	4.46E+01	3.17E+01
Heart	1.15E+02	8.43E+01	9.83E+01	7.77E+01	5.64E+01	4.13E+01	1.00E+02	7.35E+01	8.48E+01	6.73E+01	4.91E+01	3.60E+01
LeftAdrenal	1.32E+02	9.52E+01	1.08E+02	8.43E+01	6.44E+01	4.66E+01	1.62E+02	1.18E+02	1.17E+02	9.21E+01	7.95E+01	5.79E+01
LeftArmBone	1.89E+02	1.35E+02	1.40E+02	1.07E+02	9.25E+01	6.59E+01	1.86E+02	1.33E+02	1.37E+02	1.05E+02	9.12E+01	6.50E+01
LeftBreast	0.00E+00	0.00E+00	0.00E+00	0.00E+00	0.00E+00	0.00E+00	2.44E+02	1.74E+02	2.23E+02	1.67E+02	1.19E+02	8.50E+01
LeftClavicle	1.68E+02	1.21E+02	1.23E+02	9.56E+01	8.22E+01	5.92E+01	1.60E+02	1.15E+02	1.25E+02	9.77E+01	7.81E+01	5.64E+01
LeftKidney	1.38E+02	1.00E+02	1.02E+02	8.02E+01	6.77E+01	4.91E+01	1.36E+02	9.87E+01	9.98E+01	7.81E+01	6.67E+01	4.83E+01
LeftLeg	1.68E+02	1.20E+02	1.44E+02	1.10E+02	8.22E+01	5.87E+01	1.67E+02	1.19E+02	1.44E+02	1.09E+02	8.16E+01	5.84E+01
LeftLegBone	1.22E+02	8.90E+01	1.02E+02	8.02E+01	5.99E+01	4.36E+01	1.20E+02	8.74E+01	9.93E+01	7.81E+01	5.87E+01	4.28E+01
LeftLung	1.39E+02	1.01E+02	1.09E+02	8.58E+01	6.83E+01	4.93E+01	1.37E+02	9.93E+01	1.09E+02	8.58E+01	6.70E+01	4.86E+01
LeftOvary	0.00E+00	0.00E+00	0.00E+00	0.00E+00	0.00E+00	0.00E+00	1.47E+02	1.09E+02	1.33E+02	1.06E+02	7.20E+01	5.31E+01
LeftScapula	1.76E+02	1.27E+02	1.31E+02	9.98E+01	8.64E+01	6.20E+01	2.00E+02	1.43E+02	1.47E+02	1.13E+02	9.80E+01	6.99E+01
LeftTeste	1.85E+02	1.33E+02	1.21E+02	9.31E+01	9.05E+01	6.50E+01	0.00E+00	0.00E+00	0.00E+00	0.00E+00	0.00E+00	0.00E+00
LowerLargeIntestine	9.62E+01	7.04E+01	8.08E+01	6.43E+01	4.71E+01	3.45E+01	1.17E+02	8.54E+01	9.67E+01	7.66E+01	5.72E+01	4.18E+01
MaleGenitalia	1.61E+02	1.16E+02	1.60E+02	1.20E+02	7.88E+01	5.67E+01	0.00E+00	0.00E+00	0.00E+00	0.00E+00	0.00E+00	0.00E+00
MiddleLowerSpine	1.09E+02	7.92E+01	8.58E+01	6.79E+01	5.31E+01	3.88E+01	1.07E+02	7.81E+01	8.54E+01	6.73E+01	5.24E+01	3.82E+01
Pancreas	8.18E+01	6.02E+01	6.89E+01	5.50E+01	4.00E+01	2.95E+01	9.52E+01	7.00E+01	8.39E+01	6.69E+01	4.66E+01	3.43E+01
Pelvis	1.12E+02	8.18E+01	8.74E+01	6.94E+01	5.49E+01	4.00E+01	1.10E+02	8.02E+01	8.54E+01	6.73E+01	5.39E+01	3.93E+01
RibCage	1.89E+02	1.35E+02	1.46E+02	1.11E+02	9.25E+01	6.62E+01	1.81E+02	1.30E+02	1.39E+02	1.06E+02	8.84E+01	6.35E+01
RightAdrenal	1.50E+02	1.08E+02	1.01E+02	7.97E+01	7.33E+01	5.28E+01	1.46E+02	1.06E+02	1.06E+02	8.39E+01	7.13E+01	5.19E+01
RightArmBone	1.95E+02	1.39E+02	1.44E+02	1.10E+02	9.53E+01	6.83E+01	1.86E+02	1.34E+02	1.39E+02	1.06E+02	9.12E+01	6.55E+01
RightBreast	0.00E+00	0.00E+00	0.00E+00	0.00E+00	0.00E+00	0.00E+00	2.62E+02	1.86E+02	2.35E+02	1.76E+02	1.28E+02	9.12E+01
RightClavicle	1.51E+02	1.09E+02	1.12E+02	8.74E+01	7.40E+01	5.34E+01	1.71E+02	1.22E+02	1.23E+02	9.62E+01	8.36E+01	5.99E+01
RightKidney	1.33E+02	9.67E+01	9.72E+01	7.66E+01	6.52E+01	4.74E+01	1.27E+02	9.21E+01	9.21E+01	7.20E+01	6.22E+01	4.51E+01
RightLeg	1.67E+02	1.19E+02	1.44E+02	1.09E+02	8.16E+01	5.84E+01	1.72E+02	1.23E+02	1.48E+02	1.13E+02	8.43E+01	6.02E+01
RightLegBone	1.17E+02	8.48E+01	9.62E+01	7.56E+01	5.72E+01	4.15E+01	1.23E+02	8.95E+01	1.02E+02	7.97E+01	6.05E+01	4.38E+01
RightLung	1.36E+02	9.87E+01	1.07E+02	8.39E+01	6.67E+01	4.83E+01	1.37E+02	9.87E+01	1.10E+02	8.64E+01	6.70E+01	4.83E+01
RightOvary	0.00E+00	0.00E+00	0.00E+00	0.00E+00	0.00E+00	0.00E+00	8.95E+01	6.54E+01	7.00E+01	5.56E+01	4.38E+01	3.20E+01
RightScapula	1.82E+02	1.31E+02	1.36E+02	1.04E+02	8.91E+01	6.39E+01	1.85E+02	1.32E+02	1.36E+02	1.03E+02	9.05E+01	6.44E+01
RightTeste	1.39E+02	1.00E+02	9.56E+01	7.46E+01	6.80E+01	4.91E+01	0.00E+00	0.00E+00	0.00E+00	0.00E+00	0.00E+00	0.00E+00
Skull	1.85E+02	1.33E+02	1.54E+02	1.18E+02	9.05E+01	6.50E+01	1.81E+02	1.29E+02	1.50E+02	1.14E+02	8.84E+01	6.32E+01
SmallIntestine	9.41E+01	6.89E+01	7.81E+01	6.22E+01	4.61E+01	3.37E+01	1.00E+02	7.35E+01	8.27E+01	6.58E+01	4.91E+01	3.60E+01
Spleen	1.18E+02	8.58E+01	9.41E+01	7.41E+01	5.76E+01	4.20E+01	1.11E+02	8.08E+01	9.16E+01	7.25E+01	5.44E+01	3.95E+01
Stomach	1.13E+02	8.23E+01	8.85E+01	7.00E+01	5.51E+01	4.03E+01	1.14E+02	8.33E+01	8.90E+01	7.04E+01	5.59E+01	4.08E+01
Thymus	1.09E+02	7.97E+01	8.69E+01	6.85E+01	5.36E+01	3.90E+01	1.08E+02	7.81E+01	8.58E+01	6.79E+01	5.28E+01	3.82E+01
Thyroid	1.22E+02	8.90E+01	9.93E+01	7.87E+01	5.97E+01	4.36E+01	1.13E+02	8.18E+01	8.48E+01	6.69E+01	5.51E+01	4.00E+01
Trunk	1.14E+02	8.23E+01	9.93E+01	7.62E+01	5.59E+01	4.03E+01	1.14E+02	8.23E+01	9.87E+01	7.56E+01	5.59E+01	4.03E+01
UpperLargeIntestine	9.67E+01	7.10E+01	8.08E+01	6.43E+01	4.74E+01	3.47E+01	1.03E+02	7.56E+01	8.64E+01	6.89E+01	5.06E+01	3.70E+01
UpperSpine	1.38E+02	1.00E+02	1.06E+02	8.39E+01	6.77E+01	4.91E+01	1.22E+02	8.90E+01	9.72E+01	7.62E+01	5.99E+01	4.36E+01
UrinaryBladder	1.13E+02	8.27E+01	8.79E+01	6.94E+01	5.54E+01	4.05E+01	1.22E+02	8.90E+01	9.41E+01	7.46E+01	5.99E+01	4.36E+01
Uterus	0.00E+00	0.00E+00	0.00E+00	0.00E+00	0.00E+00	0.00E+00	9.67E+01	7.10E+01	7.81E+01	6.27E+01	4.74E+01	3.47E+01

Table 4: Effective dose (mSv) on Mars surface in different organs

Organ	Male Phantom						Female Phantom					
	Hydrogen		Helium		Heavy		Hydrogen		Helium		Heavy	
	Solar Min.	Solar Max.	Solar Min.	Solar Max.	Solar Min.	Solar Max.	Solar Min.	Solar Max.	Solar Min.	Solar Max.	Solar Min.	Solar Max.
Brain	1.55E+02	1.11E+02	1.18E+02	9.16E+01	7.59E+01	5.44E+01	1.44E+02	1.04E+02	1.10E+02	8.57E+01	7.03E+01	5.08E+01
Head	8.57E+01	6.16E+01	8.38E+01	6.34E+01	4.19E+01	3.02E+01	8.19E+01	5.83E+01	8.01E+01	6.02E+01	4.01E+01	2.86E+01
Heart	1.04E+02	7.59E+01	8.85E+01	6.99E+01	5.08E+01	3.71E+01	9.02E+01	6.62E+01	7.64E+01	6.06E+01	4.42E+01	3.24E+01
LeftAdrenal	1.18E+02	8.57E+01	9.68E+01	7.59E+01	5.80E+01	4.19E+01	1.46E+02	1.06E+02	1.06E+02	8.29E+01	7.16E+01	5.21E+01
LeftArmBone	1.70E+02	1.21E+02	1.26E+02	9.63E+01	8.33E+01	5.93E+01	1.68E+02	1.19E+02	1.24E+02	9.44E+01	8.20E+01	5.85E+01
LeftBreast	0.00E+00	0.00E+00	0.00E+00	0.00E+00	0.00E+00	0.00E+00	2.19E+02	1.56E+02	2.00E+02	1.50E+02	1.07E+02	7.65E+01
LeftClavicle	1.51E+02	1.09E+02	1.11E+02	8.61E+01	7.40E+01	5.32E+01	1.44E+02	1.04E+02	1.13E+02	8.79E+01	7.03E+01	5.08E+01
LeftKidney	1.24E+02	9.02E+01	9.16E+01	7.22E+01	6.09E+01	4.42E+01	1.23E+02	8.88E+01	8.98E+01	7.03E+01	6.00E+01	4.35E+01
LeftLeg	1.51E+02	1.08E+02	1.30E+02	9.90E+01	7.40E+01	5.28E+01	1.50E+02	1.07E+02	1.30E+02	9.85E+01	7.34E+01	5.26E+01
LeftLegBone	1.10E+02	8.01E+01	9.21E+01	7.22E+01	5.39E+01	3.92E+01	1.08E+02	7.86E+01	8.93E+01	7.03E+01	5.28E+01	3.85E+01
LeftLung	1.25E+02	9.07E+01	9.85E+01	7.72E+01	6.14E+01	4.44E+01	1.23E+02	8.93E+01	9.85E+01	7.72E+01	6.03E+01	4.37E+01
LeftOvary	0.00E+00	0.00E+00	0.00E+00	0.00E+00	0.00E+00	0.00E+00	1.32E+02	9.77E+01	1.19E+02	9.54E+01	6.48E+01	4.78E+01
LeftScapula	1.59E+02	1.14E+02	1.18E+02	8.98E+01	7.77E+01	5.58E+01	1.80E+02	1.29E+02	1.32E+02	1.01E+02	8.82E+01	6.29E+01
LeftTeste	1.66E+02	1.19E+02	1.09E+02	8.38E+01	8.14E+01	5.85E+01	0.00E+00	0.00E+00	0.00E+00	0.00E+00	0.00E+00	0.00E+00
LowerLargeIntestine	8.66E+01	6.34E+01	7.27E+01	5.78E+01	4.24E+01	3.10E+01	1.05E+02	7.69E+01	8.71E+01	6.89E+01	5.14E+01	3.76E+01
MaleGenitalia	1.45E+02	1.04E+02	1.44E+02	1.08E+02	7.09E+01	5.10E+01	0.00E+00	0.00E+00	0.00E+00	0.00E+00	0.00E+00	0.00E+00
MiddleLowerSpine	9.77E+01	7.13E+01	7.72E+01	6.11E+01	4.78E+01	3.49E+01	9.63E+01	7.03E+01	7.69E+01	6.06E+01	4.71E+01	3.44E+01
Pancreas	7.36E+01	5.42E+01	6.20E+01	4.95E+01	3.60E+01	2.65E+01	8.57E+01	6.30E+01	7.55E+01	6.02E+01	4.19E+01	3.08E+01
Pelvis	1.01E+02	7.36E+01	7.86E+01	6.25E+01	4.94E+01	3.60E+01	9.90E+01	7.22E+01	7.69E+01	6.06E+01	4.85E+01	3.53E+01
RibCage	1.70E+02	1.22E+02	1.31E+02	9.99E+01	8.33E+01	5.96E+01	1.63E+02	1.17E+02	1.25E+02	9.54E+01	7.96E+01	5.71E+01
RightAdrenal	1.35E+02	9.71E+01	9.12E+01	7.17E+01	6.60E+01	4.76E+01	1.31E+02	9.54E+01	9.58E+01	7.55E+01	6.42E+01	4.67E+01
RightArmBone	1.75E+02	1.25E+02	1.30E+02	9.90E+01	8.57E+01	6.14E+01	1.68E+02	1.20E+02	1.25E+02	9.58E+01	8.20E+01	5.89E+01
RightBreast	0.00E+00	0.00E+00	0.00E+00	0.00E+00	0.00E+00	0.00E+00	2.36E+02	1.68E+02	2.12E+02	1.59E+02	1.15E+02	8.20E+01
RightClavicle	1.36E+02	9.82E+01	1.00E+02	7.86E+01	6.66E+01	4.81E+01	1.54E+02	1.10E+02	1.11E+02	8.66E+01	7.53E+01	5.39E+01
RightKidney	1.20E+02	8.71E+01	8.74E+01	6.89E+01	5.87E+01	4.26E+01	1.14E+02	8.29E+01	8.29E+01	6.48E+01	5.59E+01	4.06E+01
RightLeg	1.50E+02	1.07E+02	1.30E+02	9.85E+01	7.34E+01	5.26E+01	1.55E+02	1.11E+02	1.34E+02	1.01E+02	7.59E+01	5.42E+01
RightLegBone	1.05E+02	7.64E+01	8.66E+01	6.80E+01	5.14E+01	3.74E+01	1.11E+02	8.05E+01	9.16E+01	7.17E+01	5.44E+01	3.94E+01
RightLung	1.23E+02	8.88E+01	9.63E+01	7.55E+01	6.00E+01	4.35E+01	1.23E+02	8.88E+01	9.90E+01	7.77E+01	6.03E+01	4.35E+01
RightOvary	0.00E+00	0.00E+00	0.00E+00	0.00E+00	0.00E+00	0.00E+00	8.05E+01	5.88E+01	6.30E+01	5.00E+01	3.94E+01	2.88E+01
RightScapula	1.64E+02	1.18E+02	1.23E+02	9.35E+01	8.02E+01	5.76E+01	1.66E+02	1.18E+02	1.22E+02	9.30E+01	8.14E+01	5.80E+01
RightTeste	1.25E+02	9.02E+01	8.61E+01	6.72E+01	6.12E+01	4.42E+01	0.00E+00	0.00E+00	0.00E+00	0.00E+00	0.00E+00	0.00E+00
Skull	1.66E+02	1.19E+02	1.39E+02	1.06E+02	8.14E+01	5.85E+01	1.63E+02	1.16E+02	1.35E+02	1.03E+02	7.96E+01	5.69E+01
SmallIntestine	8.47E+01	6.20E+01	7.03E+01	5.59E+01	4.15E+01	3.03E+01	9.02E+01	6.62E+01	7.45E+01	5.92E+01	4.42E+01	3.24E+01
Spleen	1.06E+02	7.72E+01	8.47E+01	6.67E+01	5.19E+01	3.78E+01	9.99E+01	7.27E+01	8.24E+01	6.53E+01	4.89E+01	3.56E+01
Stomach	1.01E+02	7.41E+01	7.96E+01	6.30E+01	4.96E+01	3.63E+01	1.03E+02	7.50E+01	8.01E+01	6.34E+01	5.03E+01	3.67E+01
Thymus	9.85E+01	7.17E+01	7.82E+01	6.16E+01	4.82E+01	3.51E+01	9.71E+01	7.03E+01	7.72E+01	6.11E+01	4.76E+01	3.44E+01
Thyroid	1.10E+02	8.01E+01	8.93E+01	7.08E+01	5.37E+01	3.92E+01	1.01E+02	7.36E+01	7.64E+01	6.02E+01	4.96E+01	3.60E+01
Trunk	1.03E+02	7.41E+01	8.93E+01	6.85E+01	5.03E+01	3.63E+01	1.03E+02	7.41E+01	8.88E+01	6.80E+01	5.03E+01	3.63E+01
UpperLargeIntestine	8.71E+01	6.39E+01	7.27E+01	5.78E+01	4.26E+01	3.13E+01	9.30E+01	6.80E+01	7.77E+01	6.20E+01	4.55E+01	3.33E+01
UpperSpine	1.24E+02	9.02E+01	9.58E+01	7.55E+01	6.09E+01	4.42E+01	1.10E+02	8.01E+01	8.74E+01	6.85E+01	5.39E+01	3.92E+01
UrinaryBladder	1.02E+02	7.45E+01	7.91E+01	6.25E+01	4.98E+01	3.65E+01	1.10E+02	8.01E+01	8.47E+01	6.72E+01	5.39E+01	3.92E+01
Uterus	0.00E+00	0.00E+00	0.00E+00	0.00E+00	0.00E+00	0.00E+00	8.71E+01	6.39E+01	7.03E+01	5.64E+01	4.26E+01	3.13E+01

Table 5: Effective dose (mSv) on Mars surface with 5 g cm⁻² Al shielding in different organs

Organ	Event 1	Event 2	Event 3	Event 4	Event 5	Event 6	Event 7	Event 8	Event 9	Event 10
Brain	8.99E+02	3.32E+02	3.53E+00	1.88E+01	9.72E+02	4.81E+02	2.19E+01	1.16E+02	4.18E+01	3.74E+01
Head	1.08E+03	7.00E+02	3.77E+00	2.42E+01	2.40E+03	1.36E+03	3.09E+01	1.97E+02	6.15E+01	1.20E+02
Heart	2.67E+02	5.70E+01	1.13E+00	4.10E+00	1.86E+02	8.97E+01	4.96E+00	2.14E+01	1.04E+01	6.05E+00
LeftAdrenal	4.89E+02	1.42E+02	2.00E+00	8.99E+00	4.31E+02	2.10E+02	1.06E+01	5.15E+01	2.09E+01	1.54E+01
LeftArmBone	1.48E+03	7.09E+02	5.58E+00	3.38E+01	2.08E+03	1.07E+03	4.00E+01	2.31E+02	7.52E+01	8.85E+01
LeftBreast	0.00E+00	0.00E+00	0.00E+00	0.00E+00	0.00E+00	0.00E+00	0.00E+00	0.00E+00	0.00E+00	0.00E+00
LeftClavicle	1.03E+03	4.22E+02	4.00E+00	2.26E+01	1.22E+03	6.11E+02	2.63E+01	1.44E+02	4.96E+01	4.86E+01
LeftKidney	5.64E+02	1.86E+02	2.26E+00	1.12E+01	5.50E+02	2.70E+02	1.30E+01	6.62E+01	2.52E+01	2.04E+01
LeftLeg	1.55E+03	8.84E+02	5.62E+00	3.51E+01	2.85E+03	1.56E+03	4.33E+01	2.64E+02	8.38E+01	1.35E+02
LeftLegBone	4.20E+02	1.24E+02	1.71E+00	7.76E+00	3.76E+02	1.84E+02	9.15E+00	4.46E+01	1.81E+01	1.35E+01
LeftLung	5.61E+02	1.78E+02	2.26E+00	1.09E+01	5.30E+02	2.59E+02	1.28E+01	6.37E+01	2.48E+01	1.93E+01
LeftOvary	0.00E+00	0.00E+00	0.00E+00	0.00E+00	0.00E+00	0.00E+00	0.00E+00	0.00E+00	0.00E+00	0.00E+00
LeftScapula	1.51E+03	7.51E+02	5.64E+00	3.51E+01	2.19E+03	1.12E+03	4.14E+01	2.44E+02	7.76E+01	9.38E+01
LeftTeste	1.30E+03	5.90E+02	4.93E+00	2.93E+01	1.71E+03	8.70E+02	3.44E+01	1.96E+02	6.46E+01	7.11E+01
LowerLargeIntestine	1.98E+02	3.91E+01	8.52E-01	2.90E+00	1.30E+02	6.28E+01	3.53E+00	1.48E+01	7.53E+00	4.13E+00
MaleGenitalia	2.01E+03	1.31E+03	7.07E+00	4.64E+01	4.34E+03	2.43E+03	5.87E+01	3.74E+02	1.15E+02	2.14E+02
MiddleLowerSpine	3.10E+02	8.33E+01	1.28E+00	5.41E+00	2.57E+02	1.25E+02	6.42E+00	3.03E+01	1.29E+01	9.00E+00
Pancreas	1.45E+02	2.18E+01	6.40E-01	1.80E+00	7.95E+01	3.81E+01	2.27E+00	8.48E+00	5.12E+00	2.31E+00
Pelvis	3.71E+02	1.14E+02	1.51E+00	6.92E+00	3.43E+02	1.68E+02	8.16E+00	4.05E+01	1.61E+01	1.26E+01
RibCage	1.59E+03	8.00E+02	5.92E+00	3.68E+01	2.35E+03	1.21E+03	4.36E+01	2.58E+02	8.20E+01	1.02E+02
RightAdrenal	6.78E+02	2.27E+02	2.70E+00	1.36E+01	6.69E+02	3.28E+02	1.59E+01	8.10E+01	3.05E+01	2.48E+01
RightArmBone	1.50E+03	7.13E+02	5.64E+00	3.41E+01	2.09E+03	1.07E+03	4.03E+01	2.33E+02	7.58E+01	8.89E+01
RightBreast	0.00E+00	0.00E+00	0.00E+00	0.00E+00	0.00E+00	0.00E+00	0.00E+00	0.00E+00	0.00E+00	0.00E+00
RightClavicle	6.54E+02	2.31E+02	2.60E+00	1.32E+01	6.79E+02	3.36E+02	1.55E+01	8.08E+01	2.98E+01	2.59E+01
RightKidney	5.24E+02	1.70E+02	2.11E+00	1.03E+01	5.04E+02	2.47E+02	1.20E+01	6.06E+01	2.33E+01	1.86E+01
RightLeg	1.55E+03	8.83E+02	5.61E+00	3.50E+01	2.84E+03	1.56E+03	4.32E+01	2.64E+02	8.37E+01	1.34E+02
RightLegBone	4.22E+02	1.27E+02	1.72E+00	7.90E+00	3.83E+02	1.88E+02	9.30E+00	4.56E+01	1.83E+01	1.39E+01
RightLung	5.26E+02	1.63E+02	2.13E+00	1.01E+01	4.89E+02	2.39E+02	1.18E+01	5.87E+01	2.31E+01	1.77E+01
RightOvary	0.00E+00	0.00E+00	0.00E+00	0.00E+00	0.00E+00	0.00E+00	0.00E+00	0.00E+00	0.00E+00	0.00E+00
RightScapula	1.49E+03	7.29E+02	5.59E+00	3.45E+01	2.12E+03	1.09E+03	4.07E+01	2.38E+02	7.61E+01	9.01E+01
RightTeste	8.92E+02	3.93E+02	3.41E+00	1.97E+01	1.14E+03	5.81E+02	2.32E+01	1.31E+02	4.38E+01	4.72E+01
Skull	1.49E+03	7.58E+02	5.53E+00	3.39E+01	2.27E+03	1.19E+03	4.06E+01	2.40E+02	7.69E+01	9.99E+01
SmallIntestine	1.85E+02	3.35E+01	8.02E-01	2.56E+00	1.15E+02	5.51E+01	3.15E+00	1.28E+01	6.85E+00	3.55E+00
Spleen	3.45E+02	9.16E+01	1.43E+00	6.04E+00	2.83E+02	1.37E+02	7.15E+00	3.36E+01	1.43E+01	9.81E+00
Stomach	3.31E+02	9.02E+01	1.37E+00	5.84E+00	2.77E+02	1.35E+02	6.92E+00	3.28E+01	1.39E+01	9.74E+00
Thymus	3.97E+02	1.16E+02	1.62E+00	7.41E+00	3.52E+02	1.71E+02	8.70E+00	4.22E+01	1.71E+01	1.25E+01
Thyroid	4.40E+02	1.27E+02	1.80E+00	8.18E+00	3.84E+02	1.87E+02	9.60E+00	4.63E+01	1.89E+01	1.36E+01
Trunk	8.81E+02	4.97E+02	3.21E+00	1.94E+01	1.63E+03	8.99E+02	2.42E+01	1.47E+02	4.73E+01	7.77E+01
UpperLargeIntestine	1.99E+02	3.86E+01	8.55E-01	2.87E+00	1.29E+02	6.23E+01	3.51E+00	1.46E+01	7.50E+00	4.09E+00
UpperSpine	5.30E+02	1.65E+02	2.14E+00	1.02E+01	4.92E+02	2.41E+02	1.19E+01	5.93E+01	2.33E+01	1.79E+01
UrinaryBladder	3.35E+02	9.35E+01	1.38E+00	5.95E+00	2.86E+02	1.40E+02	7.05E+00	3.38E+01	1.41E+01	1.02E+01
Uterus	0.00E+00	0.00E+00	0.00E+00	0.00E+00	0.00E+00	0.00E+00	0.00E+00	0.00E+00	0.00E+00	0.00E+00

Table 6: Radiation dose deposition in different organs for SEP events

Organ	Event 11	Event 12	Event 13	Event 14	Event 15	Event 16	Event 17	Event 18	Event 19	Event 20
Brain	1.86E+01	7.52E+01	9.52E+01	1.17E+03	6.77E+01	3.26E+00	1.03E+01	1.24E+01	1.30E+01	2.41E+01
Head	2.25E+01	2.85E+02	1.18E+02	5.69E+03	2.51E+02	5.22E+00	1.91E+01	3.74E+01	1.83E+01	4.77E+01
Heart	4.38E+00	1.18E+01	2.25E+01	1.14E+02	1.07E+01	6.74E-01	2.04E+00	2.16E+00	3.27E+00	5.25E+00
LeftAdrenal	9.19E+00	3.05E+01	4.69E+01	3.90E+02	2.76E+01	1.52E+00	4.67E+00	5.27E+00	6.56E+00	1.13E+01
LeftArmBone	3.25E+01	1.86E+02	1.67E+02	3.56E+03	1.66E+02	6.27E+00	2.06E+01	2.85E+01	2.31E+01	4.77E+01
LeftBreast	0.00E+00	0.00E+00	0.00E+00	0.00E+00	0.00E+00	0.00E+00	0.00E+00	0.00E+00	0.00E+00	0.00E+00
LeftClavicle	2.20E+01	9.88E+01	1.13E+02	1.67E+03	8.87E+01	3.99E+00	1.27E+01	1.59E+01	1.54E+01	2.95E+01
LeftKidney	1.12E+01	4.05E+01	5.72E+01	5.68E+02	3.66E+01	1.90E+00	5.92E+00	6.87E+00	7.88E+00	1.41E+01
LeftLeg	3.31E+01	3.07E+02	1.72E+02	6.12E+03	2.72E+02	7.07E+00	2.47E+01	4.24E+01	2.54E+01	5.98E+01
LeftLegBone	7.91E+00	2.69E+01	4.05E+01	3.52E+02	2.43E+01	1.31E+00	4.05E+00	4.62E+00	5.66E+00	9.84E+00
LeftLung	1.10E+01	3.83E+01	5.63E+01	5.15E+02	3.47E+01	1.84E+00	5.72E+00	6.56E+00	7.76E+00	1.37E+01
LeftOvary	0.00E+00	0.00E+00	0.00E+00	0.00E+00	0.00E+00	0.00E+00	0.00E+00	0.00E+00	0.00E+00	0.00E+00
LeftScapula	3.34E+01	1.97E+02	1.71E+02	3.87E+03	1.76E+02	6.56E+00	2.16E+01	3.00E+01	2.38E+01	4.98E+01
LeftTeste	2.83E+01	1.47E+02	1.45E+02	2.72E+03	1.32E+02	5.34E+00	1.73E+01	2.30E+01	2.00E+01	4.01E+01
LowerLargeIntestine	3.14E+00	8.03E+00	1.61E+01	7.19E+01	7.34E+00	4.76E-01	1.43E+00	1.49E+00	2.37E+00	3.75E+00
MaleGenitalia	4.30E+01	4.98E+02	2.26E+02	1.02E+04	4.40E+02	9.89E+00	3.57E+01	6.66E+01	3.44E+01	8.75E+01
MiddleLowerSpine	5.60E+00	1.77E+01	2.86E+01	2.17E+02	1.61E+01	9.08E-01	2.78E+00	3.10E+00	4.05E+00	6.87E+00
Pancreas	2.05E+00	4.45E+00	1.05E+01	2.89E+01	4.10E+00	2.96E-01	8.65E-01	8.69E-01	1.62E+00	2.42E+00
Pelvis	7.03E+00	2.51E+01	3.59E+01	3.52E+02	2.27E+01	1.18E+00	3.67E+00	4.26E+00	5.03E+00	8.86E+00
RibCage	3.51E+01	2.15E+02	1.80E+02	4.26E+03	1.92E+02	6.93E+00	2.29E+01	3.25E+01	2.52E+01	5.31E+01
RightAdrenal	1.36E+01	4.92E+01	6.97E+01	6.84E+02	4.45E+01	2.32E+00	7.21E+00	8.35E+00	9.55E+00	1.71E+01
RightArmBone	3.27E+01	1.87E+02	1.68E+02	3.57E+03	1.67E+02	6.31E+00	2.07E+01	2.86E+01	2.33E+01	4.81E+01
RightBreast	0.00E+00	0.00E+00	0.00E+00	0.00E+00	0.00E+00	0.00E+00	0.00E+00	0.00E+00	0.00E+00	0.00E+00
RightClavicle	1.32E+01	5.19E+01	6.74E+01	7.93E+02	4.68E+01	2.29E+00	7.20E+00	8.63E+00	9.30E+00	1.70E+01
RightKidney	1.03E+01	3.69E+01	5.28E+01	5.08E+02	3.33E+01	1.75E+00	5.43E+00	6.27E+00	7.29E+00	1.29E+01
RightLeg	3.30E+01	3.07E+02	1.72E+02	6.11E+03	2.72E+02	7.06E+00	2.47E+01	4.23E+01	2.53E+01	5.97E+01
RightLegBone	8.04E+00	2.75E+01	4.11E+01	3.64E+02	2.49E+01	1.33E+00	4.13E+00	4.72E+00	5.73E+00	9.99E+00
RightLung	1.02E+01	3.51E+01	5.23E+01	4.65E+02	3.18E+01	1.70E+00	5.29E+00	6.03E+00	7.23E+00	1.27E+01
RightOvary	0.00E+00	0.00E+00	0.00E+00	0.00E+00	0.00E+00	0.00E+00	0.00E+00	0.00E+00	0.00E+00	0.00E+00
RightScapula	3.30E+01	1.89E+02	1.69E+02	3.66E+03	1.69E+02	6.41E+00	2.10E+01	2.89E+01	2.34E+01	4.85E+01
RightTeste	1.91E+01	9.79E+01	9.78E+01	1.78E+03	8.76E+01	3.59E+00	1.16E+01	1.53E+01	1.35E+01	2.69E+01
Skull	3.23E+01	2.15E+02	1.66E+02	4.29E+03	1.91E+02	6.47E+00	2.16E+01	3.18E+01	2.36E+01	5.06E+01
SmallIntestine	2.82E+00	6.89E+00	1.44E+01	5.75E+01	6.31E+00	4.21E-01	1.25E+00	1.30E+00	2.16E+00	3.36E+00
Spleen	6.25E+00	1.93E+01	3.20E+01	2.25E+02	1.75E+01	1.01E+00	3.08E+00	3.40E+00	4.51E+00	7.60E+00
Stomach	6.03E+00	1.92E+01	3.08E+01	2.35E+02	1.74E+01	9.79E-01	3.01E+00	3.36E+00	4.35E+00	7.40E+00
Thymus	7.56E+00	2.47E+01	3.87E+01	3.06E+02	2.23E+01	1.24E+00	3.83E+00	4.29E+00	5.37E+00	9.26E+00
Thyroid	8.35E+00	2.66E+01	4.27E+01	3.19E+02	2.41E+01	1.36E+00	4.19E+00	4.66E+00	5.93E+00	1.02E+01
Trunk	1.84E+01	1.79E+02	9.57E+01	3.55E+03	1.58E+02	3.95E+00	1.39E+01	2.45E+01	1.43E+01	3.40E+01
UpperLargeIntestine	3.12E+00	7.96E+00	1.60E+01	7.11E+01	7.27E+00	4.73E-01	1.41E+00	1.48E+00	2.36E+00	3.73E+00
UpperSpine	1.03E+01	3.53E+01	5.28E+01	4.65E+02	3.20E+01	1.72E+00	5.33E+00	6.07E+00	7.29E+00	1.28E+01
UrinaryBladder	6.13E+00	2.01E+01	3.13E+01	2.57E+02	1.82E+01	1.00E+00	3.09E+00	3.49E+00	4.41E+00	7.58E+00
Uterus	0.00E+00	0.00E+00	0.00E+00	0.00E+00	0.00E+00	0.00E+00	0.00E+00	0.00E+00	0.00E+00	0.00E+00

Table 7: Radiation dose deposition in different organs for SEP events

Organ	Event 21	Event 22	Event 23	Event 24	Event 25	Event 26	Event 27	Event 28	Event 29	Event 30
Brain	5.85E+00	8.28E+01	5.81E+00	3.46E+01	6.22E+00	1.87E+01	8.62E+00	4.64E+00	9.56E+01	2.35E+00
Head	1.08E+01	3.31E+02	2.80E+01	1.63E+02	1.66E+01	5.86E+01	1.18E+01	5.36E+00	2.17E+02	2.59E+00
Heart	1.24E+00	1.06E+01	9.24E-01	5.01E+00	1.26E+00	3.62E+00	1.90E+00	1.15E+00	1.69E+01	8.33E-01
LeftAdrenal	2.73E+00	3.02E+01	2.35E+00	1.33E+01	2.82E+00	8.27E+00	4.13E+00	2.34E+00	4.13E+01	1.40E+00
LeftArmBone	1.17E+01	2.32E+02	1.51E+01	9.70E+01	1.34E+01	4.21E+01	1.57E+01	7.90E+00	2.05E+02	3.68E+00
LeftBreast	0.00E+00	0.00E+00	0.00E+00	0.00E+00	0.00E+00	0.00E+00	0.00E+00	0.00E+00	0.00E+00	0.00E+00
LeftClavicle	7.24E+00	1.15E+02	7.67E+00	4.68E+01	7.79E+00	2.37E+01	1.04E+01	5.43E+00	1.21E+02	2.65E+00
LeftKidney	3.40E+00	4.19E+01	3.11E+00	1.79E+01	3.55E+00	1.05E+01	5.11E+00	2.82E+00	5.36E+01	1.54E+00
LeftLeg	1.40E+01	3.69E+02	2.84E+01	1.72E+02	1.92E+01	6.50E+01	1.67E+01	7.96E+00	2.67E+02	3.79E+00
LeftLegBone	2.35E+00	2.71E+01	2.08E+00	1.19E+01	2.45E+00	7.24E+00	3.56E+00	2.02E+00	3.60E+01	1.19E+00
LeftLung	3.29E+00	3.89E+01	2.94E+00	1.68E+01	3.43E+00	1.01E+01	4.99E+00	2.78E+00	5.13E+01	1.54E+00
LeftOvary	0.00E+00	0.00E+00	0.00E+00	0.00E+00	0.00E+00	0.00E+00	0.00E+00	0.00E+00	0.00E+00	0.00E+00
LeftScapula	1.23E+01	2.52E+02	1.58E+01	1.03E+02	1.40E+01	4.41E+01	1.63E+01	8.09E+00	2.17E+02	3.71E+00
LeftTeste	9.84E+00	1.80E+02	1.17E+01	7.39E+01	1.09E+01	3.40E+01	1.36E+01	6.90E+00	1.70E+02	3.25E+00
LowerLargeIntestine	8.89E-01	7.12E+00	6.36E-01	3.42E+00	8.96E-01	2.56E+00	1.35E+00	8.27E-01	1.17E+01	6.36E-01
MaleGenitalia	2.03E+01	6.05E+02	4.73E+01	2.88E+02	2.96E+01	1.03E+02	2.25E+01	1.02E+01	4.01E+02	4.81E+00
MiddleLowerSpine	1.65E+00	1.74E+01	1.37E+00	7.72E+00	1.70E+00	4.96E+00	2.49E+00	1.43E+00	2.43E+01	9.14E-01
Pancreas	5.76E-01	3.72E+00	3.65E-01	1.91E+00	5.70E-01	1.60E+00	8.50E-01	5.49E-01	6.71E+00	4.99E-01
Pelvis	2.14E+00	2.63E+01	1.94E+00	1.13E+01	2.24E+00	6.63E+00	3.18E+00	1.78E+00	3.30E+01	1.06E+00
RibCage	1.30E+01	2.75E+02	1.75E+01	1.14E+02	1.51E+01	4.78E+01	1.71E+01	8.48E+00	2.32E+02	3.91E+00
RightAdrenal	4.12E+00	5.03E+01	3.77E+00	2.17E+01	4.30E+00	1.28E+01	6.23E+00	3.43E+00	6.54E+01	1.83E+00
RightArmBone	1.17E+01	2.33E+02	1.51E+01	9.72E+01	1.34E+01	4.23E+01	1.58E+01	7.97E+00	2.07E+02	3.73E+00
RightBreast	0.00E+00	0.00E+00	0.00E+00	0.00E+00	0.00E+00	0.00E+00	0.00E+00	0.00E+00	0.00E+00	0.00E+00
RightClavicle	4.13E+00	5.67E+01	4.01E+00	2.37E+01	4.37E+00	1.31E+01	6.08E+00	3.30E+00	6.65E+01	1.76E+00
RightKidney	3.12E+00	3.78E+01	2.83E+00	1.63E+01	3.25E+00	9.64E+00	4.70E+00	2.61E+00	4.90E+01	1.44E+00
RightLeg	1.40E+01	3.69E+02	2.84E+01	1.72E+02	1.92E+01	6.49E+01	1.67E+01	7.94E+00	2.67E+02	3.78E+00
RightLegBone	2.39E+00	2.78E+01	2.13E+00	1.22E+01	2.50E+00	7.37E+00	3.62E+00	2.04E+00	3.68E+01	1.19E+00
RightLung	3.04E+00	3.54E+01	2.70E+00	1.54E+01	3.17E+00	9.34E+00	4.62E+00	2.59E+00	4.72E+01	1.46E+00
RightOvary	0.00E+00	0.00E+00	0.00E+00	0.00E+00	0.00E+00	0.00E+00	0.00E+00	0.00E+00	0.00E+00	0.00E+00
RightScapula	1.19E+01	2.39E+02	1.51E+01	9.79E+01	1.35E+01	4.25E+01	1.60E+01	7.99E+00	2.10E+02	3.68E+00
RightTeste	6.61E+00	1.19E+02	7.77E+00	4.90E+01	7.33E+00	2.27E+01	9.13E+00	4.68E+00	1.13E+02	2.28E+00
Skull	1.23E+01	2.74E+02	1.79E+01	1.17E+02	1.47E+01	4.72E+01	1.59E+01	7.83E+00	2.22E+02	3.68E+00
SmallIntestine	7.97E-01	6.03E+00	5.51E-01	2.94E+00	7.99E-01	2.27E+00	1.20E+00	7.45E-01	1.01E+01	6.08E-01
Spleen	1.81E+00	1.84E+01	1.49E+00	8.28E+00	1.86E+00	5.43E+00	2.77E+00	1.61E+00	2.67E+01	1.01E+00
Stomach	1.77E+00	1.88E+01	1.48E+00	8.34E+00	1.83E+00	5.34E+00	2.69E+00	1.54E+00	2.63E+01	9.68E-01
Thymus	2.21E+00	2.40E+01	1.89E+00	1.06E+01	2.29E+00	6.72E+00	3.39E+00	1.93E+00	3.37E+01	1.12E+00
Thyroid	2.42E+00	2.55E+01	2.04E+00	1.14E+01	2.50E+00	7.32E+00	3.74E+00	2.13E+00	3.68E+01	1.24E+00
Trunk	7.91E+00	2.13E+02	1.68E+01	1.01E+02	1.11E+01	3.78E+01	9.31E+00	4.43E+00	1.51E+02	2.19E+00
UpperLargeIntestine	8.85E-01	7.06E+00	6.31E-01	3.39E+00	8.91E-01	2.55E+00	1.34E+00	8.21E-01	1.16E+01	6.43E-01
UpperSpine	3.07E+00	3.54E+01	2.71E+00	1.54E+01	3.19E+00	9.41E+00	4.67E+00	2.62E+00	4.76E+01	1.47E+00
UrinaryBladder	1.82E+00	2.01E+01	1.55E+00	8.81E+00	1.88E+00	5.52E+00	2.74E+00	1.56E+00	2.72E+01	9.80E-01
Uterus	0.00E+00	0.00E+00	0.00E+00	0.00E+00	0.00E+00	0.00E+00	0.00E+00	0.00E+00	0.00E+00	0.00E+00

Table 8: Radiation dose deposition in different organs for SEP events

Organ	Event 31	Event 32	Event 33	Event 34	Event 35	Event 36	Event 37	Event 38	Event 39	Event 40
Brain	3.27E+02	4.56E+02	3.43E+02	2.31E+02	3.01E+00	1.96E+01	2.56E+01	1.41E+01	1.33E+01	9.23E+01
Head	4.08E+02	1.38E+03	7.20E+02	3.88E+02	3.70E+00	2.87E+01	3.28E+01	1.49E+01	1.76E+01	2.30E+02
Heart	7.49E+01	8.01E+01	5.75E+01	5.37E+01	7.52E-01	4.12E+00	6.01E+00	3.70E+00	2.90E+00	1.44E+01
LeftAdrenal	1.59E+02	1.92E+02	1.46E+02	1.12E+02	1.52E+00	9.21E+00	1.26E+01	7.29E+00	6.36E+00	3.78E+01
LeftArmBone	5.76E+02	1.09E+03	7.33E+02	4.34E+02	5.19E+00	3.70E+01	4.52E+01	2.32E+01	2.42E+01	2.13E+02
LeftBreast	0.00E+00	0.00E+00	0.00E+00	0.00E+00	0.00E+00	0.00E+00	0.00E+00	0.00E+00	0.00E+00	0.00E+00
LeftClavicle	3.88E+02	5.93E+02	4.36E+02	2.78E+02	3.53E+00	2.39E+01	3.04E+01	1.63E+01	1.61E+01	1.21E+02
LeftKidney	1.95E+02	2.49E+02	1.91E+02	1.37E+02	1.83E+00	1.15E+01	1.54E+01	8.68E+00	7.90E+00	5.02E+01
LeftLeg	5.95E+02	1.60E+03	9.11E+02	5.10E+02	5.37E+00	4.01E+01	4.73E+01	2.27E+01	2.53E+01	2.81E+02
LeftLegBone	1.37E+02	1.69E+02	1.27E+02	9.70E+01	1.31E+00	7.93E+00	1.09E+01	6.29E+00	5.49E+00	3.29E+01
LeftLung	1.92E+02	2.38E+02	1.82E+02	1.34E+02	1.80E+00	1.12E+01	1.51E+01	8.62E+00	7.71E+00	4.74E+01
LeftOvary	0.00E+00	0.00E+00	0.00E+00	0.00E+00	0.00E+00	0.00E+00	0.00E+00	0.00E+00	0.00E+00	0.00E+00
LeftScapula	5.95E+02	1.17E+03	7.78E+02	4.51E+02	5.33E+00	3.86E+01	4.67E+01	2.36E+01	2.51E+01	2.28E+02
LeftTeste	5.01E+02	8.74E+02	6.10E+02	3.69E+02	4.52E+00	3.18E+01	3.92E+01	2.04E+01	2.09E+01	1.75E+02
LowerLargeIntestine	5.34E+01	5.60E+01	3.93E+01	3.87E+01	5.43E-01	2.91E+00	4.30E+00	2.69E+00	2.05E+00	9.84E+00
MaleGenitalia	7.81E+02	2.52E+03	1.35E+03	7.21E+02	7.02E+00	5.49E+01	6.25E+01	2.84E+01	3.38E+01	4.30E+02
MiddleLowerSpine	9.66E+01	1.14E+02	8.49E+01	6.85E+01	9.35E-01	5.52E+00	7.67E+00	4.52E+00	3.83E+00	2.19E+01
Pancreas	3.42E+01	3.39E+01	2.15E+01	2.56E+01	3.65E-01	1.82E+00	2.80E+00	1.82E+00	1.28E+00	5.43E+00
Pelvis	1.22E+02	1.57E+02	1.17E+02	8.68E+01	1.16E+00	7.15E+00	9.64E+00	5.52E+00	4.90E+00	3.09E+01
RibCage	6.24E+02	1.26E+03	8.28E+02	4.78E+02	5.60E+00	4.07E+01	4.90E+01	2.47E+01	2.64E+01	2.44E+02
RightAdrenal	2.38E+02	3.02E+02	2.33E+02	1.66E+02	2.22E+00	1.40E+01	1.87E+01	1.05E+01	9.65E+00	6.11E+01
RightArmBone	5.81E+02	1.10E+03	7.37E+02	4.38E+02	5.24E+00	3.72E+01	4.56E+01	2.34E+01	2.44E+01	2.14E+02
RightBreast	0.00E+00	0.00E+00	0.00E+00	0.00E+00	0.00E+00	0.00E+00	0.00E+00	0.00E+00	0.00E+00	0.00E+00
RightClavicle	2.31E+02	3.17E+02	2.37E+02	1.64E+02	2.15E+00	1.38E+01	1.81E+01	1.01E+01	9.40E+00	6.40E+01
RightKidney	1.80E+02	2.28E+02	1.74E+02	1.26E+02	1.69E+00	1.06E+01	1.42E+01	8.05E+00	7.28E+00	4.57E+01
RightLeg	5.93E+02	1.59E+03	9.10E+02	5.09E+02	5.36E+00	4.00E+01	4.72E+01	2.27E+01	2.53E+01	2.81E+02
RightLegBone	1.40E+02	1.72E+02	1.30E+02	9.84E+01	1.33E+00	8.08E+00	1.10E+01	6.36E+00	5.59E+00	3.38E+01
RightLung	1.78E+02	2.19E+02	1.67E+02	1.25E+02	1.68E+00	1.03E+01	1.40E+01	8.04E+00	7.14E+00	4.34E+01
RightOvary	0.00E+00	0.00E+00	0.00E+00	0.00E+00	0.00E+00	0.00E+00	0.00E+00	0.00E+00	0.00E+00	0.00E+00
RightScapula	5.86E+02	1.12E+03	7.55E+02	4.41E+02	5.25E+00	3.79E+01	4.60E+01	2.34E+01	2.47E+01	2.20E+02
RightTeste	3.38E+02	5.81E+02	4.06E+02	2.49E+02	3.06E+00	2.13E+01	2.65E+01	1.39E+01	1.41E+01	1.16E+02
Skull	5.76E+02	1.24E+03	7.84E+02	4.52E+02	5.19E+00	3.77E+01	4.54E+01	2.27E+01	2.44E+01	2.34E+02
SmallIntestine	4.76E+01	4.92E+01	3.35E+01	3.49E+01	4.92E-01	2.58E+00	3.85E+00	2.44E+00	1.81E+00	8.43E+00
Spleen	1.08E+02	1.24E+02	9.33E+01	7.60E+01	1.04E+00	6.12E+00	8.56E+00	5.06E+00	4.27E+00	2.38E+01
Stomach	1.04E+02	1.23E+02	9.20E+01	7.37E+01	1.01E+00	5.96E+00	8.26E+00	4.86E+00	4.13E+00	2.37E+01
Thymus	1.31E+02	1.55E+02	1.19E+02	9.17E+01	1.25E+00	7.53E+00	1.04E+01	6.01E+00	5.24E+00	3.05E+01
Thyroid	1.45E+02	1.68E+02	1.30E+02	1.01E+02	1.38E+00	8.29E+00	1.14E+01	6.67E+00	5.78E+00	3.29E+01
Trunk	3.30E+02	9.15E+02	5.12E+02	2.88E+02	3.00E+00	2.23E+01	2.63E+01	1.27E+01	1.40E+01	1.59E+02
UpperLargeIntestine	5.29E+01	5.57E+01	3.88E+01	3.85E+01	5.40E-01	2.89E+00	4.27E+00	2.67E+00	2.03E+00	9.75E+00
UpperSpine	1.80E+02	2.20E+02	1.69E+02	1.26E+02	1.70E+00	1.04E+01	1.41E+01	8.11E+00	7.22E+00	4.37E+01
UrinaryBladder	1.06E+02	1.28E+02	9.55E+01	7.51E+01	1.02E+00	6.11E+00	8.39E+00	4.90E+00	4.22E+00	2.49E+01
Uterus	0.00E+00	0.00E+00	0.00E+00	0.00E+00	0.00E+00	0.00E+00	0.00E+00	0.00E+00	0.00E+00	0.00E+00

Table 9: Radiation dose deposition in different organs for SEP events

Organ	Event 41	Event 42	Event 43	Event 44	Event 45	Event 46	Event 47	Event 48	Event 49	Event 50
Brain	6.85E+01	9.74E+00	8.86E+01	6.48E+01	7.60E+00	2.61E+00	3.62E+00	3.50E+02	7.98E+01	1.68E+01
Head	1.50E+02	3.01E+01	1.96E+02	1.00E+02	1.18E+01	5.53E+00	8.03E+00	5.63E+02	1.08E+02	3.04E+01
Heart	1.30E+01	1.70E+00	1.30E+01	1.21E+01	1.62E+00	4.83E-01	7.85E-01	6.44E+01	1.95E+01	3.47E+00
LeftAdrenal	3.04E+01	4.14E+00	3.58E+01	2.91E+01	3.57E+00	1.15E+00	1.69E+00	1.56E+02	3.98E+01	7.75E+00
LeftArmBone	1.44E+02	2.24E+01	1.99E+02	1.26E+02	1.43E+01	5.45E+00	7.35E+00	6.89E+02	1.41E+02	3.30E+01
LeftBreast	0.00E+00	0.00E+00	0.00E+00	0.00E+00	0.00E+00	0.00E+00	0.00E+00	0.00E+00	0.00E+00	0.00E+00
LeftClavicle	8.59E+01	1.25E+01	1.16E+02	8.02E+01	9.22E+00	3.27E+00	4.46E+00	4.34E+02	9.44E+01	2.06E+01
LeftKidney	3.89E+01	5.39E+00	4.82E+01	3.72E+01	4.45E+00	1.48E+00	2.10E+00	2.00E+02	4.81E+01	9.72E+00
LeftLeg	1.85E+02	3.39E+01	2.49E+02	1.39E+02	1.61E+01	6.90E+00	9.72E+00	7.69E+02	1.52E+02	3.95E+01
LeftLegBone	2.64E+01	3.63E+00	3.11E+01	2.51E+01	3.09E+00	9.99E-01	1.47E+00	1.35E+02	3.44E+01	6.72E+00
LeftLung	3.74E+01	5.14E+00	4.54E+01	3.58E+01	4.34E+00	1.42E+00	2.04E+00	1.93E+02	4.74E+01	9.43E+00
LeftOvary	0.00E+00	0.00E+00	0.00E+00	0.00E+00	0.00E+00	0.00E+00	0.00E+00	0.00E+00	0.00E+00	0.00E+00
LeftScapula	1.51E+02	2.36E+01	2.14E+02	1.33E+02	1.49E+01	5.74E+00	7.68E+00	7.25E+02	1.46E+02	3.45E+01
LeftTeste	1.19E+02	1.81E+01	1.65E+02	1.08E+02	1.22E+01	4.54E+00	6.11E+00	5.86E+02	1.22E+02	2.78E+01
LowerLargeIntestine	9.04E+00	1.18E+00	8.67E+00	8.41E+00	1.15E+00	3.36E-01	5.61E-01	4.45E+01	1.41E+01	2.45E+00
MaleGenitalia	2.76E+02	5.34E+01	3.72E+02	1.92E+02	2.23E+01	1.02E+01	1.45E+01	1.08E+03	2.04E+02	5.67E+01
MiddleLowerSpine	1.80E+01	2.44E+00	2.05E+01	1.71E+01	2.15E+00	6.80E-01	1.03E+00	9.15E+01	2.44E+01	4.65E+00
Pancreas	5.41E+00	6.90E-01	4.32E+00	4.86E+00	7.18E-01	1.98E-01	3.65E-01	2.53E+01	9.42E+00	1.53E+00
Pelvis	2.41E+01	3.34E+00	2.92E+01	2.28E+01	2.77E+00	9.11E-01	1.33E+00	1.22E+02	3.05E+01	6.06E+00
RibCage	1.61E+02	2.56E+01	2.28E+02	1.40E+02	1.58E+01	6.12E+00	8.22E+00	7.65E+02	1.53E+02	3.66E+01
RightAdrenal	4.74E+01	6.55E+00	5.90E+01	4.56E+01	5.43E+00	1.80E+00	2.55E+00	2.45E+02	5.84E+01	1.18E+01
RightArmBone	1.44E+02	2.25E+01	2.00E+02	1.27E+02	1.44E+01	5.48E+00	7.40E+00	6.93E+02	1.42E+02	3.32E+01
RightBreast	0.00E+00	0.00E+00	0.00E+00	0.00E+00	0.00E+00	0.00E+00	0.00E+00	0.00E+00	0.00E+00	0.00E+00
RightClavicle	4.78E+01	6.77E+00	6.11E+01	4.52E+01	5.35E+00	1.82E+00	2.55E+00	2.44E+02	5.68E+01	1.18E+01
RightKidney	3.56E+01	4.92E+00	4.38E+01	3.41E+01	4.10E+00	1.35E+00	1.93E+00	1.83E+02	4.44E+01	8.93E+00
RightLeg	1.85E+02	3.38E+01	2.48E+02	1.38E+02	1.60E+01	6.89E+00	9.71E+00	7.67E+02	1.51E+02	3.94E+01
RightLegBone	2.70E+01	3.71E+00	3.21E+01	2.57E+01	3.15E+00	1.02E+00	1.49E+00	1.38E+02	3.48E+01	6.84E+00
RightLung	3.45E+01	4.73E+00	4.15E+01	3.31E+01	4.02E+00	1.31E+00	1.89E+00	1.78E+02	4.41E+01	8.72E+00
RightOvary	0.00E+00	0.00E+00	0.00E+00	0.00E+00	0.00E+00	0.00E+00	0.00E+00	0.00E+00	0.00E+00	0.00E+00
RightScapula	1.47E+02	2.28E+01	2.07E+02	1.30E+02	1.46E+01	5.57E+00	7.46E+00	7.08E+02	1.43E+02	3.36E+01
RightTeste	7.96E+01	1.20E+01	1.09E+02	7.21E+01	8.22E+00	3.03E+00	4.11E+00	3.91E+02	8.26E+01	1.87E+01
Skull	1.54E+02	2.52E+01	2.15E+02	1.30E+02	1.47E+01	5.83E+00	7.91E+00	7.11E+02	1.43E+02	3.46E+01
SmallIntestine	7.90E+00	1.02E+00	7.22E+00	7.28E+00	1.02E+00	2.92E-01	5.04E-01	3.83E+01	1.27E+01	2.17E+00
Spleen	1.99E+01	2.67E+00	2.23E+01	1.90E+01	2.39E+00	7.50E-01	1.13E+00	1.01E+02	2.72E+01	5.15E+00
Stomach	1.95E+01	2.64E+00	2.23E+01	1.85E+01	2.32E+00	7.35E-01	1.10E+00	9.91E+01	2.63E+01	5.02E+00
Thymus	2.48E+01	3.36E+00	2.91E+01	2.38E+01	2.94E+00	9.40E-01	1.38E+00	1.28E+02	3.27E+01	6.34E+00
Thyroid	2.71E+01	3.65E+00	3.15E+01	2.61E+01	3.23E+00	1.03E+00	1.51E+00	1.40E+02	3.61E+01	6.96E+00
Trunk	1.05E+02	1.96E+01	1.39E+02	7.67E+01	8.99E+00	3.90E+00	5.57E+00	4.26E+02	8.52E+01	2.22E+01
UpperLargeIntestine	8.96E+00	1.17E+00	8.55E+00	8.32E+00	1.14E+00	3.32E-01	5.58E-01	4.40E+01	1.40E+01	2.43E+00
UpperSpine	3.48E+01	4.76E+00	4.19E+01	3.34E+01	4.06E+00	1.32E+00	1.91E+00	1.79E+02	4.44E+01	8.80E+00
UrinaryBladder	2.01E+01	2.74E+00	2.34E+01	1.91E+01	2.37E+00	7.59E-01	1.13E+00	1.02E+02	2.67E+01	5.15E+00
Uterus	0.00E+00	0.00E+00	0.00E+00	0.00E+00	0.00E+00	0.00E+00	0.00E+00	0.00E+00	0.00E+00	0.00E+00

Table 10: Radiation dose deposition in different organs for SEP events

Organ	Event 51	Event 52	Event 53	Event 54	Event 55	Event 56	Event 57	Event 58	Event 59	Event 60
Brain	7.23E+01	2.45E+01	1.49E+01	1.84E+02	1.42E+02	3.36E+01	7.00E+01	2.04E+02	7.03E+01	1.14E+01
Head	1.47E+02	5.34E+01	3.75E+01	3.58E+02	3.17E+02	1.41E+02	2.85E+02	2.36E+02	1.04E+02	1.70E+01
Heart	1.09E+01	4.37E+00	2.63E+00	2.79E+01	2.58E+01	5.15E+00	9.47E+00	5.21E+01	1.50E+01	2.57E+00
LeftAdrenal	2.97E+01	1.06E+01	6.40E+00	7.58E+01	6.20E+01	1.34E+01	2.68E+01	1.04E+02	3.31E+01	5.50E+00
LeftArmBone	1.58E+02	5.20E+01	3.27E+01	3.98E+02	3.01E+02	8.55E+01	1.84E+02	3.46E+02	1.31E+02	2.11E+01
LeftBreast	0.00E+00	0.00E+00	0.00E+00	0.00E+00	0.00E+00	0.00E+00	0.00E+00	0.00E+00	0.00E+00	0.00E+00
LeftClavicle	9.35E+01	3.09E+01	1.90E+01	2.38E+02	1.79E+02	4.44E+01	9.42E+01	2.38E+02	8.51E+01	1.38E+01
LeftKidney	3.97E+01	1.38E+01	8.31E+00	1.01E+02	7.99E+01	1.80E+01	3.67E+01	1.25E+02	4.13E+01	6.77E+00
LeftLeg	1.90E+02	6.64E+01	4.47E+01	4.70E+02	3.90E+02	1.48E+02	3.07E+02	3.50E+02	1.44E+02	2.33E+01
LeftLegBone	2.57E+01	9.25E+00	5.59E+00	6.56E+01	5.39E+01	1.19E+01	2.37E+01	8.99E+01	2.86E+01	4.75E+00
LeftLung	3.75E+01	1.32E+01	7.95E+00	9.56E+01	7.67E+01	1.70E+01	3.43E+01	1.23E+02	4.02E+01	6.63E+00
LeftOvary	0.00E+00	0.00E+00	0.00E+00	0.00E+00	0.00E+00	0.00E+00	0.00E+00	0.00E+00	0.00E+00	0.00E+00
LeftScapula	1.69E+02	5.49E+01	3.46E+01	4.27E+02	3.18E+02	9.03E+01	1.96E+02	3.53E+02	1.36E+02	2.19E+01
LeftTeste	1.32E+02	4.32E+01	2.68E+01	3.34E+02	2.50E+02	6.70E+01	1.44E+02	3.02E+02	1.12E+02	1.81E+01
LowerLargeIntestine	7.34E+00	3.02E+00	1.82E+00	1.87E+01	1.79E+01	3.50E+00	6.31E+00	3.77E+01	1.06E+01	1.83E+00
MaleGenitalia	2.80E+02	9.89E+01	6.82E+01	6.86E+02	5.85E+02	2.43E+02	5.03E+02	4.49E+02	1.98E+02	3.20E+01
MiddleLowerSpine	1.71E+01	6.25E+00	3.77E+00	4.35E+01	3.66E+01	7.82E+00	1.53E+01	6.43E+01	1.99E+01	3.33E+00
Pancreas	3.72E+00	1.73E+00	1.05E+00	9.49E+00	1.05E+01	1.93E+00	3.17E+00	2.54E+01	6.61E+00	1.17E+00
Pelvis	2.40E+01	8.47E+00	5.13E+00	6.12E+01	4.93E+01	1.11E+01	2.25E+01	7.92E+01	2.57E+01	4.24E+00
RibCage	1.79E+02	5.86E+01	3.71E+01	4.52E+02	3.40E+02	9.91E+01	2.14E+02	3.71E+02	1.44E+02	2.31E+01
RightAdrenal	4.86E+01	1.68E+01	1.01E+01	1.24E+02	9.75E+01	2.18E+01	4.45E+01	1.52E+02	5.03E+01	8.25E+00
RightArmBone	1.59E+02	5.23E+01	3.29E+01	4.01E+02	3.03E+02	8.58E+01	1.84E+02	3.49E+02	1.32E+02	2.12E+01
RightBreast	0.00E+00	0.00E+00	0.00E+00	0.00E+00	0.00E+00	0.00E+00	0.00E+00	0.00E+00	0.00E+00	0.00E+00
RightClavicle	4.99E+01	1.70E+01	1.04E+01	1.27E+02	9.88E+01	2.32E+01	4.80E+01	1.46E+02	4.94E+01	8.08E+00
RightKidney	3.61E+01	1.26E+01	7.59E+00	9.21E+01	7.31E+01	1.63E+01	3.32E+01	1.16E+02	3.80E+01	6.24E+00
RightLeg	1.90E+02	6.63E+01	4.46E+01	4.70E+02	3.90E+02	1.48E+02	3.07E+02	3.49E+02	1.44E+02	2.33E+01
RightLegBone	2.65E+01	9.47E+00	5.71E+00	6.76E+01	5.52E+01	1.22E+01	2.44E+01	9.10E+01	2.92E+01	4.83E+00
RightLung	3.44E+01	1.21E+01	7.32E+00	8.76E+01	7.07E+01	1.55E+01	3.13E+01	1.15E+02	3.72E+01	6.15E+00
RightOvary	0.00E+00	0.00E+00	0.00E+00	0.00E+00	0.00E+00	0.00E+00	0.00E+00	0.00E+00	0.00E+00	0.00E+00
RightScapula	1.64E+02	5.33E+01	3.34E+01	4.14E+02	3.08E+02	8.64E+01	1.87E+02	3.49E+02	1.34E+02	2.15E+01
RightTeste	8.74E+01	2.88E+01	1.79E+01	2.21E+02	1.67E+02	4.45E+01	9.52E+01	2.05E+02	7.55E+01	1.22E+01
Skull	1.68E+02	5.58E+01	3.58E+01	4.22E+02	3.25E+02	9.99E+01	2.14E+02	3.43E+02	1.34E+02	2.16E+01
SmallIntestine	6.14E+00	2.61E+00	1.57E+00	1.57E+01	1.55E+01	3.00E+00	5.28E+00	3.42E+01	9.38E+00	1.63E+00
Spleen	1.86E+01	6.89E+00	4.14E+00	4.75E+01	4.03E+01	8.47E+00	1.65E+01	7.19E+01	2.22E+01	3.71E+00
Stomach	1.85E+01	6.77E+00	4.08E+00	4.72E+01	3.96E+01	8.46E+00	1.66E+01	6.91E+01	2.15E+01	3.59E+00
Thymus	2.42E+01	8.69E+00	5.22E+00	6.16E+01	5.06E+01	1.09E+01	2.16E+01	8.58E+01	2.72E+01	4.52E+00
Thyroid	2.62E+01	9.48E+00	5.68E+00	6.69E+01	5.53E+01	1.17E+01	2.31E+01	9.49E+01	3.00E+01	4.98E+00
Trunk	1.06E+02	3.75E+01	2.55E+01	2.61E+02	2.21E+02	8.68E+01	1.79E+02	1.95E+02	8.03E+01	1.30E+01
UpperLargeIntestine	7.25E+00	2.98E+00	1.80E+00	1.85E+01	1.77E+01	3.47E+00	6.24E+00	3.75E+01	1.05E+01	1.82E+00
UpperSpine	3.47E+01	1.22E+01	7.37E+00	8.84E+01	7.12E+01	1.56E+01	3.14E+01	1.16E+02	3.76E+01	6.20E+00
UrinaryBladder	1.94E+01	7.00E+00	4.22E+00	4.94E+01	4.09E+01	8.88E+00	1.76E+01	6.99E+01	2.20E+01	3.66E+00
Uterus	0.00E+00	0.00E+00	0.00E+00	0.00E+00	0.00E+00	0.00E+00	0.00E+00	0.00E+00	0.00E+00	0.00E+00

Table 11: Radiation dose deposition in different organs for SEP events

4. Impact of Ionizing Radiation on Astronaut Health

Humankind is well-protected from ionizing radiation by our planet's atmosphere and magnetosphere. The International Space Station sits in the low-Earth orbit where it is still protected by the magnetosphere, and the only human beings to travel outside of the magnetosphere remain the Apollo astronauts. Our knowledge of the harmful impacts of radiation exposure on the human body comes mainly from the study of radiation therapy. Radiation therapy does not employ neutron exposure; therefore 1 Sv is approximately equivalent to 1 Gy in patients receiving radiotherapy treatment. Similarly, as most experimental studies utilize low photon energy, 1 Sv is approximately equivalent to 1 Gy in such publications [29]. Some knowledge also comes from historical radiation disasters such as the atomic bombings of Hiroshima and Nagasaki in 1945 and the Chernobyl disaster of 1986. Acquiring knowledge of how radiation exposure affects the human body is crucial for the future of space travel (such as to Mars), where exposure to galactic cosmic radiation and solar particle events poses a threat to astronaut health. The following literature review material focuses on the effects of radiation on various human physiological systems and the genetic material.

4.1. The Impact of Ionizing Radiation on the Physiological Systems

4.1.1. Acute Radiation Syndrome

In August 1972, a series of solar flares led to severe solar storms, solar particle events, and geomagnetic storms. This was just five months after Apollo 16 had launched in April and five months before Apollo 17 would launch in December. August 1972 was considered as a potential launch date for either Apollo 16 or 17 during the initial planning stages. If Apollo 16 or 17 had been launched during the dates of the solar storms, and specifically during the extreme solar flare of August 4th, any in-flight astronauts could have been exposed to an absorbed radiation dose of around 0.5 Gy [30]. The Centers for Disease Control and Prevention (CDC) defines 0.7 Gy as the threshold of radiation exposure at which acute radiation syndrome can occur and reports that mild symptoms can be observed at exposures as low as 0.3 Gy [31]. Acute radiation syndrome is a health concern for astronauts during SPEs. NASA have commented that there is a risk of ARS for astronauts due to the known occurrence of SPEs and the poor ability to predict SPEs [32].

Acute radiation syndrome is divided into three medically distinct presentations: Hematopoietic, gastrointestinal, and neurovascular. This is not an exhaustive list of the tissues that can be affected in acute radiation syndrome. In medical terms, 'acute' means that the illness presents severely in a short amount of time. The three divisions of the syndrome present at different thresholds of radiation exposure: The hematopoietic syndrome at 1-5 Gy, the gastrointestinal syndrome at 5-20 Gy, and the neurovascular syndrome at more

than 20 Gy. The gastrointestinal and neurovascular syndromes are unlikely to be a risk for astronauts at spaceflight-relevant radiation doses. The hematopoietic syndrome, however, may occur at doses as low as 0.3 Gy, affecting the formation of blood cells. Consequences of the hematopoietic syndrome include low numbers of white and red blood cells, which can lead to infection and anemia. The higher the radiation dose that the individual is exposed to, the lower the survival rate is. If bone marrow is sufficiently damaged during the hematopoietic presentation, it can lead to hemorrhage and impaired ability of the immune system to fight off infection, both of which can lead to death [31].

4.1.2. The Nervous System

Radiotherapy for patients with brain tumors produces a wide range of acute and delayed effects on the nervous system. This is useful information for considering the potential effects that radiation exposure may have on the nervous system of astronauts in long-term space missions. For patients who have been recently diagnosed with brain cancer and treated with radiotherapy, observed side effects include mood changes (anxiety and depression) and difficulty with reading, writing, and expression of language. For long-term survivors of radiotherapy-treated brain tumors, late side effects can also include physical and mental fatigue, anger and frustration, and difficulty concentrating. External beam radiation therapy is the most common radiation therapy used to treat brain cancers, utilizing X-rays and gamma rays. Proton therapy is a novel technique gaining momentum and is used more often for children. Radiation doses in brain tumor radiotherapy can be around 20 Gy in adults and 24 Gy in children, delivered in fractions of 1.8 to 2.0 Gy directly to the tumor. These dose rates can cause delayed cognitive impairment.

A common side effect of brain tumor radiotherapy and one of the particular concerns for astronauts is fatigue. Fatigue is an acute side effect usually observable within several weeks of the patient's first radiotherapy treatment and usually persists for one to three months after treatment has finished. A defining characteristic of radiotherapy-induced fatigue is that it is not typically alleviated by resting [33]. This is a concern for astronauts who need to be alert when partaking in dangerous interplanetary space travel and exploration. The fatigue can be accompanied by depression and cognitive dysfunction, but some symptoms can be relieved by medication such as methylphenidate. Hair loss and skin erythema (redness of the skin) are other acute side effects that often occur alongside fatigue as a result of radiotherapy [33]. It is important to note that the radiation dose employed in cancer radiotherapy is much higher than what astronauts are expected to be subjected to during interplanetary space travel. Yet, the risk of symptoms like impaired cognitive performance [34] as well as skin erythema and hair loss are well-documented [35].

Butler et al. (2006) ([33]) discuss that brain irradiation can lead to the demyelination of white matter as a delayed reaction. Myelin is a fatty sheath that wraps around neurons and allows signals to propagate through the nervous system at a higher rate. Demyelination involves damage to the myelin of the neurons. The demyelination of neurons in the brain's white matter would considerably slow the rate at which action potentials (signals) are propagated, accounting for some of the cognitive dysfunction and mood changes that can be observed in patients following radiotherapy. The cognitive dysfunction that is observed as a delayed reaction to radiotherapy involves slowing of cognitive functions, difficulty concentrating and multitasking, and decreased memory [33]. An impeded function of neurons is characteristic of the pathogenesis of several neurodegenerative diseases such as Parkinson's Disease, where there is an observed decrease in the number of dopamine-producing neurons in the substantia nigra. The substantia nigra is the part of the brain that is important for movement, thus producing the movement disorders associated with Parkinson's Disease [36]. Additionally, damaged neurons can result in decreased neurotransmitter (chemical signals) production. Low levels of neurotransmitters such as dopamine and serotonin can cause anxiety and depression. Thereby, the ability of radiation to damage neurons is potentially hazardous for astronauts.

A significant component of deep space radiation is high-energy protons. Proton radiotherapy is a novel development of high interest in medical fields as it allows for treatment of a tumor without such a high degree of damage to the surrounding healthy tissue due to an ability to control the depth of the proton beam inside the tissue. Proton radiotherapy is a commonly used treatment for rhabdomyosarcoma (RMS), a highly aggressive form of cancer that derives from muscle cells with an impaired ability to differentiate. Orbital rhabdomyosarcoma is a head and neck subtype that accounts for 10% of pediatric RMS cases and commonly affects the orbit (the socket of the skull where the eye and its appendages sit). Standard photon radiotherapy as a treatment of orbital RMS can lead to impaired vision in the irradiated eye in most patients, and 10% of patients receiving this treatment develop a later complication that requires enucleation (surgical removal of the eyeball from its orbit). Standard photon radiotherapy that utilizes X-rays and gamma-rays also renders children more prone to a second tumor development than adults.

Yock et al. (2005) carried out a study that followed seven patients treated via proton radiotherapy for orbital rhabdomyosarcomas and who had also received dactinomycin/vincristine-based chemotherapy. The patients were all treated at Massachusetts General Hospital or the Harvard Cyclotron between 1995 and 2001, with a median dose of 46.6 CGE (cobalt gray equivalent) delivered in conventional fractions. The study followed up the patients at a median time of 6.3 years following radiotherapy treatment. At the follow-up, it was found that all seven patients were disease-free, and only one patient had required enucleation and

stereotactic radiotherapy due to the treatment not being locally controlled. The remaining six patients had good vision in the radiotherapy-treated eye. There was additionally no evidence of cataract formation or neuroendocrine effects in any of the patients. All patients displayed mild to moderate orbital bony asymmetry or enophthalmos. Enophthalmos causes the eye to sink and be abnormally positioned in its socket due to an injury or medical condition. Despite this, overall results showed that healthy tissue surrounding the cancer mass was better spared by proton irradiation than by photon irradiation [37]. This is interesting considering the high abundance of protons in deep space radiation, and highlights an avenue for further research into proton irradiation in radiotherapy and space medicine.

HZE particles (high-energy nuclei) are a crucial component of galactic cosmic radiation, and it is essential to consider their biological effects compared to the standard X-rays and gamma-rays commonly used in radiotherapy. A study by Craven et al. (1994) showed calculations on the number of cell nuclei in the brain likely to be struck by HZE particles during interplanetary space travel. The study determined that 3.4% of the neuronal nuclei at the center of the brain would be crossed by an HZE particle once every three years of interplanetary space travel. As is previously discussed, neuronal damage plays a role in neurodegenerative diseases and mental illnesses. Neurons of the central nervous system could experience much damage due to being hit by a high-energy HZE particle. Neurons have a very low regeneration rate making repair and replacement in response to damage a prolonged process. The study also reports on iron as an abundant component of galactic cosmic radiation and an element capable of creating breaks in the DNA strands in neuronal nuclei. Due to the low regeneration rate of neurons, these radiation-induced DNA changes may not be phenotypically present until later in the astronaut's life. The accumulation of DNA damage and direct damage to neuronal nuclei could result in premature aging for exposed astronauts. In addition to damaging the neurons themselves, the heavy-charge radiation particles could disrupt the complex interactions (synapses) of neurons in the central nervous system, impairing the mental and physical abilities of the astronaut. Optimal cognitive and physical performance is essential for astronauts partaking in the dangerous endeavors of interplanetary space travel [34].

4.1.3. Behavioral Effects

As previously discussed, ionizing radiation can impair the central nervous system (CNS). Damages occur in basic neuronal processes, such as neuronal firing and synaptic excitability, and also in the brain structure due to white matter necrosis, demyelination, and vascular changes [38][39]. Cucinotta et al. (2009) described that some side effects are in behavior and cognition; according to their exposure, they can be classified as

acute or chronic. Acute CNS risks include altered cognitive function, reduced motor function, and behavioral changes, all of which may affect performance and human health. Chronic CNS risks are possible neurological disorders such as Alzheimer's disease, dementia, or premature aging [39]. Radiotherapy patients manifest behavioral changes, such as chronic fatigue and depression, and neurocognitive degeneration in verbal and visual memory, attention, speed of thought, and verbal fluency [39]. Children are especially susceptible to these effects. A review by Butler and Haser (2006) showed a decline in intelligence and academic achievement, including low intelligence quotient (IQ) scores, verbal abilities, and performance IQ in children after radiotherapy treatment for brain tumors [40].

Besides the hazard for the physiological systems, there is a growing concern for social and cognitive welfare in astronauts on long-term missions due to the prolonged radiation exposure and confinement they will experience [41]. As behavioral effects are difficult to quantitate, there are different tests to evaluate changes in conduct and cognitive performance. In each assay, results always depend on the age of the individual and radiation exposure dose [39]. Trivedi et al. (2012) exposed three-month-old male mice to doses of 3 Gy, 5 Gy and 8 Gy (Tele 60C0 unit gamma irradiation). 10 days post-irradiation, they detected anxiety-like symptoms in the three irradiation groups, and a decrease in locomotor activities and execution in the novel object recognition test (a paradigm used to assess object recognition and spatial memory) for 5 Gy and 8 Gy groups [38]. In another study, Pecaut et al. (2002) simulated space radiation conditions with mono-energetic protons (250 MeV) for 3 or 4 Gy doses in two-month-old female mice. Their results also evidenced deficits in locomotor activities, as well, acoustic startle habituation. However, two weeks later, the effects of radiation were negligible [42].

A recent investigation by Kiffer et al. (2009) analyzed female mice nine-months the late effects in cognition, behavior, and neuronal morphology post-exposure to lower doses of 0.1 Gy or 0.25 of 16O. Nine-months post-exposure, they estimated animal conduct changes. 0.1 Gy and 0.25 Gy induced deficiencies in object recognition memory and deficit in social novelty only at higher doses [41]. Cherry et al. (2012) found consistent results in mice three-month; they evidenced cognitive and memory space impairment after exposure to 0.1 Gy and 1 Gy of ^{56}Fe radiation at $1 \text{ GeV}/\mu$ [43]. These findings suggest that recognition memory is one of the most affected after space type radiation and that these damages may persist over time. One of the long-term effects is the possible development of neurological disorder, Alzheimer's disease (AD). AD is characterized by a progressive cognitive decline over several years. One of the causes of this decline is an ongoing chronic neuroinflammatory process. The accumulation of amyloid-beta (an abnormal protein) in the brain forms plaques; these plaques are one of the key players in neuroinflammation and is one of the

principal histopathological hallmarks. Monitoring plaque progression is a diagnostic tool for humans and allows the gauge of disease severity [44].

Mice receiving doses as low as 0.1 Gy showed alarming amyloid accumulation, behavioral deficits, and reduction in cognitive abilities. Mice do not possess the genes capable of developing symptoms related to AD. However, there are genetically modified mouse models to express proteins associated with this disease [44]. One of them is the protein ApoE-4 which tends to produce amyloid-beta accumulation that precedes the symptoms of AD [45][46]. A study by Villasana et al. (2011) with male transgenic mice expressing ApoE-4 evidenced deficiencies in spatial memory after 3 Gy radiation exposure [47]. Another study by the same author reported deficits in displaying the NOR test in female transgenic mice expressing ApoE-4 after radiation exposure of 2 Gy [48].

Rudbeck et al. (2017) evaluated spatial learning and memory with the water maze (WM) test and amyloid-beta deposits in 3 month-old APP/PSEN1 transgenic (TG) and wild-type (WT) mice irradiated with protons (150 MeV; 0.1 ± 1.0 Gy; whole body). After irradiation, TG mice performed significantly worse than WT mice in the WM test, also TG mice exhibited an increase in amyloid-beta deposits in the brain cortex. They concluded that although irradiation with protons increased $A\beta$ deposition, the complex functional and biochemical results indicate that irradiation effects are not synergistic to AD pathology [49]. Nevertheless, Alzheimer's disease is another concern that should be taken into account and needs further studies for long-term space missions.

4.1.4. The Ocular System

In 1897, Chaluppecky started the first studies of the effects of ionizing radiation on the eye. Since then, subsequent investigations have tried to demonstrate the possible harmful impairments on the ocular structures as a warning to therapists [50]. Later in 1929, a study by Rohrshneider et al. listed the oculars structures according to their sensitivity to radiation, with the lens being one of the most sensitive, followed by the conjunctiva, cornea, uvea, retina, and optic nerve [51]. The use of radiotherapy to treat different conditions in the ocular structures, such as an ocular lesion, non-neoplastic tumor, tumors of the eye, and tumors of the orbit, is well-known. Radiation doses vary between 6 Gy-12 Gy for a single dose, or between 20 Gy and 100 Gy for various doses for periods of several weeks (more than two weeks); however, the appearance of side effects after several weeks or even years of exposure is a current concern [50]. Within the damages we find: Erythema, telangiectasis (chronic dilation of the capillaries and other small blood vessels [52]), lacrimal gland atrophy, hyperemia (increased amount of blood in the vessels of an organ or tissue in the body

[53]), thinning of the cornea, and cataracts. According to The International Commission of Radiological Protection (ICRP), cataracts have become a growing concern due to the low radiation threshold necessary to detect lens opacities. For a single acute exposure, only 0.5–2.0 Gy is required. For highly fractionated or protracted exposures, 5Gy is required. And for annual dose rates for yearly highly fractionated or protracted exposure for many years is >0.1 Gy per year; however, the cataract formation is a late effect [54]. Even some epidemiological studies from Hiroshima and Nagasaki, and children survivors from Chernobyl have demonstrated that lower doses can trigger detectable opacity [55].

NASA's Lifetime Surveillance of Astronaut Health (LSAH) data provides a historical record of cataract incidence in astronauts, and the NASA Study of Cataracts in Astronauts (NASCA) aims to precisely determine the types, severity and progression rates of lens opacification in astronauts. It was a 5-year longitudinal study where the status of the lens and visual function was measured in 171 astronauts (active and retired), and in two control groups: military aviators (active and retired) and people without any military aviation background [56]. The Nidek EAS 1000 Lens Imaging System (an imaging system for the anterior eye segment, which offers the possibility of recording Scheimpflug and retro illumination images [57]) measured the status of the nuclear, cortical, and posterior subcapsular (PSC) lens of the subjects. Other characteristics measured at baseline were age, demographics, general health, nutritional intake, and solar ocular exposure [56]. At the end of the study, the conclusions recollected were: the variability and median of cortical cataracts were significantly higher for exposed astronauts than for the control group. Within the astronaut group, PSC opacity was more significant in subjects exposed to higher space radiation doses. There was no evidence of an association between space radiation and nuclear cataracts. These results suggest increased cataract risks at smaller radiation doses than have been reported previously [56]. Cucinotta et al. (2001) previously discussed these findings in another study, with 295 astronauts participating in NASA's Longitudinal Study of Astronaut Health (LSAH) and individual occupational radiation exposure data. He suggests an increased risk of cataracts for astronauts with higher lens exposure doses (>8 mGy) in comparison to other astronauts with lower exposures [58].

Another interesting phenomenon is the observation of phosphenes by crew members Apollo 11 through Apollo 17 [59]. Phosphenes are the visual sensation as flashes of light without light entering the eye induced by various stimuli (mechanical, electrical, magnetic, ionizing radiation, and some others) [60]. Apollo 11 Lunar Module pilot, Edwin Aldrin, first described these flashlights, and subsequently, the Apollo 12 and Apollo 13 crews were briefed on the phenomena and asked to report their observations. After these reports, Apollo 14, Apollo 15, and Apollo 16 dedicated a one-hour session to observe these flashlights with a simple

blindfold (designed to avoid pressure on the eyeballs). There have been reported three types of flashes, the “spot” or “starlike,” which is the most common, the “streaks” (probably caused by particles with trajectories approximately tangent to the retina) and the last one referred as “clouds” always seen in the eye periphery. The time of appearance of these flashes is on average 19.3 minutes after starting the darkness adaptation phase. Apollo 16 and Apollo 17 missions added a device known as the Apollo Light Flash Moving Emulsion Detector (ALFMED) to understand the origin of this phenomenon [59]. Chapman et al. (1972) suggest that the flashlights observed might be due to primary cosmic rays particles passing through the vitreous humor generating Cherenkov radiation or by direct ionizing interactions with the retina [61]. Over 80% of astronauts from NASA or ESA (European Space Agency) programs also have perceived phosphenes, at least in some missions [62]. It is necessary to study in-depth the possible long-term effects of this particular phenomenon.

4.1.5. The Thyroid Gland

The thyroid gland is a human organ positioned in front of the trachea and under the larynx in the neck (C5-T1). It is characterized by the presence of two lobes that are interconnected thanks to the presence of the central isthmus. It is covered by two different capsules, one given by the pretracheal layer of the deep cervical fascia and another one given by the peripheral gland of the glandular tissue. From a microscopic point of view, thyroid is organized in round-shaped structures called folliculi and the cells that create these elements are called follicular cells, responsible for the synthesis of the mature thyroid hormones. Thyroid hormones, T3 and T4, synthesized from iodine and thyroglobulin, have several effects on the human body: they increase the basal metabolic rate (increase of oxidative processes), the heat production, the oxygen delivery to the tissues, and the intestinal absorption of folates and B12.

Thyroid gland is one of the most radiosensitive organs in our body since even doses as small as 50-100 mGy have been associated with an increased risk of thyroid malignancy in children [63]. During a CT scan, the thyroid is exposed to 15.2-52 mGy, a radiation dose that would increase the cases of thyroid malignancies in up to 390 per million exposed people [64]. The exposure to ionizing radiation leads to DNA damages and increases the rates of thyroid cancer. The majority of the current information derives from past nuclear accidents, as it happened in Hiroshima (1945) and Chernobyl (1986). Although the radiation doses were high in both cases considering the current recommended thresholds for human health, the characteristics of the radiation were different in those two scenarios. In the Hiroshima bombing, people were subjected to a rapid irradiation with high-energy gamma rays and neutrons while in the Chernobyl accident, many people, especially in Belarus, were invested with beta and gamma rays plus different iodine radioisotopes.

A study conducted on Hiroshima survivors demonstrated that among 105,401 subjects, 371 thyroid cancers have been identified in the period 1958-2005 and the excess risk was higher for people who were 10 years old or less at the time of the bombing [65]. In the same study it was defined that a mean dose as low as 0.05-0.1 Gy may significantly increase the risk of thyroid cancer, a correlation that continues being linear up to doses as high as 20-29 Gy. The Chernobyl disaster was linked to an increased incidence of thyroid cancer in children by different studies. For example, researchers analyzed in the period 1992-2000 about 4,000 cases of thyroid cancer in 0-18 years old. About 75% of these cases occurred in children aged 0-14 years [66]. Ionizing radiation (IR) may induce specific genetic instability in human thyroids. In particular, two genetic alterations have been intensively studied and they both belong to the same intracellular signaling pathway: ET/PTC = genetic translocation induced by IR, whose variant 1 is characterized by a centromeric inversion on chromosome 10. It has been observed in children exposed to Hiroshima and Nagasaki bombings and its presence is correlated to a more aggressive cancer phenotype [67]. BRAF/AKAP9 = paracentric inversion on chromosome 7q, which impairs the autoinhibitory structure of BRAF, a portion of the protein that also contains RBD (Ras Binding Domain), leading to a Ras-independent activation of BRAF. It has been described in 2 cohorts of Belarussian children and adolescents exposed to radiation after the Chernobyl accident [68].

4.1.6. The Skeletal System

The skeletal system of the human body is vital for structure and movement, and damage to bones underlies several medical conditions including osteomalacia (bone softening due to malnourishment). An increased risk of bone fracture is a concern for cancer patients post-radiotherapy. Following radiotherapy treatment, radiation damage to the healthy skeletal tissue near a tumour can render it more vulnerable to fractures. For example, in breast cancer patients receiving radiotherapy, post-treatment rib fracture rates can reach as high as 19%. The standard radiation therapy for breast cancer patients involves the use of X-rays and/or gamma rays, but the experimental use of proton therapy is occurring more frequently. Radiotherapy can impede bone structure integrity through loss of minerals and damage to the important spongy bone tissue (trabecular structures). A paper by Baxter et al. (2005) investigated the relative bone fracture risk of three cancer types in women that are commonly treated via radiation therapy: cervical, rectal, and anal cancer. The study looked at women over the age of 65. Results of the paper show that women who were treated for cervical cancer by radiation therapy had a resulting increased relative risk of hip fracture of 65%. The paper subsequently identified the increased relative risk of hip fractures for rectal and anal cancers to be 66% and

214% respectively [69].

Willey et al. (2011) have made major advances in investigating the possible effects of space radiation on bone health. The researchers compare the radiation exposure of astronauts in spaceflight to that of cancer therapy patients. Radiotherapy as a cancer treatment typically involves delivering fractions of 1.8-2.0 Gy directly to the tumour mass for a few minutes. The total size and number of fractions delivered depends on the cancer type, for example, gynaecological cancers are treated with a total of 54 Gy delivered over six weeks in fractions of 1.8 Gy at a time. For comparison, in-flight astronauts exposed to a solar particle event lasting 8-24 hours would receive whole body cumulative doses of 1.0-2.0 Sv, or 1.0-2.0 Gy of protons [70]. The radiation doses that cancer radiotherapy patients receive are higher than what astronauts are expected to be exposed to in spaceflight. This somewhat weakens the comparison of radiotherapy health risks to space radiation health risks, however spaceflight-relevant radiation doses have been shown to induce bone loss. At proton doses as low as 0.5 Gy, bone loss is seen to persist at nine weeks after spaceflight-relevant radiation exposure. At a dose exposure of 1 Gy, bone loss is seen to persist at four months following the exposure. Thus, the 1.0-2.0 Gy of protons that astronauts could be exposed to during a solar particle event could ensue long-term negative effects on bone health [70].

Two major effects of spaceflight-relevant radiation exposure are a decrease in osteoblast activity, and an early increase in osteoclast activity. Osteoblasts are large cells containing a single nucleus that function in synthesising bone. Bone synthesis, however, requires a number of individual osteoblasts to work as a group of connected cells. Radiation exposure has been shown to damage osteoblast precursors and osteoprogenitors (cells that go on to develop into osteoblasts). Osteoprogenitors are specifically damaged by the oxidative stress of irradiation, which impairs the ability of the mesenchymal stem cells to undergo osteogenic differentiation. The impact of radiation-induced oxidative stress makes research on antioxidants of target interest. Antioxidants such as beta-carotene have been seen to prevent radiation-induced oxidative stress damage (see dietary mitigation strategies section) [71]. The process of osteoblast differentiation involves a key transcription factor, RUNX2. Levels of RUNX2 are seen to decrease in response to radiation exposure, suggesting a weakened ability of osteoblast precursors and osteoprogenitors to develop into fully-functioning, bone-synthesising osteoblasts. Irradiation results in a decline in the number of mesenchymal stem cells able to respond to osteogenic stimulation, which delays the recovery of the bone from the osteoblast damage. Osteoblast damage has other consequences on bone health including reducing the size of the blood vessels that supply oxygenated blood to the bones, which can cause hypoxia (inadequate oxygen supply) [70]. MC3T3-E1 is an osteoblast precursor cell line derived from the calvaria of *Mus musculus* (house mouse).

These MC3T3-E1 cells can undergo differentiation to form osteoblasts. A study by Kook et al. (2015) demonstrated the impaired capacity of MC3T3-E1 cells to differentiate into osteoblasts following radiation exposure. MC3T3-E1 cells were exposed to radiation doses ranging from 0-8 Gy (spaceflight-relevant doses). The study produced results on specific effects of irradiation on MC3T3-E1 cells. The study reported that irradiation enhances the biochemical Nrf-2/HO-1 pathway which interferes with the role of transcription factor RUNX2 to drive osteoblast development [72]. Osteoclasts are large multinucleated cells that function in the degradation of bone tissue in response to, for example, a bodily demand for calcium. The early response of osteoclasts to irradiation is the opposite to that of osteoblasts, with an initial increase in osteoclast activity. The dissolution of bones by osteoclasts involves an enzyme, tartrate-resistant acid phosphatase (TRAP5b). The prevalence of TRAP5b in the circulation can be measured using serum markers. In response to radiation exposure, it is observed that serum markers for TRAP5b are elevated in the first 24 hours. This research was produced by Willey et al. (2011) and has identified bisphosphonate antiresorptive risedronate as a potential pharmacological agent for suppressing radiation-induced increases in osteoclast activity, thereby suppressing the resulting damage to the bone tissue [70].

4.1.7. The Immune System

There are many different types of cells in the human body, each with their own defining characteristics. The regeneration rate of a particular cell type influences its sensitivity to radiation-induced damage. Immune cells (white blood cells) are one of the most radiation-sensitive cell types in the body and also have one of the highest regeneration rates. In comparison, nerve cells have one of the lowest regeneration rates and show less radiation sensitivity than immune cells. Neutrophils are the most abundant type of leukocyte (immune cell), accounting for 60-70% of the whole leukocyte pool in the body. Neutrophils regenerate every 1-5 days. Neutrophils are a crucial part of the body's immune system, and are capable of engulfing and digesting pathogenic microorganisms by a process called phagocytosis. The neutrophil releases antimicrobial products such as hydrolytic enzymes and reactive oxygen species to kill the phagocytosed pathogen. These antimicrobial products can cause damage to the surrounding healthy human tissue if their production is unregulated. To reduce the detrimental effect to the surrounding tissue, a neutrophil undergoes apoptosis (programmed cell death) after it has successfully phagocytosed and killed a pathogen. This means that the pool of neutrophils needs to be continuously replenished resulting in a high neutrophil regeneration rate. Cells that regenerate more frequently are replicating their DNA more frequently, making it more likely that harmful radiation-induced DNA mutations (see DNA damage section) will be expressed.

The effect of space radiation on the immune systems of astronauts is a big concern in space travel science. Due to the rapid regeneration rate of leukocytes, the immune system is particularly susceptible to local and systemic damage by particle irradiation. A subtype of leukocytes, lymphocytes, show increased chromosomal aberrations following long-term space missions in low Earth orbit such as in the International Space Station [73]. Lymphocytes are key to the adaptive immune response, a powerful immune response that allows the immune system to remember previous infections. Gridley et al. (2002) have carried out Earth-based experiments on the response of the immune system in mice to proton irradiation, as protons make up a significant proportion of deep space radiation [74]. It is estimated that if a solar particle event lasting 8-24 hours were to occur whilst astronauts were travelling in deep space, the exposure of the in-flight astronauts would be 1.0-2.0 Gy [30]. The experiments by Gridley and Pecaat involved delivering total doses of 0.5, 1.5, or 3.0 Gy delivered in fractions of either 1cGy or 80cGy per minute. It was observed in these experiments that such irradiation produced a linear or dose-dependent decline in the leukocyte and lymphocyte populations. B cells were identified as the most radiation-sensitive leukocytes, followed by T cells, and then natural killer cells as the least radiation-sensitive leukocytes. B cells and T cells are both adaptive immune cells, whilst natural killer cells are capable of killing virally-infected and cancerous cells. Cancer risk is increased in astronauts following radiation exposure (see increased cancer risk section), and this could be significantly worsened following a decline in the number of T cells and natural killer cells. The simulated deep space radiation not only affected leukocyte population size, but also impacted the functional capabilities of the immune cells [74]. Chancellor et al. (2018) discuss the limitations of using Earth-based radiobiology studies to predict the health risks of space radiation for astronauts. Such limitations include the discrepancies between animal and human models, difficulty simulating the distribution of radiation exposure across the entire body, and the discrepancies between terrestrial and space radiation types [75].

Research on the impairment of leukocyte function by irradiation is compiled from various journal articles by the International Atomic Energy Agency. The compiled research shows the effects of different levels of radiation exposure. After exposure to 5 Gy for an hour, concentrates of lymphocytes in saline had a significant fall in ATP levels, indicating implications for the metabolic and energy processes of the cell. At exposure to 10 Gy, leukocyte cytoplasm show increased vacuolization, indicating increased cell death. At 20 Gy, radiation exposure is high enough to eliminate leukocyte mitotic ability, impairing the ability of leukocytes to replicate. A subtype of leukocytes called granulocytes seem to be less susceptible to radiation damage than other leukocytes. Granulocytes are immune cells that can release granules containing antimicrobial chemicals to kill infecting pathogenic microorganisms. At 30 Gy, lymphocytes show decreased

responsiveness to phytohemagglutinin; a chemical that promotes the lymphocyte activation and proliferation [76]. Part of the immune system that is of concern for astronauts is the inflammatory response. Hayashi et al. (2003) took blood samples from 453 atomic bomb survivors and assessed the plasma levels of C-reactive protein (CRP) and interleukin-6 (IL-6), both of which play key roles in the inflammatory response. The study observed that exposure to just 1 Gy produced a 28% increase in the plasma levels of CRP (p-value of 0.0002), and a 9.8% increase in the plasma levels of IL-6 (p-value of 0.0003) [77]. The inflammatory response is a quick response of the body to infection, characterized by increased blood flow to the infected area to allow higher numbers of immune cells to reach the infection site. Inflammation, when unregulated, can damage healthy body tissue and can have pathological consequences. Even low-levels of ionizing radiation-induced inflammatory response are accepted as a risk factor for the development of both cancerous and non-cancerous diseases such as cardiovascular disease.

4.1.8. The Cardiovascular System

Cardiovascular disease is the world's leading cause of death and is of particular concern in cancer patients receiving radiotherapy to the thoracic area of the body. It is seen in breast cancer patients that a dose of <2 Gy can increase the risk for later development of radiation-induced cardiovascular disease. Results from survivors of the Chernobyl accident have shown that a dose as low as 0.15 Gy can significantly increase one's chances of developing radiation-induced cardiovascular disease [78]. The Chernobyl disaster resulted in the radioactive release of several radioactive elements, with the radioactive isotopes of iodine-131 and caesium-137 being two of the most prominent and most harmful to those exposed [79]. The Life Span Study of individuals who survived the atomic bombings of Hiroshima and Nagasaki in 1945 indicates that ischaemic heart disease and hypertension (high blood pressure) are the two most common late effects seen in survivors of the radiation exposure, and both are involved in cardiovascular disease [78]. Nuclear bombs generate high intensity fluxes of x-rays, gamma rays and neutrons, as well as other radioactive nuclei.

The International Space Station sits in the low-Earth orbit (LEO) where, whilst it is not protected from space radiation by Earth's ozone-rich atmosphere, it is protected by the Earth's magnetic field. The only humans to have travelled outside of the realms of the magnetic field are the Apollo astronauts. A 2016 study published in Scientific Reports investigated the effects of deep space radiation on astronauts in relation to cardiovascular disease. The study compared the cardiovascular disease mortality rates of astronauts who had never flown orbital missions in space, astronauts who had flown in low-Earth orbit (LEO), and the Apollo lunar astronauts. The study uncovered that the cardiovascular disease mortality rate was 4-5 times higher

in Apollo lunar astronauts than in LEO, or non-orbit astronauts. The study found that the cardiovascular disease mortality rate did not differ between low-Earth orbit and non-orbit astronauts, but that the Apollo lunar astronauts showed a significantly higher cardiovascular disease mortality rate [80]. This study by Delp et al (2016) has however been opposed by other publications such as Cucinotta et al. (2016) who challenged the publication and highlighted downfalls in the methodology of the study [81]. Elgart (2018) investigated the excess risk of cardiovascular disease mortality from space radiation exposure, and found no significant correlation [82].

It is interesting to investigate the cardiac abnormalities that have been observed in Apollo astronauts when considering this increased risk of radiation-induced cardiovascular disease. As is noted in section 2) Ionizing Radiation, the Apollo astronauts displayed some homeostatic disruptions including inflight cardiac arrhythmias. Cardiac arrhythmia is a condition whereby the heartbeat rate is irregular; either too slow or too fast. Throughout the Apollo 15 mission, the Lunar Module Pilot showed arrhythmias whilst the Command Module Pilot did not. The Lunar Module Pilot showed abnormal cardiac behaviour after docking with the Command Module Pilot. Firstly, at 178 hours Ground Elapsed Time (GET), there were five premature ventricular contractions experienced by the Lunar Module Pilot in just 30-seconds. Premature ventricular contractions occur when the heartbeat is initiated by the wrong “pacemaker.” A pacemaker is a structure of the heart involved in regulating the timing of the heartbeats. Premature ventricular contractions are induced when the Purkinje fibres initiate the heartbeat instead of the sinoatrial node, which is the normal pacemaker of the heart. A single premature ventricular contraction is not considered to be dangerous, but when they become frequent, they are of higher concern and can lead to arrhythmia-induced cardiomyopathy. Cardiomyopathy is a disease that damages the heart muscles and impedes the ability of the heart to pump blood. Later at 179 GET, the Lunar Module Pilot showed a very sudden onset of a nodal bigeminal rhythm, an abnormal or “off-beat” heart rhythm. Prior to the onset of the bigeminal rhythm, the Lunar Module Pilot’s heart rate peaked at 120 beats per minute. The heart rate then slowed to 95 beats per minute immediately preceding and during the arrhythmia [14]. A normal resting heart rate for an adult is between 60 to 100 beats per minute.

Different types of radiation are observed to instigate different biological effects in many tissue types, including the cardiovascular system. HZE particles (abundant in space radiation) play a role in altering gene expression which can impair cardiovascular function and induce harm. Exposure to HZE particles is also shown to impair the production of new blood vessels, the physiological process of angiogenesis. Studies have observed these effects by HZE particles to be potent at low-to-moderate doses exposures. Neutrons are shown to damage

cardiovascular tissue more severely than ground-based gamma rays. High-LET particles (such as alpha rays, protons and neutrons) are shown to induce damage to endothelial cells which can trigger the immune system's inflammatory response. Inflammation is an effective method of fighting off infections, but when it is not needed, it can cause damage to human tissue. Thus, this can lead to the subsequent development of radiation-induced cardiovascular disease if cardiac tissue is damaged. Immune cells in the inflammatory response commonly utilize reactive oxygen species as a means of killing infectious microorganisms. One of the main factors in radiation-induced damage to the cardiovascular system is oxidative stress. This has led scientists to propose a diet rich in nutrients that counteract oxidative stress, as a preventative- and counter-measure of radiation-induced cardiovascular disease. For example, nitrate, nitrite (both from green vegetables) and nicotinamide riboside (from milk and yeast-derived foods) facilitate the production of nitric oxide which can counter oxidative stress, and lycopene found in tomatoes is an antioxidant nutrient with additional radioprotective properties [78]. See more on dietary mitigation strategies in section 4.

Space science and medicine are undoubtedly intertwined. It is difficult to study the effects of space radiation on astronauts without comparison to the effect of radiotherapy on cancer patients. The Childhood Cancer Survivor Study followed a group of adults who received radiotherapy treatment for childhood cancer between 1970 and 1986, and survived at least five years after the treatment. The study reported that patients who had received radiotherapy to the chest had a significantly increased risk of developing illnesses such as cardiovascular disease and cerebral infarction (stroke). It was also reported in the study by Marmagkiolis et al. (2016) that for patients who underwent radiotherapy between 1960 and 1995, cardiovascular disease was responsible for 9-16% of mortality [83]. Hodgkin's disease is a cancer of the lymphatic system, and is commonly treated with radiotherapy. Specifically, Hodgkin's disease can be treated by external beam radiation therapy methods such as conventional radiotherapy and intensity-modulated radiation therapy (utilizing X-rays and gamma rays), but proton radiotherapy is becoming more common [84]. Following patients who received radiotherapy for Hodgkin's disease between 1960 and 1998, 10% clinically presented with apparent coronary artery disease at a median time of 9 years following radiotherapy, and 6.2% clinically presented with significant valvular dysfunction at a median time of 22 years following radiotherapy [83]. Both are involved in the development of cardiovascular disease.

4.1.9. The Pulmonary System

Over the next couple of decades, there are plans to try and land the first humans on Mars. The NASA Artemis missions aim to establish sustainable crewed exploration of the Moon by the end of the 2030s in

preparation to later send astronauts to Mars. The Martian surface poses many environmental threats to human health, including its high radiation levels and the Martian soil. Martian soil contains high levels of perchlorate. Perchlorate compounds are toxic to humans, particularly to the thyroid gland, however; some bacterial lifeforms have shown developed tolerance to perchlorates [85]. There have even been perchlorate-reducing bacteria discovered such as species of the *Dechloromonas* genus and *Wolinella succinogenes* [86]. The Martian surface sees irradiation by high levels of UVB and UVC, the more dangerous ultraviolet rays that the Earth's surface is predominantly protected from by ozone. Perchlorate irradiated by the high UV levels of the Martian surface can result in the production of increasingly more dangerous chemicals including hypochlorite and chlorite, which were shown to be lethal to the previously described perchlorate-tolerant bacterial cells [85]. Martian soil is of particular concern for the pulmonary (lung) health of astronauts due to its hazardous chemical composition, fine dust particles, and interactions with UV radiation.

A study by Lam et al. (2008) exposed laboratory mice to low and high doses of Martian soil simulant, with follow-up examinations either 7 or 90 days post-exposure. The low dose of Martian soil simulant was 0.1 mg/mouse, whilst the high dose was 1 mg/mouse. The examination that followed 7 days after the exposure showed observations of mild fibrosis (scarring) at various points throughout the mouse lungs, as well as particle-laden macrophages. Macrophages are immune cells that function in phagocytizing pathogens, and the lungs have their own macrophages called alveolar macrophages. The examination that took place 90 days following Martian soil simulant exposure showed significant amounts of particle-laden macrophages, mild-to-moderate inflammation of the alveoli (the site of oxygen and carbon dioxide gas exchange), as well as inflammation surrounding the pulmonary blood vessels and bronchioles, and debris within the alveoli [87]. These are all factors that significantly reduce the correct functioning of the lungs.

Radiotherapy is commonly used to treat non-small cell lung cancer (NSCLC), which makes up around 80% of lung cancer cases. Proton therapy is shown to induce less damage to the nearby tissue such as the heart and the esophagus than standard photon therapy [88]. One of the main concerns of radiotherapy for lung cancer is the development of radiation-induced lung fibrosis which clinically manifests in the form of a dry cough, dyspnea, and severe respiratory insufficiency. Fibrosis is the laying down of scar tissue and can occur as the result of a sustained inflammatory response whereby immune cells and fibroblast cells are attempting to fight off an infection or heal an injury [89]. Scar tissue is laid down when an area is too damaged to return to healthy tissue, and impedes the ability of that organ or tissue to carry out its original function. Damaged lung tissue that is replaced by fibrotic scar tissue will not be able to provide the adequate oxygen and carbon dioxide gas exchange needed to supply the body. It has been discussed previously that radiation can induce

oxidative stress which can mimic some of the antimicrobial defenses characteristic of the inflammatory response.

A study by Oh et al. (2012) analysed the radiation-induced lung fibrosis in 48 NSCLC patients who were treated with postoperative radiation therapy (PORT), and were not receiving simultaneous chemotherapy. The radiation dose delivered to these patients was done so in typical fractionations of 1.8-2.0 Gy/day, and at a total overall dose ranging from 44 to 65 Gy. The study used some key parameters to analyse the appearance of radiation-induced lung fibrosis. 'Vf' was the fibrosis volume, and 'V-dose' was the volume of lung tissue that received more than the reference radiation dose. The results showed a significant correlation coefficient of 0.602-0.683 ($p < 0.01$) between the dosimetric parameters of the fibrosis volume and the V-dose, meaning that as the volume of lung tissue receiving the radiation dose increased, so did the level of fibrosis or scarred lung tissue. There was also a strong correlation coefficient of 0.726 ($p < 0.01$) between the mean lung radiation dose and the fibrosis volume. A main conclusion of the study was that the fibrosis volume was seen to increase continuously with the V-dose, as the reference radiation dose increased [90]. Despite these results, caution must be taken when using radiotherapy and historical radiation disaster studies to predict the health risks of space radiation exposure for astronauts. Lifestyle factors such as the presence of underlying health conditions, physical fitness, age, and history of smoking cannot be ignored in terms of their potential influence [91].

4.1.10. The Integumentary System

The integumentary system of the body refers to the skin as well its attached hair and nails. In other animals, it includes appendages such as feathers, fur, scales and hooves. The integumentary system functions in providing a protective barrier between the body and the outside environment. For example, the skin provides a barrier to pathogenic microorganisms. The top layer of skin (the epidermis) is composed of dead cells that microbes cannot infect and that shed regularly. Additionally, the presence of keratin and fatty acids on the skin create a dry and acidic environment that is unfavourable to many pathogenic microorganisms. The skin has many other roles but notably, in humans, the skin is important for allowing the body to synthesise vitamin D. Vitamin D is made through interactions of ultraviolet radiation with compounds in the skin such as 7-dehydrocholesterol. The skin thereby provides a large surface area for exposure to ultraviolet rays from sunlight and greater vitamin D synthesis. Vitamin D is required for healthy bones and other body tissues. Whilst exposure to UV radiation is useful in vitamin D synthesis, it is also a significant risk factor for skin cancers.

Skin cancer is one of the most highly prevalent forms of cancer with over 3.5 million cases diagnosed in the U.S.A. every year. On Planet Earth, our ozone-rich atmosphere absorbs most of the harmful ultraviolet radiation and prevents it from reaching the surface. The much greater UV radiation exposure that would accompany interplanetary space travel and Mars exploration poses a threat to astronaut health. There are three main types of skin cancer including basal cell carcinoma, squamous cell carcinoma, and melanoma. Both basal cell carcinoma and squamous cell carcinoma arise from keratinocytes (skin cells that produce keratin) and are less invasive and aggressive than melanoma. Melanoma arises from melanocytes (skin cells that produce melanin pigment) and is the most aggressive form of skin cancer, being responsible for the majority of skin cancer deaths. Melanoma is more harmful as often it has already metastasised to other parts of the body (such as the brain or bones) by the time it is clinically presented. The risk of developing any of the three forms of skin cancer increases dramatically with UV radiation exposure [92]. An individual's risk of developing melanoma can be tripled with just one sunburning incident every two years.

UV radiation exposure can cause a variety of genetic mutations that contribute to skin cancer. Basal cell carcinoma can be caused by mutations of the *PTCH1* and *PTCH2* genes, which lead to the activation of transcription factors, as well as genes that promote cell proliferation and angiogenesis (blood vessel formation) [93]. Squamous cell carcinoma is commonly accompanied by mutations of the p53 tumour suppressor gene. Brash et al. (1991) report the evidence that such p53 mutations are induced by UV exposure, as the mutation induced involves two cytosine bases being replaced by two thymine base pairs. This is a specific mutation attributed only to the action of UV radiation [94]. The most common mutation associated with melanoma is a mutation of the *CDKN2A* tumour suppressor gene. A mutation of the *CDKN2A* gene can lead to uncontrolled cell proliferation. Monzon et al. (1998) report that in families with a genetic predisposition to melanoma, 20% have *CDKN2A* gene mutations [95].

Considering that on Planet Earth (with an ozone-rich atmosphere to absorb a lot of the harmful UV radiation) we still have such high rates of skin cancer, one has to assess the risks for astronauts travelling to Mars which has an atmosphere less than 1% the thickness of Earth's. Kim et al. (2006) discuss the risk of skin cancer for future astronauts partaking in missions to the Moon and Mars. The risk of UV-induced skin cancer is significant in areas of the body that experience more sunlight exposure such as the face and hands [96]. The risk is increased in individuals with fair skin accompanied by an inability to tan, red or light-coloured hair, and freckles. This is due to an associated lack of the melanin pigment that produces the colour in darker-skinned individuals [97]. There are a variety of hardware mitigation strategies that would allow for the blocking of UV radiation exposure, however, this would be likely to impact vitamin D levels in astronauts as well and

so would lead to another health consideration. The study by Kim et al. (2006) reports that astronauts on the Lunar surface during the occurrence of a solar particle event could have greatly increased risks of skin cancer development. The study also evaluated radiotherapy cases, with a study of patients with tinea capitis (fungal infection of the scalp) treated with radiation therapy who received around 0.1 to 0.5 Gy (X-rays) to the face and neck region. There was found to be a strong correlation between the ionizing radiation exposure and the development of basal cell carcinoma in these patients [96]. Ionizing radiation exposure has also been observed to induce hair loss and skin erythema (reddening of the skin) in cancer patients [33].

Mao et al. (2014) [98] analyzed numerous skin samples from female C57BL/6 mice after that they were launched in space for 13 days inside animal enclosure modules (AEMs). Several genes involved in reactive oxygen species (ROS) metabolism were upregulated (Als2, Cat, Fmo2 and Noxa1). Also, there was an alteration in the quantity of genes responsible for antioxidant defense, like Ehd2, Prdx5, Ptgs2 and Gsr (Glutathione reductase - see DNA damage section). Also, genes involved in extracellular matrix remodeling were analyzed and 11 of them appeared upregulated while 4 of them appeared downregulated. In particular, the gene coding for collagen II alpha-1 was downregulated while collagen IV alpha-1 was upregulated. At the same time researchers found an increase in many integrins, MMP15 and Timp3, the inhibitor of metalloproteinase 3. Also, MMP15 belongs to the family of the membrane-type metalloproteinases (MT-MMP) whose upregulation is a typical trait of several human cancers [98].

Su et al. (2010) [99] created a 3D skin model system to conduct simulations of exposure to ionizing radiation and to assess the consequent DNA damage. For the experiment, scientists used MCR5 cells (lung fibroblasts) and Human EpiDerm, a skin model with only primary keratinocytes, and EpiDermFT, which contains fibroblasts too. These tissues were irradiated with a Cs-137 radioactive source delivering a dose of 0.82 Gy/min. This is the first example of a 3D artificial skin which appeared to be good in order to conduct radiation experiments for astronauts. The potential damage to the skin through increased exposure to UV and other types of ionizing radiation is a concern for astronauts and showcases the need for further research in this area.

4.1.11. The Reproductive System

Oglivy-Stuart et al. (1993) outlines some of the key effects of irradiation on the reproductive system in humans. In biological males, aspermia (lack of semen in an ejaculation) can result from direct exposure of the testis to a radiation dose of >0.35 Gy, and aspermia can become permanent if the radiation dose is >2 Gy. At a considerably higher dose of >15 Gy, the production of testosterone by Leydig cells can become impaired.

In biological females, direct irradiation of the ovaries with a dose of 4 Gy may cause 100% incidence of sterility in women over 40 years of age, and 30% sterility in younger women [100]. The reproductive glands, or gonads, can be directly affected by irradiation of the abdomen, pelvis, spinal cord or testicles in radiotherapy. Cranial irradiation, such as in the treatment of a brain tumour via radiotherapy, has the potential to damage the hypothalamic-pituitary axis which has multiple consequences including unusually early occurrence of puberty (precocious puberty), unusually high levels of prolactin in the blood (hyperprolactinemia), and deficiency of gonadotropin (hormones that act on the reproductive glands). Deficiencies of the pituitary gland are also observable following the irradiation of nasopharyngeal tumours, likely as a secondary result of damage to the hypothalamus. There are many interactions of the hypothalamus and pituitary gland that are crucial to the proper functioning of the male and female reproductive systems [100].

Radiotherapy to the cranio-spinal, abdominal, or pelvic regions in women can have consequences on fertility and pregnancy. Wo et al. (2009) reported a dose-dependent relationship between ovarian radiotherapy and a premature onset of menopause. Those undergoing radiotherapy of the cranio-spinal region had consequent impairment of hormonal regulation which led to difficulty becoming pregnant later in life. Those undergoing radiotherapy to the abdominal or pelvic regions showed the consequences of birth abnormalities such as uterine and placental abnormalities, early labor, low birth weight and miscarriages [101]. Norwitz et al. (2001) reported the case of a 23-year-old woman who experienced uterine rupture at 17-weeks gestation after a history of receiving whole body irradiation therapy for treatment of childhood leukaemia. At 17-weeks gestation, after the woman reported acute abdominal pain, a pathological examination showed an atrophic (wasting away) uterus and a myometrium that had thinned to about 1-6mm, being completely absent in some areas. The study hypothesized that the prior radiation therapy the woman had experienced as a child had led to uterine injury and subsequent thinning of the myometrium. The woman also showed clinical signs of placental percreta, an abnormal condition where the placenta implants deeply into the uterine wall and is not delivered normally at childbirth, which can be life-threatening. The post-pubertal uterus is a relatively radiation-resistant organ in adult women, but the study reports that high-dose rates of radiation exposure in childhood can cause irreversible injury to the uterine musculature and vasculature [102].

4.1.12. The Digestive System

The gastrointestinal (GI) system, composed of various organs and an associated microbiome, can be severely affected after exposure to ionizing radiation. The resulting adverse effects depend on both the dose and the organ involved. Doses as low as 1 Gy can diminish gastric motility (with delayed gastric emptying) and,

in some occasions, induce sphincter incompetence, late suppression of gastric acid secretion, and release of neurohumoral factors and histamine which contributes to diarrhea [30]. One of the organs with moderate radiosensitivity of the GI system is the stomach, which sustains doses of up to 40 Gy without severe secondary complications. Adverse effects occur with doses greater than 45 Gy where the risk of developing ulcerations, perforations, and obstructions increases to 25-50% of cases, for exposures between 55 Gy and 64 Gy this percentage can grow to almost 63% of cases. The ulcerations appear after a month of exposure and present with symptoms such as intractable nausea, pain, vomiting, and hematemesis (vomiting of blood, which may be red or have an appearance similar to coffee grounds [103]) [50].

The intestine represents a particular interest as it is the portion most sensitive to radiation. Injury of the small intestine gives rise to more acute and long-term suffering and risk of death than any other abdominal viscera. Intestinal radiation toxicity is classified as acute (early) or chronic (delayed). Acute toxicity occurs during or within three months with a cumulative dose to 45 Gy or daily doses between 1.5-2.0 Gy (5-day week schedule). It leads to epithelial injury, resulting in the breakdown of the mucosal barrier and mucosal inflammation (intestinal mucositis). The clinical presentation includes vomiting, abdominal pain, and diarrhea. It occurs in 60-80% of patients who receive intraabdominal or pelvic radiotherapy [50][104]. After treatment with high daily radiation fractions of 25-30 Gy, chronic toxicity begins. Some characteristics of the internal intestinal compartments change, generating mucosal atrophy, intestinal wall fibrosis, and vascular sclerosis manifested in malabsorption syndrome, dysmotility, transit abnormalities, vitamin B12 deficiencies, diarrhea, weight loss, and acute or intermittent small bowel obstruction [64][65]. Higher doses, like 50-60 Gy, can lead to Chronic Radiation Enteritis, and symptoms are similar to 25-30 Gy doses. In both cases, it can appear from 6 months to 20 years after radiotherapy or ionizing radiation exposure [105] [104].

Ionizing radiation is also known as a risk factor for colorectal (CR) cancer due to a higher incidence of pre-malignant lesions, such as colonic polyps, after radiation exposure. Some NASA projects have tried to estimate the risk of space radiation-induced intestinal tumors. For example, a study by Fornace et al. (2008) employed the adenomatous polyposis coli (APC) (a mouse model used to demonstrate radiation-induced intestinal cancer). They studied survival and the progression of colon cancer after full body exposure of APC mice to a simulated Solar Particle Event (SPE) with varying energies using a total dose of 2 Gy over 2 hours. For reference radiation exposure, they used 2 Gy of monoenergetic proton and X-ray at a dose rate of 20 cGy/min. As a result, the SPE stimulation induced an increase percent number of polyps (A polyp is defined as any mass protruding into the lumen of a hollow viscus [106]), and invasive adenocarcinomas (a malignant epithelial tumor with a glandular organization [107]) compared to reference radiation exposure.

These findings suggest that exposure to low dose rate SPE protons has significant biological effects that may have functional consequences on colon cancer progression [108].

Another study carried out by Shubhankar et al. (2017) evaluated intestinal and colon tumorigenesis in male and female APC mice exposed to different doses (10 or 50 cGy) of energetic heavy-ion radiation (^{56}Fe or ^{58}Si) and monitored 150 days after radiation exposure. Intestinal tumorigenesis and intestinal tumor size in male and female mice was similar for both radiation types for high and low dose rates tested. Colon tumor frequency in male and female mice after high and low dose rate energetic heavy ions was also not significantly different. In conclusion, intestinal and colonic tumor frequency and size were similar, suggesting that carcinogenic potential of energetic heavy ions is independent of dose rate [109].

The human microbiome is the collection of microbes that live in and on our bodies, and it plays an essential role in health [110]. As previously mentioned, the GI tract has a microbiome associated; it includes viruses, archaea, fungi, protists, and the main population of bacteria. The GI microbiome in each individual has vital functions, which includes production of vitamins, carbohydrate fermentation, absorption of nutrients, and the suppression of pathogenic microbial growth creating a more hostile environment [111] [112]. It also has connections to other body systems, including the digestive system, immune system, endocrine system, and, notably, the nervous system where it's in the gut-brain axis. This axis has an influence on a multitude of factors and disorders, including cognition and mental health [113].

Dysbiosis is the disturbance and imbalance of the GI microbiome's regular composition. It can occur after diet changes, enteric infections, antibiotic treatment, and radiation exposure [112]. Dysbiosis triggers the release of pro-inflammatory cytokines that eventually aggravate mucosal damage. It also seems to be associated with several gastrointestinal diseases, systemic conditions such as Type I and II diabetes, autoimmune disorders, neurodegenerative diseases, obesity, and psychiatric episodes [113][112].

A study in fecal samples from 19 rhesus macaques, *Macaca mulatta*, exposed to 7.4 Gy cobalt-60 gamma-radiation evidenced significant differences in the microbiome populations four days after irradiation. Ten animals demonstrated diarrhea after these days, revealing an increase in *Lactobacillus reuteri*, *Veillonella* sp. and *Dialister* sp., and a decrease of *Lentisphaerae* and *Verrucomicrobia* phylum and *Bacteroides* genus in comparison with non-diarrhea animals. These differences show the potential association between the prevalence of microbiomes and differential susceptibility to radiation-induced diarrhea [114]. Studies on radiotherapy patients have also evidenced variations in microbial populations, and in some cases, the most considerable changes could be associated with episodes of post-irradiation diarrhea [112].

The spaceflight environment comprises several factors that can influence the GI microbiome, including

microgravity and radiation [113]. An investigation carried out at the International Space Station (ISS) evaluated if the microbial communities of the GI tract, skin, nose, and tongue changed in nine astronauts during a six month mission. As a result, the main differences occurred in the GI tract. The researchers identified relative abundance and the acquisition or loss of bacteria species, besides the increase of some pro-inflammatory cytokines. On the other hand, nose, skin, and tongue microbiome composition presented fewer changes, and these can be linked to astronauts' hygiene habits. All the variations occurred very early during the space mission, and were maintained for at least 60 days after the return to Earth [115]. These results are consistent with the NASA twin study. For this study, they compared a pair of identical twin astronauts from NASA, one of them spent 340 days in the ISS, and the other stayed on Earth. After this period, they evaluated changes in telomere length, gene regulation, gut microbiome composition, body weight, carotid artery dimensions, subfoveal choroidal and retinal thickness, serum metabolites, immune response and cognitive performance [116]. A paper by Siddiqui et al. (2020) suggests that space radiation is responsible for the gut microbiome alterations in astronauts since radiotherapy patients present similar symptoms after acute radiation exposure [117].

4.2. The Impact of Ionizing Radiation on the Genetic Material

4.2.1. Reactive Oxygen Species

Several oxidative events are prone to happen in human cells after exposure to ionizing radiation. The main biological consequences occur as a direct effect of electromagnetic waves on the cellular genetic information or due to the ionizing radiation-induced radiolysis of water [118], the substance that represents the majority of the intracellular environment [119]. There is also scientific evidence of specific mtDNA mutations linked to the alteration of the cellular oxidative metabolism causing a rise in ROS production [120][121]. Water is able to produce different reactive species when lysed by ionizing radiation and, considering an aerobic cellular environment in conditions of a physiological pH, the most relevant chemical compounds are O₂⁻, OH, and H₂O₂ (H₂ tends to evaporate and does not have the same dangerous effects of the other cited chemical species) [118]. The combination of ROS, other organic radicals and molecular hydrogen may lead to the synthesis of peroxides, responsible for lipid peroxidation. Ionizing radiation may also activate NO synthases (NOS) [122] which produce nitric oxide, a chemical compound capable of interacting with superoxide radicals in order to produce peroxynitrite groups capable of interacting with other intracellular targets [123]. ROS and RNS are often produced by activated M1 macrophages that make use of these chemical species in order to destroy pathogens, especially during chronic inflammations. There is strong

evidence that chronic inflammations may lead to the onset of several human tumours [124][125] and, for this reason, the oxidative and nitrosative burst caused by ionizing radiation may represent a risk factor for cancer (discussed further in the cancer risk section).

In 1972, Harman proposed that mitochondria may represent a biological clock because they tend to accumulate genetic mutations, a process also accelerated by the relatively close distance from the Electron Transport Chain (ETC) [126]. mtDNA mutations can disrupt the structure of ETC complexes in the external mitochondrial membrane causing an undesired electronic leakage responsible for the conversion of O₂ into O₂⁻, especially considering complexes I and III. A well-known mtDNA mutation is called Common Mutation (CD), consisting of a 4.977 bp deletion that affects the genetic information for 5 different tRNA and several subunits of complexes I, III and IV [127]. There is evidence that CD can be induced by ionizing radiation [128] and, using minor doses of EM waves, other genetic alterations have been observed (e.g. 4934del). An important substance involved in the cellular redox homeostasis is glutathione (GSH), a tripeptide composed by glutamic acid, cysteine and glycine. The enzyme glutathione peroxidase uses GSH as coenzyme in order to convert a peroxide group in water and alcohol ($2 \text{ GSH} + \text{ROOH} \rightarrow \text{GSSG} + \text{ROH} + \text{H}_2\text{O}$). For this reason, usually the ratio 2GSH/GSSG is used in medical biochemistry in order to evaluate the redox potential of the considered cell. Also, GSH participates in several biological processes like the metabolism of sulphur-containing amino acids, the reduction of disulphide linkages and the stabilization of ROS and RNS. An important research study [129] led by Shimizu et al. (1998) demonstrated the protective role of glutathione on the irradiated right hemiserebrum of white rabbits. Results showed that ionizing radiation causes an increase in the levels of GSH and γ -glutamylcysteine synthetase (γ -GCS). For the experiment, X-rays with a dose rate of 3 Gy/min were used in order to irradiate the whole right hemiserebrum. With an intrathecal injection, S-methyl GSH (15.6 $\mu\text{mol/Kg}$) and buthionine sulphoximine (2.3 $\mu\text{mol/Kg}$), an inhibitor of γ -GCS, were administered in 400 μL of isotonic saline. After six hours from the administration and the exposure to radiation, brains were removed and then examined. The quantitative method to assess DNA damage was analysing the levels of 8-OHdG with HPLC and, with a 20 Gy dose, a peak was observed 3 hours following irradiation. Also, 8-OHdG seemed to be proportional to the radiation doses:

Normal control = 5.00 ± 3.12 fmol/mg DNA

5 Gy = 10.5 ± 0.13 fmol/mg DNA

10 Gy = 21.83 ± 0.13 fmol/mg DNA

20 Gy = 31.85 ± 3.92 fmol/mg DNA

A radiation dose of 20 Gy resulted in a 173% increase in GSH levels in the irradiated hemicerebrum and a similar, but lesser increase was observed in the non-irradiated left hemicerebrum. A Northern Blot was conducted in order to analyse the quantity of gamma-GCS mRNA and the results showed an impressive increase 6 hrs following exposure to 20 Gy radiation (6600 ± 950 vs. 2200 ± 140 PSL, that is photostimulated luminescence). Finally, treatments only with S-methyl GSH 6 hrs following 20 Gy of radiation resulted in a 31% decrease in the formation of 8-OHdG while treatments only with BSO resulted in an increase of 8-OHdG by 193%.

4.2.2. DNA Damage

As previously discussed, astronauts are constantly exposed to ionizing radiation (IR), and this radiation can lead to several impairments of the human physiological systems. Regarding the cellular level, the type (high-LET or low-LET radiation) and energy of IR critically affects how the DNA is damaged. This in turn may influence the cell's survival and the means by which the damaged DNA is repaired. IR leads to breaks in the DNA, and these breaks can occur either directly or indirectly [130]. DNA breaks are produced indirectly by low-LET radiation (gamma rays and X rays), which distributes its energy in random motion around the DNA [131], splitting nearby water molecules, and creating hydrogen and reactive oxygen species (ROS). These highly reactive species may react with nearby DNA, producing closely opposed single-strand DNA breaks (SSBs). These lesions are referred to as "clustered damage." W.J. Cannan and D.S. Pederson defined these lesions in their review as more than a single DNA lesion, created by a single track of radiation, that reside within one or two helical turns of DNA. Low or high LET radiation doses as low as 1 Gy (100 rad) can produce clustered lesions. Monte Carlo-based modeling of radiation tracks suggests that low and high LET radiation can generate, respectively, up to 10 and 25 lesions per damage cluster [n]. It is today believed that SSB are firstly independently created and then they happen to locate themselves in the same site on complementary strands, generating a DSB [131]. The ROS generate additional DNA damage, including oxidized bases and sites of base losses [130].

High LET radiation is a particular risk for astronauts traveling beyond the protection of the Van Allen radiation belts, and also to cancer patients treated with heavy ion radiation therapy. This radiation deposits energy much more densely and leads to direct DNA damage with greater complexity, potentially in greater amounts per unit dose, which the cell finds more difficult to repair [131]. Direct DNA damage entails a collision between a high-energy particle and a strand of DNA, breaking the phosphodiester backbone which induces DSB, this leads to fragmentation of the molecule and gives rise to structural chromosomal aberrations

[132]. DSB are the most genotoxic events that can happen to the genetic material [133]. In fact, usually the DNA repair system uses the complementary strand in order to insert the correct bases but after a DSB the information is missing on both strands. Cells react to these genetic lesions with Holliday's junctions or the NHEJ system whose aberrant action has already been reported several times in cancerous cells. These mechanisms are highly mutagenic and they may be responsible for the onset of genetic mutations causing diseases like cancers.

Considering the previous image, showing the frequency and the number of DSB derived by a simulation with 10,000 100-MeV proton beams, the energy of the colliding particles is so high that in literature there is evidence that they may cause non-random DSB, less than 25 per considered cluster. Astronauts that stay in the terrestrial atmosphere are partially protected by the Van Allen Belt while astronauts who travel beyond may be exposed to higher doses of ionizing radiation, increasing the cancer risk too [134]. According to a study published in 2000 by Dahm-Daphi et al. (2000), the number of DSB caused by ionizing radiation increases linearly with radiation in a range of several hundred Gy [135]. When a DSB is created in human cells, a molecular complex, called MRN, binds to it and facilitates the activation of ATM. It autophosphorylates allowing the activation and the consequent phosphorylation of many targets in the surrounding chromatin [136]. An important pattern found in many early DSBs is the phosphorylation of the histone variant H2AX (also called γ -H2AX). When DDR (DNA Damage Response) proteins accumulate in the damaged sites, the formation of foci (also called IRIFs, Ionizing Radiation-Induced Foci) starts [137]. Usually the biomolecular pathways started by DDR proteins lead to the cell cycle arrest in G1/S or G2/M. Mammalian cells make use of two major pathways in order to repair DSBs, that are NHEJ and HR.

In the 1970s sucrose gradient sedimentation was used to measure DSBs in irradiated mammals [138] and was substituted by some electrophoretic protocols in the 1980s (e.g. PGFE and Comet Assay). Today, thanks to the advancements in genomics, it is possible to determine the non-random distribution of IR-induced DSBs across the genome, evaluating the heterogeneous cell response too. Since proteins must accumulate in order to be detected, NHEJ is really difficult to highlight because its proteins are usually expressed and only 1-2 additional proteins are necessary to repair a DSB. Instead, HR can be detected thanks to the accumulation of proteins like RAD51, RAD52 or BRCA2 but it is not useful for non-cycling cells and makes up only 15% of total DSBs. FRAP (fluorescence recovery after photobleaching) can be used to get information about the mobility and the binding rates of recruited proteins on DSBs. Also, it is possible to create miniaturized classic antibodies called scFvs (single-chain variable fragments) that consist of the variable regions of heavy and light chains linked to a peptide. Recently a phosphospecific scFv was created in order to detect IRIFs

in living cells [139]. Using the CHO-K1 cell line and 1.0 Gy of 200 kVp X-rays [140], Mori et al. (2018) managed to deduce the induction probability density of DSBs based on the measured DNA amount and the calculated dose per nucleus. This research takes into account the different phases of the cell cycle and the variation of DNA quantity were analyzed via PI staining. Also, researchers analyzed the plateau and the logarithmic phase of the growth curve in the CHO-K1 cell culture. The number of IRIFs was estimated via fluorescence microscopy and flow cytometry, analyzing the presence of γ -H2AX with fluorescent primary antibodies, and a Monte-Carlo simulation was then conducted in order to calculate the distribution of energy deposition per nucleus, deducing the DSB number per nucleus.

A control group of CHO-K1 cells was cultured in order to deduce the background of DNA damage and the cell cycle distribution. In the Monte-Carlo simulation, to obtain the probability density of the number of DSBs per nucleus, the number j was assigned to each cell and DSBs can be approximated by the following formula:

$$DSB_j = k \times Dose_j \times DNA_j \times BG_j$$

Where k is the DSB induction yield (~ 30 [1/Gy/cell]), $Dose_j$ is the absorbed dose imparted to the nucleus [Gy], DNA_j is the relative DNA amount and BG_j [1/cell] represents the number of DSB $_j$ before the irradiation. These two last parameters are derived from the quantitative analysis of the CHO-K1 cell control group. Also, to analyze the dependence of DSB induction on cell cycle, two conditions were created:

Plateau phase = 78.9% G0/G1, 12.6% S and 8.48% G2/M;

Logarithmic phase = 32.4% G0/G1, 56.9% S and 10.7% G2/M;

The energy deposition for cell nucleus gave a Gaussian distribution with a peak at 1 Gy and a standard deviation of 0.22 Gy (plateau) and 0.23 (logarithmic). For the non-irradiated group the number of foci by microscopy was 8.07 ± 10.45 while for 1.0 Gy irradiated group was 39.82 ± 18.51 . The number of samples are respectively 1.0×10^5 and 2.0×10^5 . When it comes to BG_j , the distribution of the background DSB number per cell nucleus has two peaks through the analysis of DNA profile in the logarithmic growth phase: the lower is mainly composed of G1 and G2/M cells while the higher one was composed of S cells. According to their experiment the median value of DBS per cell was 37.31, the lower and upper quartile values were 30.53 and 46.64 for the plateau phase and 52.58, 41.98 and 66.14 in the logarithmic phase. The cited model strongly agrees with the experimental data for both the plateau and logarithmic growth conditions. New forms of quantitative analysis of DSBs have been developed. Li et al. (2011) created [141] a γ -H2AX/MDC1-luc 2

reporter gene inserted in lentiviral particles and vehiculated to cancer cells in order to determine the number of DNA breaks. The H2AX and BRCT domain of MDC1 were respectively fused at the N-terminal and C-terminal of the firefly luciferase, which was therefore separated in half. When a DSB occurs, H2AX is converted into γ -H2AX and, by interacting with MDC1, the two halves of the luc 2 enzyme are brought together, reconstituting the luminescent protein. To test the reporter gene, they exposed cells with different doses of ionizing radiation and a clear dose-dependent response in reporter activities was found.

Ionizing radiation exposure caused a rapid activation of the reporter within 30 minutes of exposure but after 24 hours, thanks to the successful response of DSBs in the irradiated cells the activation dropped significantly. Surprisingly, after 24 hours, the reporter activity started to grow again reaching a peak at around day 5, and dropping again after day 12. It has been hypothesized that this second wave of reporter gene activation may be related to irradiated cell apoptosis (programmed cell death), during which whole strand breaks are routinely generated and γ -H2AX-MDC1 interactions could occur. Also, this period overlaps with an increase in caspase 3 and PARP levels, supporting the apoptotic theory. Anyway, it cannot be excluded that it may represent a symptom of a persistent genetic instability found in cells after exposure to ionizing radiation. The main objective of this reporter system was evaluating the number of DSBs in vivo in intact tissues. Its function was studied on tumor xenografts in nude mice and the irradiation was a single dose of 6 Gy.

4.3. The Impact of Ionizing Radiation on Cancer Risk

The day-to-day life on Earth exposes us to different types of radiation than what astronauts in the International Space Station (ISS) are exposed to. Francis A. Cucinotta compares the induced cancer risk from exposure to galactic cosmic rays containing HZE ions, to that from exposure to ground-based radiation including X-rays and gamma rays [142]. HZE ions are high-energy nuclei present in galactic cosmic rays. Much of the oncological effects of HZE ions are unknown due to there being no human data available. Astronauts in low Earth orbit (LEO) undergo exposure to galactic cosmic rays, as will future astronauts embarking on interplanetary space travel, making the development of this knowledge critical. Whilst there is no human data, animal studies have been carried out on tumours in mice and rats to analyse the tumours induced by HZE ions. Results have shown that tumours induced by HZE ion exposure have higher rates for becoming metastatic (spreading throughout the body), and also show an increase in the tumour grade [142]. Tumour grading is a process used in medical pathology to describe the observed cell abnormality and growth rate deviations of the tumour, to define how dangerous the tumour is overall. Exposure to HZE particles has been observed to result in the production of reactive oxygen species, inflammation, and impairment of DNA

signalling pathways, all of which play a role in cancer development [143]. These experiments also show that tumours induced by HZE ions are more lethal in terms of increased initiation and promotion of the tumour in comparison to ground-based gamma rays [142].

Cucinotta discusses the radiation exposure limits set by NASA to protect astronauts from increased cancer risk; “NASA’s radiation limits sets a 3% cancer fatality rate as the upper bound of acceptable risk and considers uncertainties in risk predictions using the upper 95% confidence level of the assessment.” [142]. Cucinotta also carried out mathematical analysis of the cancer risks experienced by astronauts in low Earth orbit, such as in the ISS. The analysis led to a major finding that female astronauts could exceed NASA’s radiation-induced cancer mortality limits after just 18 months in low Earth orbit (i.e. the ISS), and male astronauts may exceed these same limits in 24 months. Female astronauts are expected to exceed the limit in a shorter time period due to an on average lower body mass, and the presence of a number of female-specific cancers including breast cancer, ovarian cancer, and uterine cancer [142]. As with cardiovascular disease, Elgart et al. (2018) did not observe an excess risk of cancer mortality in early NASA astronauts from radiation exposure [82]. Barcellos-Hoff et al. (2015) discuss how the accuracy of predicting astronaut cancer risk from radiation exposure is limited by a lack of understanding of how space radiation could induce cancer growth [144].

Other factors play a role in the cancer risk following radiation exposure. Tore Straume discusses how age influences radiation-induced lifetime cancer risk in the Handbook of Cosmic Hazards and Planetary Defense. The radiation-induced risk of developing cancer is shown to decrease with age due to the latency period of cancer which can be two decades or longer. A younger individual exposed to radiation has more remaining lifetime for the resulting cancer to develop, whilst an older individual is likely to present a different competing fatal-health condition before the radiation-induced cancer develops. Straume also discusses the 3% radiation exposure induced death from cancer career exposure limit set by NASA, and reports on estimates of how long astronauts could embark on interplanetary space travel before exceeding these limits: “Assuming 20 g/cm², A1 shielding and average solar minimum conditions, the maximum duration would be about 150-200 days, not sufficient for a mission to Mars.” [145].

As has been previously mentioned, radiation-induced inflammation has the ability to instigate increased cancer risk. The experimental ultraviolet-irradiation of laboratory mice has shown the increased angiogenesis and metastasis as a result of the UV-induced inflammatory response of neutrophils [146]. Angiogenesis is the formation of new blood vessels and is essential for delivering adequate nutrients to the cancerous region to sustain its growth. Metastasis is the spread of cancer from a different part of the body from where it

started. The effects of UV radiation are of particular interest for future Mars missions considering the lack of a protective ozone layer on the red planet [147]. This UV-induced angiogenesis and metastasis was particularly observed in melanoma cells. Melanoma is a type of skin cancer derived in the melanocytes (pigment-producing cells of the skin) [146]. Advanced angiogenesis and metastasis are both characteristic of more pathological and life-threatening tumours. In addition with the ability of HZE particles to induce more potent tumours, the radiation-induced inflammatory response has the potential to worsen the outcome further. The radiation exposure that astronauts travelling to Mars are estimated to undergo accompanies undeniable risks for development of cancer. This shows the importance that further research is done into how we can mitigate such potential harm.

5. Radiation Mitigation Strategies

As science studies more about the severity and impact of the radiation astronauts will face in future manned missions, there is still much to learn about possible methods of minimizing both the overall exposure and biological damage. Protection from radiation for space missions gets broken up into three categories: monitoring, medical supplies, and shielding [148]. Currently, space agencies like NASA's Johnson Space Center track the severity of solar radiation in addition to the constant stream of galactic cosmic radiation [149]. Scientists are reviewing how dietary supplements, such as antioxidants, have a potential in arming the body against the damage caused by space radiation [150]. Teams are working on both passive and active shielding methods designed to absorb and deflect a percentage of particles that would otherwise harm astronauts in short and long-term doses. And while all these methods may protect astronauts on their journey to places like Mars, research is still being performed on what in-situ resources, such as Martian soil, can be used for habitat shielding while on the surface. Even though the astronauts' health is the first priority of manned space missions, what they take with them is still limited to the mass the spacecraft can carry, and ultimately the cost. While there is still so much to learn regarding the effectiveness of these and other methods studied for the protection of astronaut health and safety, it is important to take a step back and review where we are now before we can understand where we have to go tomorrow, and - more importantly - how we get there.

5.1. Radiation Environment Tracking

In order to limit the threat of radiation, the simplest method of prevention often involves tracking potentially harmful exposure levels before they reach astronauts. This involves monitoring solar particle events (SPEs)

as well as galactic cosmic radiation (GCRs) [149]. Tracking current radiation environments and accurately predicting future threats can help identify the safest times to schedule missions and send astronauts who are already in interstellar space sufficient warnings to use extra shielding [148, 149]. Solar activity fluctuates in 11-year cycles where radiation spikes occur as solar particle events more often at the “solar maximum” of the cycle [149, 151]. SPEs are relatively lower energy and typically happen during solar flares [151, 152]. NASA’s Johnson Space Center’s models for solar activity is still in the early stages of development, but the goal is to build a predictive map of when SPEs are likely to occur [149]. Galactic cosmic radiation occurs as a stream of high energy particles that is generally only affected by solar activity; for example, GCRs are generally lower during solar maximum [149, 151]. In addition to differing energy levels, the plethora of space radiation also involves different base chemicals and particles [151, 152]. These are just some of the elements that make effective space radiation monitoring both difficult and critical to space missions. Mapping the radiation environment not only helps planning and warning, but can also model astronauts’ expected dose on space missions. Predicting solar flares, more accurate mapping of the type and energy of space particles, and understanding astronauts’ long-term dosing limits are all necessary for understanding the effectiveness of all types of radiation mitigation strategies.

5.2. Medicine and Dietary Strategies

5.2.1. Probiotics

This review has presented the different pathological impacts of ionizing radiation on the physiological systems and genetic material of the human body. A potential mitigation strategy to reduce radiation-induced harm is related to the dietary use of probiotics, antioxidants and vitamins. Probiotics are defined as live microorganisms that confer a health benefit on the host when ingested in adequate amounts [153]. Previously, studies on Earth have shown that probiotics provide several benefits to human health, including competition against pathogens, treatment for dysbiosis in the GI tract, reduction of gastrointestinal distress, production of beneficial metabolites, interactions with host cells that promote immune and psychological health, and protection from infection. Some studies have shown that probiotics can help alleviate some human illnesses associated with space flight conditions, for example, on US crew space flights; there have been some reports of antibiotic-associated diarrhea (DAA) due to prescribed antibiotics for the crew [154]. A study by Ouwehand et al. (2014) demonstrates that the use of capsules with three different strains of probiotics reduces the incidence of DAA in patients receiving antibiotic treatment [155]. Cases of respiratory infections have also been reported in space crews [154]. The administration of probiotics in tablets or capsules to patients with

the same symptoms on Earth has been shown to reduce the symptoms, duration, and fever during infection [156]. Probiotics are also a promising strategy to protect our microbiome and normal tissues from radiation. On Earth, radiotherapy is one of the most common sources of IR and its human health impairments have been evaluated during and after the treatment [157]. A paper from Kumar et al. (2012) found that a diet supplemented with probiotics may have therapeutic potential to decrease the risk of cardiovascular disease on rats with induced hypercholesterolemia [158]. Therefore, a programmed regimen of probiotics could reduce the incidence of radiation-induced cardiovascular disease (RICVD) presented in this review.

Jaroslav Timko carried out a clinical trial with a group of 42 radio-oncology patients who had undergone adjuvant postoperative radiation therapy (RT) after abdominal and pelvic cancer. They were given a supplement with probiotics started on the first day and lasted until the end of the RT. At the end of the study, it was concluded that prophylactic probiotic therapy can be used in the prevention of radiation-induced diarrhea described previously [159]. An extensive review by G.L. Douglas and A.A. Voorhies presents that probiotics could help alleviate some other conditions associated with space flight, such as dermatitis, rashes, and psychological distress [154]. Despite the positive health benefits, probiotics must be carefully selected and evaluated for spaceflight based on their strain-specific benefits and relevance to likely crew conditions.

5.2.2. Antioxidants and Vitamins

Brown et al. (2010) carried out an experiment where they exposed laboratory mice of the strain C57BL/6 to a whole-body radiation dose of 8 Gy. The mice were 7-8 weeks old, and underwent the radiation exposure either on a normal diet, or a normal diet supplemented with antioxidants. The antioxidant supplementation diet included antioxidants L-selenomethionine, sodium ascorbate, N-acetyl cysteine, alpha-lipoic acid, alpha-tocopherol succinate, and co-enzyme Q10. There were distinct groups of 14-20 mice each that were started on the antioxidant diet either immediately, 12 hours after, or 48 hours after radiation exposure. The study found an overarching conclusion that in a group of 18 mice, 78% survived what would have been a lethal whole-body irradiation when on an antioxidant-supplemented diet. Antioxidants are believed to counteract the cellular damage induced by the production of free radicals and reactive oxygen species imparted by ionizing radiation [160].

The effects of two antioxidants (beta-carotene and alpha-tocopherol) on the acute side effects of radiation exposure were investigated in patients with stage I or II squamous cell carcinoma of the head and neck. Beta-carotene is a provitamin A (a substance that the body can convert into vitamin A) found in many orange-coloured fruits and vegetables including cantaloupe, pumpkin, and carrots. Alpha-tocopherols are

compounds with vitamin E activity that are sourced mainly from olives and sunflower oils. In the U.S.A., consumption of the gamma-tocopherol counterpart is more common from dietary sources including soybeans. The squamous cell carcinoma patients were divided into two groups. A group of 273 patients formed the supplementation arm, and 267 patients formed the placebo arm. All patients were over 18 years old. In the placebo group (those not receiving supplementation of B-carotene or a-tocopherol), 24.8% reported severe side effects from the radiation therapy treatment. Comparatively, only 19.2% of the group receiving antioxidant supplementation reported severe side effects. The positive protective effect of antioxidants was only observed when both B-carotene and a-tocopherol were administered, but not when a-tocopherol was administered alone. When the two antioxidants were administered in combination, the larynx was one of the most protected tissues from the side effects of radiotherapy. Common side effects of radiotherapy for the head and neck are those that affect the larynx such as sore throat and difficulty swallowing. Those patients who received the combination antioxidant treatment also reported less sleep disturbances than those patients not receiving any antioxidant supplementation [161].

Although antioxidant supplementation is shown through this study to reduce some of the adverse side effects of radiotherapy, other studies suggest that antioxidants can interfere with the efficacy of radiotherapy treatment. Patients being treated for oral cavity cancer via radiotherapy participated in a study investigating the antioxidant effects of a vitamin E rinse before and after each 2 Gy fraction of radiotherapy. The rinsing solution contained 400 mg of vitamin E. At the 2-year follow-up period, the overall survival of those patients was observed to be reduced in the group who had done the vitamin E rinse in comparison to the placebo group. This was attributed to an interference of the vitamin E with the treatment, however; an overall 36% reduction in the side effect of symptomatic mucositis was also observed [162]. This shows a requirement for clinicians to weigh up the risks and benefits of using antioxidants to prevent radiotherapy-induced harm.

Burns et al. (2007) carried out experimental models of rat skin exposure to space radiation with acute doses ranging from 0.5 to 10 Gy. Inflammation was observed to play a key role in the induction of cancer by radiation exposure. One of the main radiation types used in the experiment was iron radiation (which is an abundant component of space radiation). The researchers found that vitamin A had protective abilities against 47% of radiation-induced neoplasms (abnormal/excessive growths). Vitamin A was found to suppress the expression of numerous (80%) genes involved in the inflammatory response and thereby suppress the acute inflammatory response [163]. This research supports the importance of a high beta-carotene (provitamin A) abundance in the diet of future astronauts.

The interference of antioxidants with radiotherapy is not of much concern for the safety of astronauts, who are

presumably not being treated for cancer whilst in spaceflight. The protective effects of antioxidants against radiation damage are of higher interest for space travel science. It is promising that a diet high in fruits and vegetables, and the utilization of antioxidant supplements could play a role in mitigating the harmful effects of space radiation on astronaut health. Using male C57BL/6J mice, it has been demonstrated that dried plums may show a radioprotective role against IR. In particular, researchers have tested the antioxidant properties of dried plums against low-LET gamma-rays radiation and a combination of protons and HZE ions, mimicking space radiation. In the simulation, after 11 days from the irradiation, mice showed a reduction in the bone loss usually induced by radiation. It has been postulated the natural polyphenols (gallic acid, caffeoyl-quinic acids, coumaric acid and rutin) present in dried plums may contribute to the reduction of IR effects on the human bone [164] and it would be interesting to analyze if there would be similar results for bone cells in microgravity conditions.

5.3. Mitigation Hardware

To this day, the easiest form of engineering countermeasures against radiation is considered to be the passive method of putting enough absorbing mass between the astronaut and space and hence, passive shielding is acknowledged to be the most feasible method for protecting against space radiation [165]. However, some of the biggest challenges every space mission has to overcome are mass requirements and the technology available. Only some mass can be sent to space. The more massive a spacecraft is, the more difficult and expensive it is to launch, or the fewer critical items it can take with it. Engineers have used this opportunity to explore concepts for active radiation shielding, that are driven by ideas that reduce the cost and mass required for equipment that keeps radiation exposure within sustainable limits. In this Section, we analyze both of these radiation mitigation methods, along with the proposed strategies to reduce energy levels during the human stay on the surface of Mars.

5.3.1. Active Shielding

Active radiation protection includes any hardware that actively blocks or deflects galactic cosmic radiation or solar particle event radiation. Since the 1970s, three such types of shielding have been explored to actively protect against space radiation: electrostatic, plasma, and magnetic [165]. Currently, few studies have been conducted regarding active shielding concepts that use electrostatic methods. Electrostatic shields use electrically charged spheres to direct charged particles around the craft and create a “safe zone” that is minimally affected by radiation [166, 167, 168]. Many studies of electrostatic shields measure effectiveness by how much of the particles’ flux is changed with the field’s voltage [167].

In the 1980s, it was reported that designing shields that used electrostatic fields to deflect protons was difficult because they had very high voltage requirements and were “inherently insatiable” because concepts were hard to design and required particles to be oppositely charged to the electrostatic spheres [169]. Later in 2005, electrostatic shields were re-examined and calculations showed that the order of magnitudes of voltage and sphere radii were too large or unrealistic to make any difference in deflecting galactic cosmic radiation ion energies [168]. In 2004, a study on the use of novel asymmetric electrostatic shields was published, which was hypothesised to address many of the shortcomings in previous research on electrostatic shielding [167, 168]. The effectiveness of asymmetric electrostatic fields was examined against both low and high energy particles, including iron; essentially, the fields were more effective at changing the flux of low-energy particles than they were at changing high-energy particles, and the field’s effectiveness increased as the field’s voltage increased [167].

A later example of the most developed electrostatic shield concepts uses electrostatically inflated membrane structures (EIMS) made of aluminized Mylar to create a charge flux strong enough to deflect solar radiation [168, 170]. The EIMS had 10 kV of charging, 5 keV of energy for electron flux, and 5 mA of current. Again, it was found that low-energy particles were completely blocked and the fluxes of high-energy particles were only reduced; this meant that the shield totally blocked solar particle events and was 70% more effective than the best hydrogen-rich passive shielding against galactic cosmic radiation [170]. It was also concluded that electrostatic fields are very power-hungry for the voltages needed for adequate absorption of particles, but the issue can be overcome by designing the electrostatic fields to deflect particles instead of stop them. Additionally, the fields resulted significantly more effective at deflecting solar particle energy than galactic cosmic radiation due to the differences in particle energies. [170]. This design was a modular implementation of electrostatic fields and comprised of lightweight Gossamer structures that had the potential for easy deployment on spacecraft. Some of the biggest drawbacks to the design were unpredicted vibrations in the structures that showed more study of EIMS is required before they can effectively be used for protecting a spacecraft on a journey to Mars [170]. Many of the studies regarding electrostatic field designs simply do not have the same heritage of research, materials, and development as other active shielding architectures do. This lack of heritage affects the concept’s ability to become a design that is robust enough for spaceworthiness. In fact, much of the technology required for electrostatic shields to be feasible enough for use in interplanetary missions is still in development [166].

Plasma shields use a combination of electrostatic and magnetic fields where an electrostatic charge creates a pocket of electrons (the plasma) that are held in place by a magnetic field [168, 171]. Much like the

electrostatic shields, in plasma shields voltage plays a big role in the effectiveness of the electron cloud around the spacecraft. A magnetic field generated by superconducting coils would have to be strong enough to contain the plasma around the craft. The biggest issues with implementing such a concept are the voltage outputs, the plasma stability and how the plasma would affect the rest of the spacecraft systems [171].

It is possible to use space plasma for both propulsion and radiation protection by creating a “mini-magnetosphere” that can shield up to energies 200 times greater than the magnet itself with a bending power in the order of 1 Tm [172] [173]. Plasma shields show a lot of potential for architectures that can be multipurpose and modular, but lack the development and study needed for spaceflight. Much like the electrostatic shields, implementations of plasma shields for radiation protection require more robust study before they can be used for a mission to Mars. Magnetic shields are currently the most popular and developed concepts for active radiation protection. Much like how the magnetosphere protects the Earth’s surface from the most harmful radiation, the idea is to use power to generate a magnetic field that surrounds the spacecraft. Given enough energy in the right configuration for the spacecraft, instead of using charged particles in the form of plasma, the magnetic field itself will either absorb or deflect oncoming particles before they reach the spacecraft. While it is difficult to protect against all radiation particles, the goal is to deflect enough particles to minimize the effects of harmful radiation dosing to astronauts and equipment for long space missions.

The International Space Station (ISS) uses a device called the Alpha Magnetic Spectrometer (AMS-02), a 5-by-4-by-3-meter superconducting magnet that detects and deflects cosmic particles in its path [174] [151, 175]. While the AMS-02 generates a field strength of 0.14 T [174], it is isolated to the AMS to prevent interactions with Earth’s magnetosphere and causing navigation issues with the ISS. The AMS-02 measures the deflection of galactic cosmic radiation and solar particle events the ISS encounters [175]. Not only did the AMS-02 help develop our understanding of the cosmic particles we will encounter on manned space missions, it has also provided excellent groundwork for conceptualizing improvements to active shielding for such missions.

Starting from the AMS-02, different magnet geometries and field strengths were simulated to model the effects those fields have on the reduction of radiation dosing for long missions [151]. One of the best, developed designs is the “Double Helix”, presenting several superconducting magnetic cylindrical solenoids with two layers of helical cable windings tilted opposite to each other that would generate a toroidal magnetic field surrounding the spacecraft.

In particular, two different Double Helix magnet strengths, measured in Tesla (T), were evaluated: the 2T, 4Tm Double Helix coils, with a field strength of 2 T and a bending power of 4 Tm; and the 8 T, 16 Tm

Effective Reduction in Annual Radiation Dosing								
Passive Shield*			2T, 4Tm Double Helix			8T, 16Tm Double Helix		
37%	28%	29%	50%	41%	40%	68%	61%	58%
With passive shielding			21%	18%	16%	50%	46%	41%

Table 12: The percent reduction of the annual radiation dosing from freespace using passive shielding, 2T, 4Tm Double Helix, and 8T, 16Tm Double Helix; includes the additional reduction in dosing both Double Helix designs offer in addition to the spacecraft's passive shield.*

*Passive shield was defined as the "spacecraft" with a 1.5 cm aluminum shielding. BFO - Blood Forming Organs.

Double Helix, with a field strength of 8 T and a bending power of 16 Tm. This was then compared to both freespace and the presence of a passive spacecraft shield of aluminum [151]. Table 12 shows the annual dosing (at solar minimum) for skin, blood forming organs (BFO), and the body.

As it results, the Double Helix is more effective than passive shielding. While the 2T, 4Tm Double Helix could reduce radiation doses by 40%, the 8T, 16Tm Double Helix configuration could reduce them by 60% at the cost of more power and mass. In addition, the shield would effectively reduce the constant level of galactic cosmic radiation during an interplanetary mission to doses of 26-28 rem/y at solar maximum and 37 rem/y at solar minimum; both annual doses well below the maximum of 50 rem/y allowed for astronauts. Based on the energy of the particles the shield was simulated to deflect, the Double Helix would also be very effective in protecting against random solar particle events, should they arise during a several-year voyage to Mars.

Since the study was published in 2012, any future Mars missions using this or similar concepts would have at least eight years of new heritage technology at its disposal. Reviewing past architectures is often the first step in designing new and innovative technologies. One of the biggest challenges in choosing the best type of active shielding for long-duration space missions has much to do with the lack of concepts in the architecture space. For example, the lack of studies using alternative types of active shielding to magnetic fields hints that magnetic field-based designs comprise the majority of concepts. The maturity and continued study of this superconducting magnet design shows great potential for realistically making long-lasting, semi-modular designs for long space missions [151]. Other designs can show engineers the potential for using multiple shielding types to meet the redundancies necessary for a manned exploration mission, or even designs more easily repaired with in-situ resources [170]. Much further research and development is needed for making spaceworthy active shielding alternatives robust enough to help us safely send astronauts to Mars. In the

meantime, superconducting magnet designs are a great place to start modeling the effectiveness in dosing reduction by using updated radiation environment simulations.

5.3.2. *Passive Shielding*

Passive radiation shielding is one of the countermeasures for exposure to space radiation. This protection includes the usage of a sufficient amount of material to absorb the energy from the cosmic radiation. Earlier, research studies on passive shielding focused on using additional mass for the primary purpose of space radiation protection. However, using additional mass just for the purpose of radiation shielding is impractical due to the limited launch capability of rockets and mass required to sustain astronauts for extended periods of time for missions beyond Low Earth Orbits. Furthermore, adding extra thickness does not reduce much the incoming energy. From up to a point, energy levels are nearly constant, or the extra thickness even increases the dose in some cases because of the creation of secondary particles. Therefore, there had been suggestions about alternate passive shielding options like the use of advanced structural materials, food or astronaut waste.

Some general statements which influence the selection criteria of candidate materials in shielding are the following. Firstly, due to human health and safety as a primary concern, shielding designs need to be conservative and adhere to the so-called "ALARA" principle. ALARA stands for "as low as reasonably achievable". It is a safety principle designed to minimize radiation doses. Secondly, materials must be lightweight and should have desirable characteristics such as structural, mechanical and thermal, along with their space radiation shielding properties. The common materials which are considered with regard to the space radiation shielding experiments are aluminium, copper, polyethylene, water and graphite. These materials are frequently present in current spacecraft designs. They are chemically well-defined and have the required physical properties.

The effectiveness of a material as a radiation shield generally increases with decreasing atomic number [176]. Materials with most electrons per unit mass, least mean excitation energy and least tight binding energies are the best energy absorbers [177]. These conditions make hydrogen the most favored material. A series of measurements were conducted using a particle beam, 1 GeV/nuc ^{56}Fe , which is a representative of heavy ion component of Galactic Cosmic Rays (GCR), and various shielding materials including composites, light elements and heavy elements in [178]. Results from these measurements confirmed that hydrogen is the most effective shielding material. Since hydrogen is highly effective, polyethylene (CH_2), which has two hydrogen atoms and one carbon atom molecule per molecule, is also an effective shielding material. Apart from these,

its availability, non-toxicity and chemically stable nature under typical conditions make polyethylene the most convenient reference material for shielding tests.

Graphite occupied a special significance in these tests as well, as carbon is present in the molecular formula of polyethylene and the atomic mass of this carbon component is divisible by 4. Another reason behind the selection of graphite is that it is a component of carbon composites. The mechanical and radiation shielding properties of carbon fibers and carbon composites enables them to function as the multifunctional superstructure of future spacecraft or planetary surface habitats [179]. Dosimetric measurements were carried out for each one of these materials at shielding depths ranging from 5-20 g/cm² in 5 g/cm² intervals, finding a similar response with aluminium composites.

The shielding effectiveness of any given material at a specific depth can be compared to the reference value of 1.000 corresponding to polyethylene (e.g. [180]). A shielding effectiveness value is the ability of a given material to reduce absorbed dose and dose equivalent at a given depth x . In other words, it quantifies how well a material can absorb or deflect the radiation it encounters. For a set of values at a given depth, the value nearest or exceeding 1.000 means that the corresponding material performs well relative to polyethylene. In the above study, two important depths were tested, 5 g/cm² (bulkhead) and 20 g/cm² (storm shelter). Results have shown that whether based on absorbed dose or dose equivalent, water is the most effective space radiation shielding material relative to polyethylene. Shielding properties observed for water could be of practical significance as water is a necessary consumable and large quantities of it will be required by the crew in long interplanetary missions. As for the other materials tested in [180], copper had the worst behavior, followed by aluminium and graphite.

Despite so many merits, the main drawback of polyethylene is its poor mechanical properties. Therefore, one of the main priorities of space agencies today is to develop a highly efficient radiation shielding material which is also capable of withstanding the typical loads occurring during a mission. Nanoparticles of carbon and boron can play a major role in the design of such materials as they have a high modulus and great electrical and thermal properties. According to [181], carbon nanotubes enhance the mechanical properties of polyethylene and provide a good load transfer to the matrix. Other studies like [182] have shown that carbon nanotubes and nanoclays have the potential to reduce the harmful effects of ionizing radiation and to create multifunctional composite materials. Other than that, boron based composites are found to be reliable materials for radiation shielding. This is due to the neutron absorbing ability of ¹⁰B isotope which has a wide cross-section.

In [183], numerical analysis was performed with the HZETRN2015 code on typical aerospace materials such

as Kapton, Aluminium, PPS, PEEK and RTM6 to highlight the performance of polyethylene in radiation protection. This was followed by investigation of shielding properties of polyethylene based nanocomposites at different percentages of fillers, considering the three types of radiation: GCR, SPE and particles in LEO environment. Results have shown that Medium Density Polyethylene (MDP) is the most effective polymer in reduction of equivalent dose from the three sources of radiation (SPE, GCR, LEO). It was confirmed in the simulations that high hydrogen content is important in limiting the damage by both protons and heavy nuclei. Aerospace-grade epoxy RTM6 has also shown good radiation protection properties. This numerical analysis also suggested that graphene oxide (GO) could be a useful reinforcement of polyethylene matrices for the fabrication of composites which are multifunctional and have radiation shielding properties in the space environment.

On general, radiation shielding performances of a given material are studied in three steps. Firstly, Monte Carlo simulations are used to validate the shielding capabilities of a material. If results are promising, the material properties are further evaluated by ions irradiation particle accelerator facilities. It is expected that ions in these tests are the most abundant ones in space. Lastly, materials which perform the best in both these steps undergo a characterization in space. Currently, the ISS is the best available laboratory to test material response in space radiation. Even though it is within the protection of Earth's magnetic field, the radiation spectrum in ISS at high altitudes replicates the spectrum of outer space radiation [184]. Measurements were performed in the ISS during the ALTEA shield project on Polyethylene and Kevlar for the investigation of shielding effectiveness. Three detectors of ALTEA were used which were capable of merging radiation measurements with ISS position [185]. Therefore, it was possible to select measurements in the orbital tract that will best represent the radiation expected in a deep space environment. Moreover, as these three detectors were identical, they could be used concurrently. Results have shown that Kevlar has a good radiation shielding performance, and hence is comparable to polyethylene. It is also resistant to impacts, which is important for debris shielding, making it a good candidate. Moreover, since it is available as a fabric, it may be adapted for use in Extra Vehicular Activity (EVA) suits or for extra shielding in some specific locations of habitat, like the crew sleeping quarters. These features make Kevlar an optimal candidate for future integrated approach in space missions.

In space applications, every kilogram of mass has a significant impact upon the mission cost and feasibility. While dense materials or thick layers of material are great at attenuating the energy levels of incoming radiation, they also contribute to increasing the amount of mass. Additionally, in space, the goal is to keep radiation from getting into the area where the astronauts are located. For long duration space missions, the

habitat of astronauts can be a bit larger than most Earth-based radiation sources so the volume enclosed by the shield would be much larger. This will require even more shielding material. So, passive shielding can be prohibitively heavy when used as the sole method of radiation protection for long duration space flights. These studies and results are proof that future research on passive shielding should not be just towards “better materials”, but the focus should be an integrated and harmonious approach to the shielding issue. This approach will consider different passive elements, use of multipurpose materials and possibly active shielding as well along with pharmaceutical countermeasures.

5.3.3. *Martian Habitats*

The next step of human exploration into space is establishing a human presence on planet Mars with a permanent habitat on the surface, but this adventure comes with its challenges. One of these is the danger derived from the absence of a magnetic field that, just like on Earth, would protect the surface from Galactic Cosmic Rays (GCRs) and Solar Energetic Particles (SEPs). The Martian atmosphere is a natural low-energy cutoff for incoming particles and only SEP events with a strong high-energy component can be observed on the surface. GCRs are the main contribution to the surface radiation and are modulated by the solar activity variation in time [186]. GCRs are present on Mars as a continuous radiation background and the long exposure makes them one of the main risks for future exploration missions [187].

Mars is characterized by an extremely rarefied atmosphere (the average surface pressure is of 610 Pa) that is <1% thinner than that of Earth and, as analysed by [188], the surface radiation environment depends inversely on the atmospheric pressure: the measured dose rate decreases when the pressure increases; and in general, the column depth in the vertical direction is much smaller than toward the horizon [186]. It's also worth mentioning how the flux of GCR particles changes in anti-correlation with solar activity due to the solar wind. The surface dose rate is in fact anti-correlated with the atmospheric depth for solar modulation potentials smaller than ~900-1000 MV; while for stronger solar activities the anti-correlation vanishes, and the shielding effect disappears [186]. This means that at weaker solar activities there are more lower-energy primary GCR particles that are more affected by the atmospheric shielding. Therefore it is reasonable to consider the atmospheric shielding effect on the surface of Mars during the periods of solar minimum. By considering a Mars elevation map (e.g. [189]), we can consider the northern plains, as well as the Hellas Planitia, as the best settlement areas, in terms of radiation shielding, where the atmosphere can work as an additional protection to astronauts during extravehicular activities.

Since carrying shielding material from Earth to Mars could highly affect the mission costs, one of the most

favoured shielding solutions that can be employed on the surface of Mars is the usage of in-situ resources as building material for a habitat: in this case surface regolith. In conformity to this, it is also worth mentioning the possibility of setting up a settlement underground, inside caves or lava tubes, which will be explored later. It has been demonstrated that the absorbed dose and equivalent dose rate induced by GCR particles vary with height above and below the Martian surface and with the subsurface composition. In particular, to the end of [190] that considers the possibility of employing surface regolith as a shielding material, different depths below the surface were taken into account (which could be intended as different thickness values and how they mitigate radiation). The two most reasonable options to employ on Mars are:

1. A homogeneous mixture of 50% water and 50% basaltic andesite rock by weight, presumably realistic at the Martian North Pole (bulk density of 1.4 g/cm³);
2. An iron rich sandstone (dry regolith) as analyzed by “ChemCam” on board of Curiosity (bulk density of 2.2 g/cm³);

Results show the 50% water mixture is a lot more effective than dry regolith, making a water-rich material more recommended in the construction of a Mars habitat. Considering that the equivalent dose limit of radiation that astronauts can receive on the surface of Mars has been calculated to be 500 mSv/year, the walls of the habitat in question are recommended to present at least a 10-cm thick portion of this material. It must be taken into consideration that the Mars environment is also home to induction - in other words, secondary radiation - produced in the atmosphere and local surface, so using only in-situ resources might not be enough, or could even turn out negative. The issue can be controlled by adding polymer binders to the regolith, but this kind of research still requires further development [191].

Lava tubes have been identified in the northern shield of Alba Mons by the Viking orbiter, in the Tartarus Colles by the HiRISE camera on MRO, and on Olympus Mons, based on MGS/MOC images. According to studies conducted on Earth, caves tend to maintain stable environmental conditions [192], resulting less stressful on equipment than the wide diurnal swings on the surface. They have roofs tens of meters thick - around 20 meters on Mars [193] - making the environment relatively safe from solar radiation, cosmic rays, wind, dust storms and micrometeorites. For these reasons they are a favourable solution to set up a habitat. Constructions inside a lava tube could be simple inflatable structures, making them lighter and faster to set up, and maintained more easily than surface structures.

When designing a Mars habitat, it will also be necessary to consider the psychological health of the astronauts other than their safety against radiation. For example, surface habitats built in regolith will be unable to have windows and a completely closed environment may play an important role on the psychology of the crew

during long-term missions. Similarly, being able to relax and work efficiently right under tens of meters of rock shouldn't be underestimated, regardless of the unlikelihood of cave-ins in lava caverns that have survived for thousands, millions, or billions of years.

It seems that the best solutions to creating a habitat to effectively shield radiation on Mars are two, both involving in-situ regolith. The best one, in regards to blocking out the most of radiation, is setting up the habitat inside an underground cave, thus exploiting the shielding properties of Mars' surface itself. In fact, data shows that a depth of ten meters would already be able to entirely dissolve the effect of radiation. On the other hand, if the mission profile requires an on-surface habitat, the best solution would then be to use a mixture of regolith and water as building material, with a minimum thickness of 10 cm in order to keep the received radiation dose below the limit that astronauts can receive in a year.

Nevertheless, other materials may be useful too. Simulations suggested that hydrogen-based materials are indeed more effective in terms of radiation in the Martian environment too. Specifically, materials with similar properties with polyethylene, like cyclohexane, PMMA, Mylar and Kevlar, appeared to have almost identical behavior against cosmic rays, whereas liquid hydrogen outweighed by far any other material. Other alternatives, like carbon fiber or aluminium, still reduce dose levels at a sufficient percent though [194]. It is then advocated to combine materials such as Martian regolith and aluminium in order to employ the in-situ resources and the spacecraft carrying astronauts.

Considering the great shielding properties of water it could also be interesting to consider placing water storage containers strategically on the walls and ceiling of the habitat and to have them continuously refilled by the recycling systems. Previous research suggests that a layer of water 7-cm thick reduces the ionizing radiation transmitted through it by half. However, a drawback to water is that ionizing cosmic radiation is mostly gamma rays and protons that, if captured by the water, become H⁺ ions which could acidify the shielding water in time, making it unsafe to drink.

A similar concept has been talked about using human wastes [195] as in fact urine and water present the same shielding effectiveness and feces are able to shield even when removing water for recycling purposes, making it doubly useful. The same was considered for plants too, and fungi in particular were tested on the International Space Station, revealing that 1.7 mm could already decrease radiation levels by 1.82-5.04% [196].

Other materials – like polyethylene, as discussed in the passive shielding section – present the main drawback of weight. Should they be chosen to build the structure of the habitat, in fact, they would need to be carried from Earth to Mars in great quantity, meaning enormous costs. However, another and more interesting

application of these materials could be found in spacesuits for extravehicular activities on the surface or in the structure of pressurized rovers, where regolith would be more hardly applicable. A concept of a personal radiation shielding suit using water and human waste liquids has already been studied [197].

Considering the addition of weight to the spacecraft as a consequence to using passive shielding, an active shielding solution may be more fitting to protect the astronauts during transit from Earth to Mars and back. The usage of active shielding for Mars habitats can also be taken into consideration the way it was explored in Section 6.3.1 by implementing a toroidal configuration [198]. If the habitat presents a semi-cylindrical shape, large barrel toroidal magnets can surround it and be able to block a significant portion of ionizing radiation. However, given the non-negligible weight of a magnetic-field generating system, further studies and simulations should be carried out in order to assess the efficiency of both shielding solutions compared to their weight. Additionally, an active shielding is not convenient on the surface of Mars, in terms of energy consumption, compared to passive. The only energy consumption derived from passive shielding is that required by the set-up phase – if we consider the energy needed by robotic 3D printers to build a habitat in regolith above the surface, or the one needed to inflate modules below the surface. On the other hand, for an active shielding, the energy required continuously in time should also be taken in consideration. Superconductors require a large amount of power and must also support a cooling system [199]. These concepts make active shielding more expensive and with roughly the same shielding result. Consequently, in order to assess its feasibility, further research should not only focus on power management, but also on the transportation of the system from Earth to Mars and its set-up on the surface.

6. Discussion and Conclusions

The impact of radiation on astronaut health in crewed missions has always been a concern on numerous missions to the ISS and the Lunar surface. Most of these missions were short-duration, posing little risk to astronauts from GCRs or major events emitting solar-origin particles. Long-duration missions to the ISS do provide insight into the possible impact of radiation on astronauts, although their duration has been much lower compared to planned missions to Mars, and their proximity to the Earth makes them better shielded compared to interplanetary missions. Because of the distance and orbital considerations, the planned crewed missions to Mars are long-duration missions, exposing astronauts to enhanced radiation from GCRs and SEPs up to a level we have never witnessed before in human spaceflight. While SEPs are hard to predict and their intensity can vary drastically, however, due to the lower energy range of incident particles, typical radiation shields such as the 5 g cm^{-2} aluminum shield are very effective in protecting astronauts from their impact.

GCRs on the other hand, are continuous background radiation and their flux can be estimated very accurately. Nevertheless, the energy of the particles involved is much higher and typical shielding used in spacecraft does not provide much protection. Secondary productions from GCRs, especially thermal neutrons pose a threat to astronauts in long-duration missions to Mars.

Organ	Male Phantom				Female Phantom			
	No shield		Shield		No shield		Shield	
	Solar Min.	Solar Max.	Solar Min.	Solar Max.	Solar Min.	Solar Max.	Solar Min.	Solar Max.
Brain	1.74E+03	1.27E+03	1.56E+03	1.15E+03	1.61E+03	1.19E+03	1.45E+03	1.07E+03
Eyes	1.91E+03	1.40E+03	1.72E+03	1.27E+03	1.77E+03	1.31E+03	1.60E+03	1.18E+03
Head	1.03E+03	7.54E+02	9.29E+02	6.79E+02	9.87E+02	7.15E+02	8.88E+02	6.43E+02
Heart	1.20E+03	8.97E+02	1.08E+03	8.08E+02	1.04E+03	7.81E+02	9.37E+02	7.03E+02
LeftAdrenal	1.35E+03	1.00E+03	1.22E+03	9.02E+02	1.62E+03	1.20E+03	1.46E+03	1.08E+03
LeftArmBone	1.89E+03	1.37E+03	1.71E+03	1.24E+03	1.86E+03	1.35E+03	1.68E+03	1.22E+03
LeftBreast	0.00E+00	0.00E+00	0.00E+00	0.00E+00	2.59E+03	1.87E+03	2.33E+03	1.68E+03
LeftClavicle	1.68E+03	1.23E+03	1.51E+03	1.11E+03	1.62E+03	1.20E+03	1.46E+03	1.08E+03
LeftKidney	1.38E+03	1.03E+03	1.25E+03	9.23E+02	1.36E+03	1.01E+03	1.23E+03	9.06E+02
LeftLeg	1.75E+03	1.27E+03	1.58E+03	1.15E+03	1.74E+03	1.27E+03	1.57E+03	1.14E+03
LeftLegBone	1.27E+03	9.42E+02	1.14E+03	8.47E+02	1.24E+03	9.22E+02	1.11E+03	8.30E+02
LeftLung	1.42E+03	1.05E+03	1.28E+03	9.44E+02	1.40E+03	1.04E+03	1.26E+03	9.34E+02
LeftOvary	0.00E+00	0.00E+00	0.00E+00	0.00E+00	1.56E+03	1.18E+03	1.40E+03	1.06E+03
LeftScapula	1.77E+03	1.29E+03	1.59E+03	1.16E+03	2.00E+03	1.45E+03	1.80E+03	1.31E+03
LeftTeste	1.80E+03	1.31E+03	1.62E+03	1.18E+03	0.00E+00	0.00E+00	0.00E+00	0.00E+00
LowerLargeIntestine	9.97E+02	7.48E+02	8.97E+02	6.73E+02	1.21E+03	9.02E+02	1.09E+03	8.12E+02
MaleChest	2.08E+03	1.50E+03	1.87E+03	1.35E+03	0.00E+00	0.00E+00	0.00E+00	0.00E+00
MaleGenitalia	1.75E+03	1.28E+03	1.58E+03	1.15E+03	0.00E+00	0.00E+00	0.00E+00	0.00E+00
MiddleLowerSpine	1.11E+03	8.26E+02	9.96E+02	7.43E+02	1.09E+03	8.16E+02	9.84E+02	7.34E+02
Pancreas	8.48E+02	6.39E+02	7.63E+02	5.75E+02	1.00E+03	7.54E+02	9.00E+02	6.78E+02
Pelvis	1.14E+03	8.50E+02	1.02E+03	7.65E+02	1.12E+03	8.31E+02	1.00E+03	7.48E+02
RibCage	1.91E+03	1.39E+03	1.72E+03	1.25E+03	1.83E+03	1.33E+03	1.65E+03	1.20E+03
RightAdrenal	1.47E+03	1.08E+03	1.32E+03	9.73E+02	1.45E+03	1.08E+03	1.31E+03	9.73E+02
RightArmBone	1.95E+03	1.42E+03	1.76E+03	1.28E+03	1.87E+03	1.37E+03	1.68E+03	1.23E+03
RightBreast	0.00E+00	0.00E+00	0.00E+00	0.00E+00	2.77E+03	2.00E+03	2.49E+03	1.80E+03
RightClavicle	1.51E+03	1.12E+03	1.36E+03	1.00E+03	1.70E+03	1.25E+03	1.53E+03	1.12E+03
RightKidney	1.33E+03	9.87E+02	1.20E+03	8.88E+02	1.27E+03	9.36E+02	1.14E+03	8.43E+02
RightLeg	1.74E+03	1.27E+03	1.57E+03	1.14E+03	1.80E+03	1.31E+03	1.62E+03	1.18E+03
RightLegBone	1.20E+03	8.94E+02	1.08E+03	8.05E+02	1.27E+03	9.43E+02	1.15E+03	8.49E+02
RightLung	1.39E+03	1.03E+03	1.25E+03	9.24E+02	1.40E+03	1.04E+03	1.26E+03	9.32E+02
RightOvary	0.00E+00	0.00E+00	0.00E+00	0.00E+00	9.10E+02	6.80E+02	8.19E+02	6.12E+02
RightScapula	1.83E+03	1.33E+03	1.65E+03	1.20E+03	1.85E+03	1.34E+03	1.66E+03	1.21E+03
RightTeste	1.37E+03	1.01E+03	1.23E+03	9.05E+02	0.00E+00	0.00E+00	0.00E+00	0.00E+00
Skin	2.15E+03	1.56E+03	1.94E+03	1.41E+03	2.06E+03	1.51E+03	1.85E+03	1.35E+03
Skull	1.91E+03	1.40E+03	1.72E+03	1.26E+03	1.87E+03	1.36E+03	1.68E+03	1.22E+03
SmallIntestine	9.72E+02	7.29E+02	8.75E+02	6.56E+02	1.03E+03	7.76E+02	9.31E+02	6.98E+02
Spleen	1.20E+03	8.96E+02	1.08E+03	8.07E+02	1.14E+03	8.53E+02	1.03E+03	7.68E+02
Stomach	1.15E+03	8.56E+02	1.03E+03	7.71E+02	1.16E+03	8.65E+02	1.04E+03	7.79E+02
Thymus	1.12E+03	8.31E+02	1.01E+03	7.48E+02	1.10E+03	8.18E+02	9.92E+02	7.36E+02
Thyroid	1.25E+03	9.36E+02	1.13E+03	8.43E+02	1.13E+03	8.41E+02	1.02E+03	7.57E+02
Trunk	1.20E+03	8.77E+02	1.08E+03	7.90E+02	1.19E+03	8.76E+02	1.07E+03	7.88E+02
UpperLargeIntestine	1.00E+03	7.52E+02	9.01E+02	6.77E+02	1.07E+03	8.02E+02	9.63E+02	7.22E+02
UpperSpine	1.40E+03	1.04E+03	1.26E+03	9.34E+02	1.25E+03	9.28E+02	1.12E+03	8.35E+02
UrinaryBladder	1.15E+03	8.57E+02	1.03E+03	7.72E+02	1.24E+03	9.22E+02	1.11E+03	8.30E+02
Uterus	0.00E+00	0.00E+00	0.00E+00	0.00E+00	9.92E+02	7.46E+02	8.93E+02	6.72E+02

Table 13: Total Effective Dose (mSv) from GCRs in various organs, with and without shielding, in a crewed Mars mission of 600 days in cruise and 400 days on the surface

Organ	Cruise				Surface			
	No shield		Shield		No shield		Shield	
	Median	Max	Median	Max	Median	Max	Median	Max
Brain	3.41E+01	1.17E+03	6.34E+00	2.17E+02	2.84E+00	9.74E+01	5.28E-01	1.81E+01
Eyes	3.75E+01	1.29E+03	6.97E+00	2.39E+02	3.13E+00	1.07E+02	5.81E-01	1.99E+01
Head	8.08E+01	5.69E+03	1.50E+01	1.06E+03	6.73E+00	4.74E+02	1.25E+00	8.81E+01
Heart	5.63E+00	2.67E+02	1.05E+00	4.96E+01	4.69E-01	2.22E+01	8.72E-02	4.13E+00
LeftAdrenal	1.34E+01	4.89E+02	2.48E+00	9.10E+01	1.11E+00	4.08E+01	2.07E-01	7.58E+00
LeftArmBone	8.04E+01	3.56E+03	1.49E+01	6.62E+02	6.70E+00	2.97E+02	1.24E+00	5.51E+01
LeftBreast	0.00E+00	0.00E+00	0.00E+00	0.00E+00	0.00E+00	0.00E+00	0.00E+00	0.00E+00
LeftClavicle	4.56E+01	1.67E+03	8.48E+00	3.10E+02	3.80E+00	1.39E+02	7.07E-01	2.59E+01
LeftKidney	1.80E+01	5.68E+02	3.34E+00	1.06E+02	1.50E+00	4.73E+01	2.78E-01	8.80E+00
LeftLeg	1.09E+02	6.12E+03	2.03E+01	1.14E+03	9.11E+00	5.10E+02	1.69E+00	9.48E+01
LeftLegBone	1.19E+01	4.20E+02	2.21E+00	7.81E+01	9.90E-01	3.50E+01	1.84E-01	6.50E+00
LeftLung	1.69E+01	5.61E+02	3.14E+00	1.04E+02	1.41E+00	4.68E+01	2.62E-01	8.70E+00
LeftOvary	0.00E+00	0.00E+00	0.00E+00	0.00E+00	0.00E+00	0.00E+00	0.00E+00	0.00E+00
LeftScapula	8.39E+01	3.87E+03	1.56E+01	7.19E+02	6.99E+00	3.22E+02	1.30E+00	5.99E+01
LeftTeste	6.58E+01	2.72E+03	1.22E+01	5.05E+02	5.49E+00	2.26E+02	1.02E+00	4.21E+01
LowerLargeIntestine	3.94E+00	1.98E+02	7.33E-01	3.69E+01	3.28E-01	1.65E+01	6.11E-02	3.07E+00
MaleChest	8.00E+01	3.53E+03	1.49E+01	6.56E+02	0.00E+00	0.00E+00	0.00E+00	0.00E+00
MaleGenitalia	1.54E+02	1.02E+04	2.85E+01	1.90E+03	1.28E+01	8.53E+02	2.38E+00	1.59E+02
MiddleLowerSpine	7.77E+00	3.10E+02	1.44E+00	5.76E+01	6.48E-01	2.58E+01	1.20E-01	4.80E+00
Pancreas	2.37E+00	1.45E+02	4.40E-01	2.69E+01	1.97E-01	1.21E+01	3.66E-02	2.24E+00
Pelvis	1.12E+01	3.71E+02	2.08E+00	6.89E+01	9.34E-01	3.09E+01	1.74E-01	5.74E+00
RibCage	9.05E+01	4.26E+03	1.68E+01	7.91E+02	7.54E+00	3.55E+02	1.40E+00	6.59E+01
RightAdrenal	2.17E+01	6.84E+02	4.04E+00	1.27E+02	1.81E+00	5.70E+01	3.37E-01	1.06E+01
RightArmBone	8.08E+01	3.57E+03	1.50E+01	6.63E+02	6.73E+00	2.97E+02	1.25E+00	5.52E+01
RightBreast	0.00E+00	0.00E+00	0.00E+00	0.00E+00	0.00E+00	0.00E+00	0.00E+00	0.00E+00
RightClavicle	2.35E+01	7.93E+02	4.36E+00	1.47E+02	1.96E+00	6.61E+01	3.63E-01	1.23E+01
RightKidney	1.63E+01	5.24E+02	3.03E+00	9.75E+01	1.36E+00	4.37E+01	2.52E-01	8.12E+00
RightLeg	1.09E+02	6.11E+03	2.03E+01	1.14E+03	9.09E+00	5.09E+02	1.69E+00	9.47E+01
RightLegBone	1.22E+01	4.22E+02	2.26E+00	7.85E+01	1.01E+00	3.52E+01	1.88E-01	6.54E+00
RightLung	1.55E+01	5.26E+02	2.87E+00	9.78E+01	1.29E+00	4.38E+01	2.39E-01	8.15E+00
RightOvary	0.00E+00	0.00E+00	0.00E+00	0.00E+00	0.00E+00	0.00E+00	0.00E+00	0.00E+00
RightScapula	8.12E+01	3.66E+03	1.51E+01	6.80E+02	6.77E+00	3.05E+02	1.26E+00	5.67E+01
Skin	8.89E+01	3.92E+03	1.65E+01	7.29E+02	7.41E+00	3.27E+02	1.38E+00	6.08E+01
RightTeste	4.41E+01	1.78E+03	8.20E+00	3.31E+02	3.68E+00	1.48E+02	6.84E-01	2.76E+01
Skull	8.84E+01	4.29E+03	1.64E+01	7.98E+02	7.37E+00	3.58E+02	1.37E+00	6.65E+01
SmallIntestine	3.45E+00	1.85E+02	6.42E-01	3.43E+01	2.88E-01	1.54E+01	5.35E-02	2.86E+00
Spleen	8.52E+00	3.45E+02	1.58E+00	6.41E+01	7.10E-01	2.87E+01	1.32E-01	5.34E+00
Stomach	8.40E+00	3.31E+02	1.56E+00	6.15E+01	7.00E-01	2.76E+01	1.30E-01	5.13E+00
Thymus	1.08E+01	3.97E+02	2.00E+00	7.38E+01	8.96E-01	3.31E+01	1.67E-01	6.15E+00
Thyroid	1.16E+01	4.40E+02	2.15E+00	8.18E+01	9.65E-01	3.67E+01	1.79E-01	6.82E+00
Trunk	6.20E+01	3.55E+03	1.15E+01	6.59E+02	5.17E+00	2.96E+02	9.60E-01	5.50E+01
UpperLargeIntestine	3.91E+00	1.99E+02	7.27E-01	3.69E+01	3.26E-01	1.65E+01	6.06E-02	3.08E+00
UpperSpine	1.55E+01	5.30E+02	2.89E+00	9.86E+01	1.29E+00	4.42E+01	2.40E-01	8.22E+00
UrinaryBladder	8.84E+00	3.35E+02	1.64E+00	6.22E+01	7.37E-01	2.79E+01	1.37E-01	5.18E+00
Uterus	0.00E+00	0.00E+00	0.00E+00	0.00E+00	0.00E+00	0.00E+00	0.00E+00	0.00E+00

Table 14: Maximum and median effective dose (mSv) from all SEP events in various organs, with and without shielding

Using the GEANT4 numerical model, we use the predicted model spectra of GCRs and historical major SEPs to compute their impact on a human phantom. We calculated the integrated effective dose deposited in

various organs of the human body during the entirety of the mission. We consider a case of a mission which will take 600 days in the cruise phase and the astronauts will spend 400 days on the surface of Mars. While the radiation dose levels used in medical studies are different from what is expected for the astronauts, as shown in the following two tables, they are the only studies available to us for comparison. This represents a knowledge gap in the health risks associated with spaceflight-relevant radiation doses, and provides direction for future research in the field.

One observation that can be made from the data presented in Table 13 is that many of the radiation dose limits set by the ESA, RSA, JAXA, and NASA would be exceeded in a Mars mission. The International Commission on Radiological Protection (ICRP) guides space agencies on the appropriate dose limits for astronauts and cosmonauts. The European Space Agency (ESA), Russian Space Agency (RSA), and Japanese Space Agency (JAXA) set their dose limits based on this guidance. The ESA and RSA have set career dose limits of 1 Sv for their astronauts and cosmonauts [200]. It can be seen in the table that many individual organs are expected to receive a radiation dose greater than 1 Sv in the described Mars mission, therefore exceeding the career dose limit set by the ESA and RSA. Based on the latest report published by NASA regarding the limits of radiation exposure, the total career effective radiation dose due to space missions should not exceed 600 mSv [201]. Considering the results of our computational simulation, both in absence and presence of shielding structures, many internal organs would be potentially irradiated with higher doses, leading to severe health hazards which should be necessarily addressed in the preparation of future Mars missions. NASA suggests implementing ALARA (as low as reasonably achievable) principles to guarantee specific standards for radiation safety, based on the duration of radiation exposure, the distance from the radiation source and the shielding material and structures.

In addition to career dose limits, the ESA has also set annual dose limits for specific parts of the body such as 0.5 Sv, 1.0 Sv, and 3.0 Sv for the blood-forming organs, the eye, and the skin, respectively [200]. The bone marrow of the spine is one of the key parts of the body for the formation of blood and blood cells. The above Table shows that the MiddleLower spine and Upper spine can be expected to receive radiation doses ranging from 0.734 Sv to 1.40 Sv. It is important to note that the dose limits set by the ESA for the blood-forming organs are annual dose limits, so it is possible that these radiation doses would not exceed these limits over the outlined 1000 day mission. However, it could be exceeded if radiation dose is at the upper limit of what is predicted and when taking into account other parts of the body involved in blood-formation such as the bone marrow of the skull and ribcage.

There are some radiation doses derived from our calculations that are consistent with nuclear accidents or

exposure to radiotherapy, which are the only reliable sources of comparison in the existing literature to define an objective correlation between ionizing radiation and the onset of related pathologies in the human body. It is also necessary to consider that organs are differently radiosensible, which means that a similar dose might trigger cellular events with different gravity in the considered tissues and systems.

There are notable physiological systems that are affected by low doses of radiation. For example, mice exposed to doses as small as 0.1 or 0.25 Gy have displayed deficiencies in recognition memory nine-months after the exposure took place [41]. Mice receiving doses as small as 0.1 Gy have also showed damages associated with neurodegenerative disease such as amyloid accumulation, and changes to behaviour and cognition [43]. The above table shows that the brain can receive radiation doses within the range of 1.07 Sv to 1.74 Sv. With such small doses associated with accumulating brain damage in mice, it is worth considering if these radiation doses associated with space travel could have long-term effects on astronauts after returning to Earth. Other organs affected by low doses of radiation include the thyroid gland and the cardiovascular system. Exposure of the thyroid gland to radiation doses as low as 50-100mGy has been associated with increased thyroid malignancies in children [63]. Likewise, studies of Chernobyl survivors have shown that exposure to as little as 0.15 Gy of radiation can increase an individual's chances of developing radiation-induced cardiovascular disease [78].

The above table show that the left lung and right lung are predicted to receive radiation doses ranging from 0.00287 Sv to 0.561 Sv. These are low doses however the Martian environment poses other threats to pulmonary health, such as the presence of harmful perchlorates in the Martian soil [85]. The skin is another organ which has been observed to be sensitive to low doses of radiation. Irradiation of the face and neck with 0.1 to 0.5 Gy in patients with tinea capitis has been strongly correlated with the development of basal cell carcinoma [96]. Additionally, the digestive system is reported to exhibit reduced gastric motility after irradiation at doses as low as 1 Gy [30].

The radioprotection of the human reproductive system represents a fundamental and critical step to preserve the ability to procreate and lead to a healthy and successful pregnancy, especially in terms of a potential future colonization. There is evidence of an increased risk for male gonadic cells to develop testicular germ cell tumour (TGCT) in patients who undergo diagnostic scans with doses that might exceed 20 mSv of direct and indirect radiation [202]. Considering that our simulation accounts for doses of 1800 mSv and 1370 mSv, for the left and right testis respectively, it might be assumed that the exposure to an even higher radiation dose is correlated with the reported cancer development. In addition, the shielding strategies evaluated in the simulation happen not to be strong enough to significantly impact on the radiation dose delivered to the

male reproductive system.

Similar conclusions might be derived analysing the female reproductive system in our computational system, considering that ovaries, uterus, and female breasts would be exposed to radiation doses that largely exceed the limit recently imposed by NASA for space missions. There is limited evidence in literature of an association between radiation exposure and the onset of ovarian cancer but, based on the results deriving from a cohort of 62,534 female nuclear bomb survivors, a positive but not significant correlation between ovarian cancer and ionizing radiation can be pointed out [203]. A decreasing trend in relative cancer risk with increased age at exposure was evidenced, along with a stronger correlation with type 2 ovarian cancers (serous and undifferentiated carcinomas), which happen to develop de novo, with chromosomal instabilities and a more aggressive clinical phenotype. Considering the same cohort of nuclear bomb survivors, there is no significant correlation between ionizing radiation and cervical cancer but there is suggestive evidence of a radiation-related increase in corpus cancer rates, especially in females irradiated before the age 20 years when physiological changes take place in the endometrial tissue [204]. Based on the higher radiosensitivity exhibited by the younger female population, it would be reasonable to furtherly investigate the correlation between age and vulnerability to ionizing radiation in the future, to better identify the most suitable candidates for long-term Mars space missions.

Finally, in the same experimental cohort, there is an increased prevalence of female breast cancer in subjects exposed to nuclear radiation before age 20 years and the age of menarche appears to be statistically correlated with a higher vulnerability to the biological effects of ionizing radiation and the onset or related breast cancer [205]. Our simulation also describes a significant radiation dose for male breast cancer, which could be a significant radiation dose for male astronauts based on the chosen minimum cut-offs. Despite this consideration, it is necessary to report an eventual risk of male breast cancer derived by the exposure to ionizing radiation, as evidenced by studies conducted with patients who underwent X-ray chest treatments, with an increased risk from 20 to 35 years after the initial exposure and a decline after three or four decades after the last registered exposure [206].

The evident discrepancy between radiation doses used in medical studies and the radiation doses that astronauts are expected to encounter during a Mars mission represents a research gap to be filled in the field of space medicine. With the central nervous system, thyroid gland, cardiovascular system, skin, digestive system, and reproductive systems all shown to be affected by low doses of radiation, we advocate that it is important to understand the potential effects of the radiation doses predicted for a Mars mission. This includes the long-term effects, such as alterations to DNA, after astronauts have returned to Earth.

A number of mitigation strategies has also been discussed. Medicine and dietary strategies include probiotics, antioxidants and vitamins. Development of active shielding hardware is an active area of research, although none of these approaches have been certified a safe rating for human spaceflight by any of the agencies. Passive shielding techniques are more developed and both data and simulations provide a number of options for consideration in these long-duration missions. In general, hydrogen-rich materials provide the best shielding. Finally, various types of habitats, which will provide ample shielding from the harsh radiation environment have been discussed. The best options are using a mixture of regolith and water for constructing walls and construction inside lava tubes, which will provide a safe environment from surface radiation, dust storms and micrometeorites.

Acknowledgements

This work was supported by the New York University Abu Dhabi (NYUAD) Institute Research Grant G1502 and the ASPIRE Award for Research Excellence (AARE) Grant S1560 by the Advanced Technology Research Council (ATRC). We thank the Young Scientist Program of the Blue Marble Space Institute of Science for enabling this collaboration. Computations were carried out on High Performance Computing (HPC) resources at NYUAD.

References

- [1] D. V. Reames, Particle acceleration at the Sun and in the heliosphere, *Space Sci. Rev.* 90 (1999) 413–491. doi:10.1023/A:1005105831781.
- [2] F. Mekhaldi, R. Muscheler, F. Adolphi, A. Aldahan, J. Beer, J. R. McConnell, G. Possnert, M. Sigl, A. Svensson, H.-A. Synal, et al., Multiradionuclide evidence for the solar origin of the cosmic-ray events of ad 774/5 and 993/4, *Nature communications* 6 (1) (2015) 1–8.
- [3] E. Cliver, H. Hayakawa, J. J. Love, D. Neidig, On the size of the flare associated with the solar proton event in 774 ad, *The Astrophysical Journal* 903 (1) (2020) 41.
- [4] I. Usoskin, S. Koldobskiy, G. Kovaltsov, A. Gil, I. Usoskina, T. Willamo, A. Ibragimov, Revised global database: fluences of solar energetic particles as measured by the neutron-monitor network since 1956, *Astronomy & Astrophysics* 640 (2020) A17.

- [5] N. Brehm, M. Christl, F. Adolphi, R. Muscheler, H.-A. Synal, F. Mekhaldi, C. Paleari, H.-H. Leuschner, A. Bayliss, e. a. Nicolussi, Tree rings reveal two strong solar proton events in 7176 and 5259 bce, *Nature Portfolio* doi : 10.21203/rs.3.rs-753272/v1.
- [6] A. M. Hillas, Can diffusive shock acceleration in supernova remnants account for high-energy galactic cosmic rays?, *Phys. G: Nucl. Part. Phys.* 31 (2005) R95–R131. doi : 10.1088/0954-3899/31/5/R02.
- [7] I. Büsching, A. Kopp, M. Pohl, R. Schlickeiser, C. Perrot, I. Grenier, Cosmic- Ray Propagation Properties for an Origin in Supernova Remnants, *Astrophys. J.* 619 (2005) 314–326. doi : 10.1086/426537.
- [8] J. P. Wefel, The Composition of the Cosmic Rays: An Update, in *Cosmic Rays, Supernovae and the Interstellar Medium*, Springer Netherlands, 1991. doi : 10.1007/978-94-011-3158-2.
- [9] E. R. Benton, E. Benton, Space radiation dosimetry in low-earth orbit and beyond, *Nuclear Instruments and Methods in Physics Research Section B: Beam Interactions with Materials and Atoms* 184 (1-2) (2001) 255–294.
- [10] D. Atri, A. L. Melott, Cosmic rays and terrestrial life: a brief review, *Astroparticle Physics* 53 (2014) 186–190.
- [11] H. E. J. Koskinen, E. K. J. Kilpua, *Physics of Earth’s Radiation Belts: Theory and Observations*, Astronomy and Astrophysics Library, Springer, Cham, 2022. doi : 10.1007/978-3-030-82167-8.
- [12] F. E. Garrett-Bakelman, M. Darshi, S. J. Green, R. C. Gur, L. Lin, B. R. Macias, M. J. McKenna, C. Meydan, T. Mishra, J. Nasrini, et al., The nasa twins study: A multidimensional analysis of a year-long human spaceflight, *Science* 364 (6436) (2019) eaau8650.
- [13] R. A. English, R. E. Benson, J. V. Bailey, C. M. Barnes, *Apollo experience report: Protection against radiation*, Tech. rep. (1973).
- [14] R.S.Johnston, L.F.Dietlein, C.A.Berry, *Biomedical results of apollo*, Scientific and Technical Information Office, National Aeronautics and Space Administration 368.
- [15] D. M. Hassler, C. Zeitlin, R. Wimmer-Schweingruber, S. Böttcher, C. Martin, J. Andrews, E. Böhm, D. Brinza, M. Bullock, S. Burmeister, et al., The radiation assessment detector (rad) investigation, *Space science reviews* 170 (1) (2012) 503–558.

- [16] B. Ehresmann, C. Zeitlin, D. M. Hassler, R. F. Wimmer-Schweingruber, E. Böhm, S. Böttcher, D. E. Brinza, S. Burmeister, J. Guo, J. Köhler, et al., Charged particle spectra obtained with the mars science laboratory radiation assessment detector (msl/rad) on the surface of mars, *Journal of Geophysical Research: Planets* 119 (3) (2014) 468–479.
- [17] J. Köhler, C. Zeitlin, B. Ehresmann, R. F. Wimmer-Schweingruber, D. M. Hassler, G. Reitz, D. Brinza, G. Weigle, J. Appel, S. Böttcher, et al., Measurements of the neutron spectrum on the martian surface with msl/rad, *Journal of Geophysical Research: Planets* 119 (3) (2014) 594–603.
- [18] D. M. Hassler, C. Zeitlin, R. F. Wimmer-Schweingruber, B. Ehresmann, S. Rafkin, J. L. Eigenbrode, D. E. Brinza, G. Weigle, S. Böttcher, E. Böhm, et al., Mars’ surface radiation environment measured with the mars science laboratory’s curiosity rover, *science* 343 (6169) (2014) 1244797.
- [19] P. B. Saganti, F. A. Cucinotta, J. W. Wilson, L. C. Simonsen, C. Zeitlin, Radiation climate map for analyzing risks to astronauts on the mars surface from galactic cosmic rays, *2001 Mars Odyssey* (2004) 143–156.
- [20] F. A. Cucinotta, *Space radiation cancer risk projections for exploration missions: uncertainty reduction and mitigation*, DIANE Publishing, 2002.
- [21] J. Wilson, J. Miller, A. Konradi, F. Cucinotta, *Shielding strategies for human space exploration*, Tech. rep. (1997).
- [22] S. Agostinelli, J. Allison, K. a. Amako, J. Apostolakis, H. Araujo, P. Arce, M. Asai, D. Axen, S. Banerjee, G. Barrand, et al., Geant4—a simulation toolkit, *Nuclear instruments and methods in physics research section A: Accelerators, Spectrometers, Detectors and Associated Equipment* 506 (3) (2003) 250–303.
- [23] S. Guatelli, B. Mascialino, M. G. Pia, W. Pokorski, Geant4 anthropomorphic phantoms, in: *2006 IEEE Nuclear Science Symposium Conference Record*, Vol. 3, IEEE, 2006, pp. 1359–1362.
- [24] Basic anatomical and physiological data for use in radiological protection: reference values. a report of age- and gender-related differences in the anatomical and physiological characteristics of reference individuals. ICRP publication 89, *Ann ICRP* 32 (3-4) (2002) 5–265.
- [25] P. M. O’Neill, Badhwar–o’neill 2010 galactic cosmic ray flux model—revised, *IEEE Transactions on Nuclear Science* 57 (6) (2010) 3148–3153.

- [26] D. Atri, C. MacArthur, I. Dobbs-Dixon, Modeling solar proton event-induced martian surface radiation dose, arXiv preprint arXiv:2012.00568.
- [27] A. V. Ivantchenko, V. N. Ivanchenko, J.-M. Q. Molina, S. L. Incerti, Geant4 hadronic physics for space radiation environment, *International journal of radiation biology* 88 (1-2) (2012) 171–175.
- [28] E. Millour, F. Forget, A. Spiga, M. Vals, V. Zakharov, L. Montabone, Mars climate database, in: *From Mars Express to ExoMars*, 27-28 February 2018, Madrid, Spain, 2018.
- [29] N.Dainiak, J.O.Waselenko, J.O.Armitage, T.J.MacVittie, A.M.Farese, The hematologist and radiation casualties, *Hematology Am Soc Hematol Educ Program* 2003 (2003) 473–496. doi:10.1182/asheducation-2003.1.473.
- [30] J.A.Jones, F.Karouia, L.Pinsky, O.Cristea, Radiation and radiation disorders, *Principles of Clinical Medicine for Space Flight* (2020) 39–108doi:10.1007/978-1-4939-9889-0_2.
- [31] Acute radiation syndrome: A fact sheet for clinicians, Centers for Disease Control and Prevention. URL <https://www.cdc.gov/nceh/radiation/emergencies/arsphysicianfactsheet.htm>
- [32] Risk of acute radiation syndromes due to solar particle events (sps), National Aeronautics and Space Administration; Human Research Roadmap. URL <https://humanresearchroadmap.nasa.gov/Risks/risk.aspx?i=97>
- [33] J.M.Butler, S.R.Rapp, E.G.Shaw, Manging the cognitive effects of brain tumor radiation therapy, *Current Treatment Options in Oncology* 7 (2006) 517–523. doi:10.1007/s11864-006-0026-5.
- [34] P.A.Craven, J.M.Rycroft, Fluxes of galactic iron nuclei and associated hze secondaries, and resulting radiation doses, in the brain of an astronaut, *Advances in Space Research* 14 (1994) 873–878. doi:10.1016/0273-1177(94)90552-5.
- [35] J.R.Letaw, R.Silberberg, C.H.Tsao, Radiation hazards on space missions outside the magnetosphere, *Advances in Space Research* 9 (1989) 285–291. doi:10.1016/0273-1177(89)90451-1.
- [36] J.Lotharius, P.Brundin, Pathogenesis of parkinson’s disease: dopamine, vesicles and α -synuclein, *Nature Reviews Neuroscience* 3 (2002) 932–942. doi:10.1038/nrn983.
- [37] T.Yock, R.Schneider, A.Friedmann, J.Adams, B.Fullerton, N.Tarbell, Proton radiotherapy for orbital rhabdomyosarcoma: Clinical outcome and a dosimetric comparison with photons, *International*

Journal of Radiation Oncology*Biography*Physics 63 (2005) 1161–1168. doi:10.1016/j.ijrobp.2005.03.052.

- [38] R.Trivedi, A.R.Khan, P.Rana, S.Haridas, B.Hemanth Kumar, K.Manda, R.K.Rathore, R.P.Tripathi, S.Khushu, Radiation-induced early changes in the brain and behavior: Serial diffusion tensor imaging and behavioural evaluation after graded doses of radiation, *J. Neurosci. Res.* 90 2009–2019. doi:10.1002/jnr.23073.
- [39] F.Cucinotta, H.Wang, J.Huff, Risk of acute or late central nervous system effects from radiation exposure, *Human Health and Performance Risks of Space Exploration Missions NASA SP 6* (2009) 191–212.
- [40] R.W.Butler, J.K.Haser, Neurocognitive effects of treatment for childhood cancer, *Ment. Retard. Dev. Disabil. Res. Rev.* 12 (2006) 184–191. doi:10.1002/mrdd.20110.
- [41] K.Frederico, A.Tyler, A.Julie, G.Thomas, W.Jing, S.Vijayalakshmi, B.Marjan, A.Antiño, Late effects of 160-particle radiation on female social and cognitive behavior and hippocampal physiology, *Radiat Res* 1 191 (2009) 278–294. doi:10.1667/RR15092.1.
- [42] M.J.Pecaut, P.Haerich, C.N.Zuccarelli, A.Smith, E.Zendejas, G.Nelson, Behavioral consequences of radiation exposure to simulated space radiation in the c57bl/6 mouse: Open field, rotorod, and acoustic startle, *Cognitive, Affective, and Behavioral Neuroscience* 2 (2002) 329–340. doi:10.3758/CABN.2.4.329.
- [43] J.D.Cherry, B.Liu, J.L.Frost, C.A.Lemere, J.P.Williams, J.Olschowka, M.O'Banion, Galactic cosmic radiation leads to cognitive impairment and increased $\alpha\beta$ plaque accumulation in a mouse model of alzheimer's disease, *PLoS One* 7 e53275. doi:10.1371/journal.pone.0053275.
- [44] J.D.Cherry, B.Liu, J.L.Frost, C.A.Lemere, J.P.Williams, J.A.Olschowka, M.Kerry O'Banion, Galactic cosmic radiation leads to cognitive impairment and increased $\alpha\beta$ plaque accumulation in a mouse model of alzheimer's disease, *PLoS ONE* 7 (2012) e53275. doi:10.1371/journal.pone.0053275.
- [45] M.C.Donohue, R.A.Sperling, R.Petersen, S.Chung-Kai, M.Weiner, P.Aisen, Association between elevated brain amyloid and subsequent cognitive decline among cognitively normal persons, *JAMA* 317 (2017) 2305–2316. doi:10.1001/jama.2017.6669.

- [46] E.H.Corder, A.M.Saunders, W.J.Strittmatter, D.E.Schmechel, P.C.Gaskell, G.W.Small, A.D.Roses, J.L.Haines, M.A.Pericak-Vance, Gene dose of apolipoprotein e type 4 allele and the risk of alzheimer's disease in late onset families, *Science* 261 (1993) 921–3. doi : 10.1126/science.8346443.
- [47] L.Villasana, T.Benice, J.Raber, Long-term effects of 56fe irradiation on spatial memory of mice: Role of sex and apolipoprotein e isoform, *International Journal of Radiation Oncology* 80 (2011) 567–573. doi : 10.1016/j.ijrobp.2010.12.034.
- [48] L.Villasana, C.Poage, P.van Meer, J.Raber, Passive avoidance learning and memory of 56fe sham-irradiated and irradiated human apoe transgenic mice, *Radiats Biol. Radioecol.* 48 (2008) 167–170.
- [49] E.Rudbeck, J.A.Bellone, K.Bonnick, A.Szűcs, S.Mehrotra-Carter, J.Badaut, A.Nelson, R.Hartman, R.Vikolinský, Low-dose proton radiation effects in a transgenic mouse model of alzheimer's disease-implications for space travel, *PLoS ONE* 12 (2017) e0186168. doi : 10.1371/journal.pone.0186168.
- [50] J.M.Vaeth, G.R.Merrian, A.Szechter, E.F.Focht, Radiation effects and tolerance, normal tissue. 6th annual san francisco cancer symposium, san francisco, calif., october 1970: Proceedings, *Front Radiat Ther Oncol* 6 (1970) 346–385. doi : 10.1159/000392817.
- [51] W.Rohrsehneider, Experimental studies on changes in normal eye tissue after x-ray irradiation, *Graefes Archiv for Ophthalmology* 121 (1929) 537–559. doi : 10.1007/BF01854351.
- [52] T.Flore, Ataxia, telangiectasia a brief description, *Costa Rica and Central America Medical Journal LXVIII* 597 (2011) 163–168.
- [53] R.M.Bliss, Hyperaemia, *Journal of tissue viability* 8 (1998) 4–13. doi : 10.1016/s0965-206x(98)80028-4.
- [54] D.Fish, A.Kim, C.Ornelas, S.Song, S.Pangarkar, The risk of radiation exposure to the eyes of the interventional pain physician, *Radiology Research and Practicedoi* : 10.1155/2011/609537.
- [55] E.A.Ainsbury, S.D.Bouffler, W.Dörr, J.Graw, C.R.Muirhead, A.A.Edwards, J.Cooper, Radiation cataractogenesis: A review of recent studies, *Radiat Res* 172 (2009) 1–9. doi : 10.1667/RR1688.1.
- [56] L.Chylack, L.Peterson, A.Feiveson, M.Wear, F.Manuel, W.Tung, D.Hardy, L.Marak, F.Cucinotta, Nasa study of cataract in astronauts (nasca). report 1: Cross-sectional study of the relationship of

- exposure to space radiation and risk of lens opacity, *Radiation Research* 172 (2009) 10–20. doi: 10.1667/RR1580.1.
- [57] A.Wegener, O.Hockwin, H.Laser, C.Strack, Comparison of the nidek eas 1000 system and the topcon sl-45 in clinical application, *Ophthalmic Res. Supply* 1 (1992) 55–62. doi:10.1159/000267209.
- [58] F.A.Cucinotta, F.K.Manuel, J.Jones, G.Iszard, J.Murrey, B.Djojonegro, M.Wear, Space radiation and cataracts in astronauts, *Journal of Radiation Research* 156 (2001) 460–466. doi:10.1667/0033-7587(2001)156[0460:SRACIA]2.0.CO;2.
- [59] L.Pinsky, W.Osborne, J.V.Bailey, R.E.Benson, L.F.Thompson, Light flashes observed by astronauts on apollo 11 through apollo 17, *Science* 183 (1974) 957–959. doi:10.1126/science.183.4128.957.
- [60] I.Bokkon, Phosphene phenomenon: a new concept, *Biosystems* 92 (2008) 168–174. doi:10.1016/j.biosystems.2008.02.002.
- [61] P.Chapman, L.Pinsky, R.Benson, T.Budinger, Observations of cosmic-ray-induced phosphenes on apollo 14.
URL <https://ntrs.nasa.gov/citations/19720010081>
- [62] W.G.Sannita, L.Narici, P.Picozza, Positive visual phenomena in space: A scientific case and a safety issue in space travel., *Vision Res* 46 (2006) 2159–2165. doi:10.1016/j.visres.2005.12.002.
- [63] B.Sinnott, E.Ron, A.B.Schneider, Exposing the thyroid to radiation:a review of its current extent, risks, and implications, *Endocrine Reviews* 31 (2010) 756–773. doi:10.1210/er.2010-0003.
- [64] M.Mazonakis, A.Tzedakis, J.Damilakis, N.Gourtsoyiannis, Thyroiddose from common head and neck ct examinations in children: is there an excess riskfor thyroid cancer induction?, *European Radiology* 17 (2007) 1352–1357. doi:10.1007/s00330-006-0417-9.
- [65] M.L.Iglesias, A.Schmidt, A.A.Ghuzlan, L.Lacroix, F.Vathaire, S.Chevillard, M.Schlumberger, Radiation exposure and thyroid cancer: a review, *Archives of Endocrinology and Metabolism* 61 (2017) 180–187. doi:10.1590/2359-3997000000257.
- [66] H.Acar, B.Cakabay, F.Bayrak, T.Evrenkaya, Effects of the chernobyldisaster on thyroid cancer incidence in turkey after 22 years, *ISRN Surgery* 257943. doi:10.5402/2011/257943.

- [67] S.Nagataki, Y.Shibata, S.Inoue, N.Yokoyama, M.Izumi, K.Shimaoka, Thyroid diseases among atomic bomb survivors in nagasaki, *JAMA* 272 (1994) 364–370.
- [68] R.Ciampi, J.A.Knauf, R.Kerler, M.Gandhi, Z.Zhu, M.N.Nikiforova, H.M.Rabes, J.A.Fagin, Y.E.Nikiforov, Oncogenic akap9-braf fusion is a novel mechanism of mapk pathway activation in thyroid cancer, *The Journal of Clinical Investigation* 115 (2005) 94–101. doi:10.1172/JCI23237.
- [69] N.N.Baxter, E.B.Habermann, J.E.Tepper, S.B.Durham, B.A.Virnig, Risk of pelvic fractures in older women following pelvic irradiation, *JAMA* 294 (2005) 2587–2593. doi:10.1001/jama.294.20.2587.
- [70] J.S.Willey, S.A.J.Lloyd, G.A.Nelson, T.A.Bateman, Ionizing radiation and bone loss: Space exploration and clinical therapy applications, *Clinical reviews in bone and mineral metabolism* 9 (2011) 54–62. doi:10.1007/s12018-011-9092-8.
- [71] I. et al, Randomized trial of antioxidant vitamins to prevent acute adverse effects of radiation therapy in head and neck cancer patients, *Journal of Clinical Oncology* 23 (2016) 5805–5813. doi:10.1200/JCO.2005.05.514.
- [72] S.Kook, K.Kim, H.Ji, D.Lee, J.Lee, Irradiation inhibits the maturation and mineralization of osteoblasts via the activation of nrf2/ho-1 pathway, *Molecular and Cellular Biochemistry* 410 (2015) 255–266. doi:10.1007/s11010-015-2559-z.
- [73] R.Fernandez-Gonzalo, S.Baatout, M.Moreels, Impact of particle irradiation on the immune system: From the clinic to mars, *Frontiers in Immunology* doi:10.3389/fimmu.2017.00177.
- [74] D.Gridley, M.J.Pecaut, R.Dutta-Roy, G.Nelson, Dose and dose rate effects of whole-body proton irradiation on leukocyte populations and lymphoid organs: Part i, *Immunology Letters* 80 (2002) 55–66. doi:10.1016/S0165-2478(01)00306-6.
- [75] J.C.Chancellor, R.S.Blue, K.A.Cengel, S.M.Auñón-Chancellor, K.H.Rubins, H.G.Katzgraber, A.R.Kennedy, Limitations in predicting the space radiation health risk for exploration astronauts, *npj Microgravity* 4. doi:10.1038/s41526-018-0043-2.
- [76] J.B.Castelino, P.V.Holland, G.P.Jacobs, M.Lapidot, M.Markovic, Effects of ionizing radiation on blood and blood components: a survey, International Atomic Energy Agency: Vienna, Austria.
URL <https://www.iaea.org/publications/5586/effects-of-ionizing-radiation-on-blood-and-blood-co>

- [77] T.Hayashi, Y.Kusunoki, M.Hakoda, Y.Morishita, Y.Kubo, M.Maki, F.Kasagi, K.Kodama, D.G.Macphee, S.Kyoizumi, Radiation dose-dependent increases in inflammatory response markers in a-bomb survivors, *International Journal of Radiation Biology* 79 (2003) 129–136. doi: 10.1080/0955300021000038662.
- [78] R.L.Hughson, A.Helm, M.Durante, Heart in space: effect of the extraterrestrial environment on the cardiovascular system, *Nature Reviews Cardiology* 15 (2018) 167–170. doi:10.1038/nrcardio.2017.157.
- [79] Chernobyl: Assessment of radiological and health impacts - 2002 update of chernobyl: Ten years on, OECD Nuclear Energy Agency.
URL <http://www.oecd-nea.org/rp/pubs/2003/3508-chernobyl.pdf>
- [80] M.D.Delp, J.M.Charvat, C.L.Limoli, R.K.Globus, P.Ghosh, Apollo lunar astronauts show higher cardiovascular disease mortality: Possible deep space radiation effects on the vascular endothelium, *Scientific Reports* 6 (2016) 29901. doi:10.1038/srep29901.
- [81] F.A.Cucinotta, N.Hamada, M.P.Little, No evidence for an increase in circulatory disease mortality in astronauts following space radiation exposures, *Life Sciences in Space Research* 10 (2016) 53–56. doi:<https://doi.org/10.1016/j.lssr.2016.08.002>.
- [82] S.R.Elgart, M.P.Little, L.J.Chappell, C.M.Milder, M.R.Shavers, J.L.Huff, Z.S.Patel, Radiation exposure and mortality from cardiovascular disease and cancer in early nasa astronauts, *Scientific Reports* 8. doi:10.1038/s41598-018-25467-9.
- [83] K.Marmagkiolis, W.Finch, D.Tsitlakidou, T.Josephs, C.Iliescu, J.F.Best, E.H.Yang, Radiation toxicity to the cardiovascular system, *Current Oncology Reports* 18. doi:10.1007/s11912-016-0502-4.
- [84] B.S.Chera, C.Rodríguez, C.G.Morris, D.Louis, D.Yeung, Z.Li, N.P.Mendenhall, Dosimetric comparison of three different involved nodal irradiation techniques for stage ii hodgkin's lymphoma patients: Conventional radiotherapy, intensity-modulated radiotherapy, and three-dimensional proton radiotherapy, *International Journal of Radiation Oncology*Biophysics* 75 (2009) 1173–1180. doi:10.1016/j.ijrobp.2008.12.048.
- [85] J.Wadsworth, C.S.Cockell, Perchlorates on mars enhance the bacteriocidal effects of uv light, *Scientific Reports* 7. doi:10.1038/s41598-017-04910-3.

- [86] J.D.Shrouf, T.E.Scheetz, T.L.Casavant, G.F.Parkin, Isolation and characterization of autotrophic, hydrogen-utilizing, perchlorate-reducing bacteria, *Appl Microbiol Biotechnol* 67 (2005) 261–268. doi : 10.1007/s00253-004-1725-0.
- [87] C.Lam, J.T.James, R.McCluskey, S.Cowper, J.Balis, C.Muro-Cacho, Pulmonary toxicity of simulated lunar and martian dusts in mice: 1. histopathology 7 and 90 days after intratracheal instillation, *Inhalation Toxicology* 14 (2008) 901–916. doi : 10.1080/08958370290084683.
- [88] T.Auberger, K.Seydl, T.Futschek, A.Sztankay, R.A.Sweeney, P.Lukas, Photons or protons: precision radiotherapy of lung cancer, *Strahlentherapie und Onkologie* 183 (2007) 3–6. doi : 10.1007/s00066-007-2002-9.
- [89] N.Ding, J.J.Li, L.Sun, Molecular mechanisms and treatments of radiation-induced lung fibrosis, *Current Drug Targets* 14 (2013) 1347–1356. doi : 10.2174/13894501113149990198.
- [90] Y.Oh, O.K.Noh, H.Jang, M.Chun, K.Park, K.Park, M.Kim, H.Park, The features of radiation induced lung fibrosis related with dosimetric parameters, *Radiotherapy and Oncology* 102 (2012) 343–346. doi : 10.1016/j.radonc.2012.02.003.
- [91] F.A.Cucinotta, L.J.Campbell, Updates to astronaut radiation limits: Radiation risks for never-smokers, *Radiation Research* 176 (2011) 102–114. doi : 10.1667/RR2540.1.
- [92] F.R.de Gruijl, Skin cancer and solar uv radiation, *European Journal of Cancer* 35 (1999) 2003–2009. doi : 10.1016/S0959-8049(99)00283-X.
- [93] H.S.Kim, Y.S.Kim, C.Lee, M.S.Shin, J.W.Kim, B.G.Jang, Expression profile of sonic hedgehog signaling-related molecules in basal cell carcinoma, *PLoS One* 14. doi : 10.1371/journal.pone.0225511.
- [94] D.E.Brash, J.A.Rudolph, J.A.Simon, A.Lin, G.J.McKenna, H.P.Baden, A.J.Halperin, J.Pontén, A role for sunlight in skin cancer: Uv-induced p53 mutations in squamous cell carcinoma, *PNAS* 88 (1991) 10124–10128. doi : 10.1073/pnas.88.22.10124.
- [95] J.Monson, L.Liu, H.Brill, A.M.Goldstein, M.A.Tucker, L.From, J.McLaughlin, D.Hogg, N.J.Lassam, Cdkn2a mutations in multiple primary melanomas, *N Engl J Med* 338 (1998) 879–887. doi : 10.1056/NEJM199803263381305.

- [96] M.Y.Kim, K.A.George, F.A.Cucinotta, Evaluation of skin cancer risks for lunar and mars missions, *Advances in Space Research* 37 (2006) 1798–1803. doi:10.1016/j.asr.2006.03.032.
- [97] R.A.Sturm, Skin colour and skin cancer - mc1r, the genetic link, *Melanoma Research* 12 (2002) 405–416. doi:10.1097/00008390-200209000-00001.
- [98] X.W.Mao, M.J.Pecaut, L.S.Stodieck, V.L.Ferguson, T.A.Bateman, M.L.Bouxsein, D.S.Gridley, Biological and metabolic response in sts-135 space-flown mouse skin, *Free Radical Research* 48 (2014) 890–897. doi:10.3109/10715762.2014.920086.
- [99] Y.Su, J.A.Meador, C.R.Gear, A.S.Balajee, Analysis of ionizing radiation-induced dna damage and repair in three-dimensional human skin model system, *Experimental Dermatology* 19 (2010) e16–e22. doi:10.1111/j.1600-0625.2009.00945.x.
- [100] A.L.Oglivy-Stuart, S.M.Shalet, Effect of radiation on the human reproductive system, *Environmental Health Perspectives* 109 (1993) 109–116. doi:10.1289/ehp.93101s2109.
- [101] J.Y.Wo, A.N.Viswanathan, Impact of radiotherapy on fertility, pregnancy, and neonatal outcomes in female cancer patients, *Journal of Radiation Oncology*Biology*Physics* 73 (2009) 1304–1312. doi:10.1016/j.ijrobp.2008.12.016.
- [102] E.R.Norwitz, H.M.Stern, H.Grier, A.Lee-Paritz, Placental percreta and uterine rupture associated with prior whole body radiation therapy, *Obstetrics and Gynecology* 98 (2001) 929–931. doi:10.1016/S0029-7844(01)01435-1.
- [103] I.D.Wilson, Hematemesis, melena, and hematochezia, *Clinical Methods: The History, Physical, and Laboratory Examinations*. 3rd edition 85.
URL <https://www.ncbi.nlm.nih.gov/books/NBK411/>
- [104] M.Hauer-Jensen, J.Wang, M.Boerma, Q.Fu, J.W.Denham, Radiation damage to the gastrointestinal tract: mechanisms, diagnosis, and management, *Curr Opin Support Palliat Care* 1 (2007) 23–29. doi:10.1097/spc.0b013e3281108014.
- [105] V.S.Theis, R.Sripadam, V.Ramani, S.Lal, Chronic radiation enteritis, *Clinical Oncology* 22 (2010) 70–83. doi:10.1016/j.clon.2009.10.003.

- [106] N.Shussman, S.D.Wexner, Colorectal polyps and polyposis syndromes, *Gastroenterology Report* 2 (2014) 1–15. doi:10.1093/gastro/got041.
- [107] Polyp. medical subjects headings., National Center for Biotechnology Information.
URL <https://www.ncbi.nlm.nih.gov/mesh?Db=mesh&Cmd=DetailsSearch&Term=%22Adenocarcinoma%22%5BMeSH+Terms%5D>
- [108] A.Fornace, K.Batten, S.Byers, A.Cheema, K.Datta, L.Girard, H.Li, M.Lopa, H.Ressom, J.Richardson, A.Roig, J.Shay, W.Wright, Y.Xie, Nscor: Space radiation and intestinal tumorigenesis: Risk assessment and counter measure development, National Aeronautics and Space Administration (NASA).
URL <https://lnda.jsc.nasa.gov/Experiment/exper/13864>
- [109] S.Suman, S.Kumar, B.Moon, A.J.Fornace, A.Datta, Low and high dose rate heavy ion radiation-induced intestinal and colonic tumorigenesis in *apc 1638n/+* mice, *Life Sciences in Space Research* 13 (2017) 45–50. doi:10.1016/j.lssr.2017.04.003.
- [110] H.Lorenzi, D.Pierson, M.Gillis, S.Mehta, M.Ott, M.Torralba, Study of the impact of long-term space travel on the astronaut’s microbiome (microbiome), National Aeronautics and Space Administration (NASA).
URL <https://lnda.jsc.nasa.gov/Experiment/exper/1836#data>
- [111] R.Kennedy, Biological effects of space radiation and development of effective countermeasures, *Life Sciences in Space Research* 1 (2014) 10–43. doi:10.1016/j.lssr.2014.02.004.
- [112] T.Kumagai, F.Rahman, A.M.Smith, The microbiome and radiation-induced bowel injury: Evidence for potential mechanistic role in disease pathogenesis, *Nutrients* 10. doi:10.3390/nu10101405.
- [113] C.Jones, C.M.Davis, K.S.Sfanos, The potential effects of radiation on the gut-brain axis, *Journal of Radiation Research* 193 (2020) 209–222. doi:10.1667/RR15493.1.
- [114] K.Kalkeri, K.Walters, W.Van Der Pol, B.McFarland, N.Fisher, F.Koide, C.Morrow, V.Singh, Changes in the gut microbiome community of nonhuman primate following radiation injury, preprint (version 1), *Research Square* doi:10.21203/rs.3.rs-38247/v1.
- [115] A.A.Voorhies, C.Mark Ott, S.Mehta, L.Duane, B.Pierson, A.Crucian, M.Cherie, M.Torralba, K.Moncera, Y.Zhang, E.Zurek, H.Lorenzi, Study of the impact of long-duration space mis-

- sions at the international space station on the astronaut microbiome, *Scientific Reports* 9. doi: 10.1038/s41598-019-46303-8.
- [116] F. et al, The nasa twins study: A multidimensional analysis of a year-long human spaceflight, *Science* 364. doi:10.1126/science.aau8650.
- [117] R.Siddiqui, N.Akbar, N.Khan, Gut microbiome, and human health under the space environment, *J Appl Microbiol* doi : 10.1111/jam.14789.
- [118] E.I.Azzam, J.Jay-Gerin, D.Pain, Ionizing radiation-induced metabolic oxidative stress and prolonged cell injury, *Cancer Letters* 327 (2012) 48–60. doi:10.1016/j.canlet.2011.12.012.
- [119] G.M.Cooper, *The cell: A molecular approach*, 2nd edition. Sunderland (MA): Sinauer Associates. *The Molecular Composition of Cells.*
URL <https://www.ncbi.nlm.nih.gov/books/NBK9879/>
- [120] K.Kawamura, F.Qi, J.Kobayashi, Potential relationship between the biological effects of low-dose irradiation and mitochondrial ros production, *Journal of Radiation Research* 59 (2018) ii91–ii97. doi:10.1093/jrr/rrx091.
- [121] A.Hahn, S.Zuryn, Mitochondrial genome (mtdna) mutations that generate reactive oxygen species, *Antioxidants* 8 (2019) 392. doi:10.3390/antiox8090392.
- [122] L.K.Folkes, P.O’Neill, Dna damage induced by nitric oxide during ionizing radiation is enhanced at replication, *Nitric Oxide* 34 (2013) 47–55. doi:10.1016/j.niox.2013.04.005.
- [123] D.Jourd’heuil, F.L.Jourd’heuil, P.S.Kutchukian, R.A.Musah, D.A.Wink, M.B.Grisham, Reaction of superoxide and nitric oxide with peroxynitrite. implications for peroxynitrite-mediated oxidation reactions in vivo, *Journal of Biological Chemistry* 276 (2001) 28799–28805. doi:10.1074/jbc.m102341200.
- [124] G. Multhoff, M. Molls, J. Radons, Chronic inflammation in cancer development, *Frontiers in Immunology* 2. doi:10.3389/fimmu.2011.00098.
- [125] R.Singh, M.K.Mishra, H.Aggarwal, Inflammation, immunity, and cancer, *Mediators Inflamm* (2017) 1–1doi:10.1155/2017/6027305.

- [126] D.Harman, The biologic clock: The mitochondria?, *J Am Geriatr Soc* 20 (1972) 145–147. doi: 10.1111/j.1532-5415.1972.tb00787.x.
- [127] H.Nie, H.Shu, R.Vartak, A.C.Milstein, Y.Mo, X.Hu, H.Fang, L.Shen, Z.Ding, J.Lu, Y.Bai, Mitochondrial common deletion, a potential biomarker for cancer occurrence, is selected against in cancer background: A meta-analysis of 38 studies, *PLoS One* 8 (2013) e67953. doi:10.1371/journal.pone.0067953.
- [128] L.Wang, Y.Kuwahara, L.Li, T.Baba, R.Shin, Y.Ohkubo, K.Ono, M.Fukumoto, Analysis of common deletion (cd) and a novel deletion of mitochondrial dna induced by ionizing radiation, *Int J Radiat Biol* 83 (2007) 433–442. doi:10.1080/09553000701370878.
- [129] T.Shimizu, M.Iwanaga, A.Yasunaga, Y.Urata, S.Goto, S.Shibata, T.Kondo, Protective role of glutathione synthesis on radiation-induced dna damage in rabbit brain, *Cell Mol Neurobiol* 18 (1998) 299–310. doi:10.1023/A:1022525214871.
- [130] W.J.Cannan, D.S.Pederson, Mechanisms and consequences of double-strand dna break formation in chromatin, *Journal of Cellular Physiology* 231 (2016) 3–14. doi:10.1002/jcp.25048.
- [131] S.J.McMahon, K.Prise, Mechanistic modelling of radiation responses, *Cancers* 11 (2019) 205. doi:10.3390/cancers11020205.
- [132] J.Puerta-Ortiz, J.Morales-Aramburo, Biological effects of ionizing radiation, *Journal of Cardiology* 27 (2020) 61–71. doi:10.1016/j.rccar.2020.01.005.
- [133] J.R.Chapman, M.R.G.Taylor, S.J.Boulton, Playing the end game: Dna double-strand break repair pathway choice, *Molecular Cell* 47 (2012) 497–510. doi:10.1016/j.molcel.2012.07.029.
- [134] H.J.Schaefer, Radiation dosage in flight through the van allen belt, *Aerospace Medicine* 30 (1959) 631–639.
- [135] J.Dahm-Daphi, C.Sass, W.Alberti, Comparison of biological effects of dna damage induced by ionizing radiation and hydrogen peroxide in cho cells, *Int J Radiat Biol* 76 (2009) 67–75. doi:10.1080/0955300090139023.
- [136] M.F.Lavin, M.Gatei, P.Chen, A.Kijas, S.Kozlov, Chapter 263 - atm mediated signalling defends the integrity of the genome, *Handbook of Cell Signalling (Second Edition)* (2010) 2171–2183doi: 10.1016/B978-0-12-374145-5.00263-1.

- [137] A.A.Goodarzi, P.A.Jeggo, Irradiation induced foci (irif) as a biomarker for radiosensitivity, *Mutation Research/Fundamental and Molecular Mechanisms of Mutagenesis* 736 (2012) 39–47. doi : 10.1016/j.mrfmmm.2011.05.017.
- [138] J.Vignard, G.Mirey, B.Salles, Ionizing-radiation induced dna double-strand breaks: a direct and indirect lighting up, *Radiother Oncol* 108 (2013) 362–369. doi : 10.1016/j.radonc.2013.06.013.
- [139] G.Vielemeyer, H.Yuan, S.Moutel, R.Saint-Fort, D.Tang, C.Nizak, B.Goud, Y.Wang, F.Perez, Direct selection of monoclonal phosphospecific antibodies without prior phosphoamino acid mapping, *J Biol Chem* 284 (2009) 20791–20795. doi : 10.1074/jbc.M109.008730.
- [140] R.Mori, Y.Matsuya, Y.Yoshii, H.Date, Estimation of the radiation-induced dna double-strand breaks number by considering cell cycle and absorbed dose per cell nucleus, *J Radiat Res* 59 (2018) 253–260. doi : 10.1093/jrr/rrx097.
- [141] W.Li, F.Li, Q.Huang, J.Shen, F.Wolf, Y.He, X.Liu, A.Hu, J.S.Bedford, C.Lil, Quantitative, non-invasive imaging of radiation-induced dna double-strand breaks in vivo, *Cancer Res* 71 (2011) 4130–4137. doi : 10.1158/0008-5472.CAN-10-2540.
- [142] F.A.Cucinotta, Space radiation risks for astronauts on multiple international space station missions, *PLoS One* 9. doi : 10.1371/journal.pone.0096099.
- [143] D.M.Sridharan, A.Asaithamby, S.M.Bailey, S.V.Costes, P.W.Doetsch, W.S.Dynan, A.Kronenberg, K.N.Rithidech, J.Saha, A.M.Snijders, E.Werner, C.Wiese, F.A.Cucinotta, J.M.Pluth, Understanding cancer development processes after hze-particle exposure: Roles of ros, dna damage repair and inflammation, *Radiat Res* 183 (2015) 1–26. doi : 10.1667/RR13804.1.
- [144] M. H. Barcellos-Hoff, E. A. Blakely, S. Burma, A. J. Fornace Jr., S. Gerson, L. Hlatky, D. G. Kirsh, U. Luderer, J. Shay, Y. Wang, M. M. Weil, Concepts and challenges in cancer risk prediction for the space radiation environment, *Life Sciences in Space Research* 6 (2015) 92–103.
- [145] T.Straume, Medical concerns with space radiation and radiobiological effects, *Handbook of Cosmic Hazards and Planetary Defense* (2015) 259–293doi : 10.1007/978-3-319-03952-7_4.
- [146] T. et al, Ultraviolet-radiation-induced inflammation promotes angiotropism and metastasis in melanoma, *Nature* 507 (2014) 109–113. doi : 10.1038/nature13111.

- [147] C.S.Cockell, D.C.Catling, W.L.Davis, K.Snook, R.L.Kepner, P.Lee, C.P.McKay, The ultraviolet environment of mars: Biological implications past, present, and future, *Icarus* 146 (2000) 343–359. doi:10.1006/icar.2000.6393.
- [148] R. R. Dubey, W. Jordan, M. Kim, J. L. Shinn, L. C. Simonsen, J. W. Wilson, Radiation Analysis for the Human Lunar Return Mission, Technical Paper NASA TP-3662, NASA Langley Research Center, Hampton, VA 23681-2199 (Sep. 1997).
URL <https://ntrs.nasa.gov/archive/nasa/casi.ntrs.nasa.gov/19970031679.pdf>
- [149] L. Tran, How NASA Will Protect Astronauts From Space Radiation at the Moon, library Catalog: www.nasa.gov (Aug. 2019).
URL <http://www.nasa.gov/feature/goddard/2019/how-nasa-protects-astronauts-from-space-radiation>
- [150] S. L. Brown, A. Kolozsvary, J. Liu, K. A. Jenrow, S. Ryu, J. H. Kim, Antioxidant Diet Supplementation Starting 24 Hours after Exposure Reduces Radiation Lethality, *Radiation Research* 173 (4) (2010) 462–468. doi:10.1667/RR1716.1.
URL <http://www.bioone.org/doi/10.1667/RR1716.1>
- [151] R. Battiston, W. Burger, V. Calvelli, R. Musenich, V. Choutko, V. Datskov, A. D. Torre, F. Venditti, C. Gargiulo, G. Laurenti, S. Lucidi, S. Harrison, R. Meinke, Active Radiation Shield for Space Exploration Missions Publisher: INFN Open Access Repository. doi:10.15161/OAR.IT/1449018317.78.
URL <https://www.openaccessrepository.it/record/21047?ln=en>
- [152] P. Meyer, R. Ramaty, W. R. Webber, Cosmic rays—astronomy with energetic particles, *Physics Today* 27 (10) (1974) 23–32. doi:10.1063/1.3128914.
URL <http://physicstoday.scitation.org/doi/10.1063/1.3128914>
- [153] World Health Organisation, Food and Agriculture Organisation, Probiotics in food: health and nutritional properties and guidelines for evaluation, WHO/FAO, Geneva/Rome/ Switzerland/Italy.
- [154] G.L.Douglas, A.A.Voorhies, Evidence based selection of probiotic strains to promote astronaut health or alleviate symptoms of illness on long duration spaceflight missions, *Beneficial Microbes* 8 (2017) 1–12. doi:10.3920/BM2017.0027.

- [155] A.C.Ouwehand, C.DongLian, X.Weijian, M.Stewart, J.Ni, T.Stewart, L.E.Miller, Probiotics reduce symptoms of antibiotic use in a hospital setting: a randomized dose response study, *Vaccine* 32 (2014) 458–463. doi:10.1016/j.vaccine.2013.11.053.
- [156] M.Vrese, P.Wrinkler, P.Rautenberg, T.Harder, C.Noah, C.Laue, S.Ott, J.Hampe, S.Schreiber, K.Heller, J.Schrezenmier, Effect of lactobacillus gasseri pa 16/8, bifidobacterium longum sp 07/3, b. bifidum mf 20/5 on common cold episodes: a double blind, randomized, controlled trial, *Clinical Nutrition* 24 (2005) 481–491. doi:10.1016/j.clnu.2005.02.006.
- [157] H.Abdollahi, Probiotic-based protection of normal tissues during radiotherapy, *Nutrition* 30 (2014) 495–496. doi:10.1016/j.nut.2013.09.006.
- [158] M.Kumar, S.Rakesh, R.Nagpal, R.Hemalatha, A.Ramakrishna, V.Sudarshan, R.Ramagoni, M.Shujaiddin, V.Verma, A.Tiwari, B.Singh, R.Kumar, Probiotic lactobacillus rhamnosus gg and aloe vera gel improve lipid profiles in hypercholesterolemic rats, *Nutrition* 29 (2012) 574–579. doi:10.1016/j.nut.2012.09.006.
- [159] J.Timko, Probiotics as prevention of radiation-induced diarrhea, *Journal of Radiotherapy in Practice* 9 (2010) 201–208. doi:10.1017/S1460396910000087.
- [160] S.L.Brown, A.Kolozsvary, J.Liu, K.A.Jenrow, S.Ryu, J.H.Kim, Antioxidant diet supplementation starting 24 hours after exposure reduces radiation lethality, *Radiation Research* 173 (2010) 462–468. doi:10.1667/RR1716.1.
- [161] I.Bairati, F.Meyer, M.Gélinas, A.Fortin, A.Nabid, F.BrochetJean-Philippe Mercier, B.Têtu, F.Harel, B.Abdous, É.Vigneault, S.Vass, P.del Vecchio, J.Roy, Randomized trial of antioxidant vitamins to prevent acute adverse effects of radiation therapy in head and neck cancer patients, *Journal of Clinical Oncology* 23 (2016) 5805–5813. doi:10.1200/JCO.2005.05.514.
- [162] P.R.Ferreira, J.F.Fleck, A.Diehl, D.Barletta, A.Braga-Filho, A.Barletta, L.Ilha, Protective effect of alpha-tocopherol in head and neck cancer radiation-induced mucositis: A double-blind randomized trial, *Journal of the Sciences and Specialties of the Head and Neck* 26 (2004) 313–321.
- [163] F.J.Burns, M.R.Tang, K.Frenkel, A.Nádas, F.Wu, A.Uddin, R.Zhang, Induction and prevention of carcinogenesis in rat skin exposed to space radiation, *Radiation and Environmental Biophysics* 46 (2007) 195–199. doi:10.1007/s00411-007-0106-3.

- [164] A.Schreurs, Y.Shirazi-Fard, M. et al, Dried plum diet protects from bone loss caused by ionizing radiation, Sci Rep 6. doi:10.1038/srep21343.
- [165] R. W. Langley, Space Radiation Protection, Technical Report NASA SP-8054, NASA Langley Research Center, Hampton, VA 23681-2199 (Jun. 1970).
URL <https://strives-uploads-prod.s3.us-gov-west-1.amazonaws.com/19710015599/19710015599.pdf?AWSAccessKeyId=AKIASEVSKC45ZTTM42XZ&Expires=1599505466&Signature=Bedx0hth3yv213mMuRpYGTtidXg%3D>
- [166] J. Barthel, N. Sarigul-Klijn, A review of radiation shielding needs and concepts for space voyages beyond Earth's magnetic influence, Progress in Aerospace Sciences 110 (2019) 100553. doi:10.1016/j.paerosci.2019.100553.
URL <https://linkinghub.elsevier.com/retrieve/pii/S0376042119300090>
- [167] P. Metzger, R. Youngquist, J. Lane, Asymmetric electrostatic radiation shielding for spacecraft, in: 2004 IEEE Aerospace Conference Proceedings (IEEE Cat. No.04TH8720), IEEE, Big Sky, MT, USA, 2004, pp. 626–637. doi:10.1109/AERO.2004.1367649.
URL <http://ieeexplore.ieee.org/document/1367649/>
- [168] L. Townsend, Critical analysis of active shielding methods for space radiation protection, in: 2005 IEEE Aerospace Conference, IEEE, Big Sky, MT, USA, 2005, pp. 724–730. doi:10.1109/AERO.2005.1559364.
URL <http://ieeexplore.ieee.org/document/1559364/>
- [169] L. W. Townsend, Galactic Heavy-Ion Shielding Using Electrostatic Fields, Technical Report N84-33453, NASA Langley Research Center, Hampton, VA 23681-2199 (Sep. 1984).
URL <https://strives-uploads-prod.s3.us-gov-west-1.amazonaws.com/19840025382/19840025382.pdf?AWSAccessKeyId=AKIASEVSKC45ZTTM42XZ&Expires=1599508876&Signature=2rMCia%2FJjnGD3pnZJqvjt8Vemn0%3D>
- [170] R. K. Tripathi, Meeting the Grand Challenge of Protecting Astronaut's Health: Electrostatic Active Space Radiation Shielding for Deep Space Missions, Technical Report HQ-E-DAA-TN33876, NASA Langley Research Center, Hampton, VA 23681-2199.
URL <https://ntrs.nasa.gov/archive/nasa/casi.ntrs.nasa.gov/20160010094.pdf>

- [171] R. H. Levy, F. W. French, Plasma radiation shield - Concept and applications to space vehicles., *Journal of Spacecraft and Rockets* 5 (5) (1968) 570–577. doi:10.2514/3.29306.
URL <https://arc.aiaa.org/doi/10.2514/3.29306>
- [172] R. Winglee, Advances in magnetized plasma propulsion and radiation shielding, in: *Proceedings. 2004 NASA/DoD Conference on Evolvable Hardware, 2004.*, IEEE, Seattle, WA, USA, 2004, pp. 340–347. doi:10.1109/EH.2004.1310849.
URL <http://ieeexplore.ieee.org/document/1310849/>
- [173] X.-H. Jia, S.-X. Jia, F. Xu, Y.-Q. Bai, J. Wan, H.-T. Liu, R. Jiang, H.-B. Ma, S.-G. Wang, Study of magnetic field expansion using a plasma generator for space radiation active protection, *Chinese Physics C* 37 (9) (2013) 098201. doi:10.1088/1674-1137/37/9/098201.
URL <https://iopscience.iop.org/article/10.1088/1674-1137/37/9/098201>
- [174] AMS in a Nutshell | The Alpha Magnetic Spectrometer Experiment.
URL <https://ams02.space/what-is-ams/ams-in-nutshell>
- [175] K. Rainey, Alpha Magnetic Spectrometer (AMS): How It Works, library Catalog: www.nasa.gov (Oct. 2015).
URL http://www.nasa.gov/mission_pages/station/research/news/ams_how_it_works.html
- [176] S. Guetersloh, C. Zeitlin, L. Heilbronn, J. Miller, T. Komiyama, A. Fukumura, Y. Iwata, T. Murakami, M. Bhattacharya, Polyethylene as a radiation shielding standard in simulated cosmic-ray environments, *Nuclear Instruments and Methods in Physics Research Section B: Beam Interactions with Materials and Atoms* 252 (2) (2006) 319–332.
- [177] J. W. Wilson, F. F. Badavi, F. A. Cucinotta, J. L. Shinn, G. D. Badhwar, R. Silberberg, C. Tsao, L. W. Townsend, R. K. Tripathi, Hzetrn: Description of a free-space ion and nucleon transport and shielding computer program.
- [178] C. Zeitlin, S. B. Guetersloh, L. H. Heilbronn, J. Miller, Measurements of materials shielding properties with 1 gev/nuc 56fe, *Nuclear Instruments and Methods in Physics Research Section B: Beam Interactions with Materials and Atoms* 252 (2) (2006) 308–318.

- [179] N. R. Council, et al., *Managing space radiation risk in the new era of space exploration*, National Academies Press, 2008.
- [180] J. DeWitt, E. Benton, *Shielding effectiveness: A weighted figure of merit for space radiation shielding*, *Applied Radiation and Isotopes* 161 (2020) 109141.
- [181] S. Kanagaraj, F. R. Varanda, T. V. Zhil'tsova, M. S. Oliveira, J. A. Simões, *Mechanical properties of high density polyethylene/carbon nanotube composites*, *Composites Science and Technology* 67 (15-16) (2007) 3071–3077.
- [182] S. Nambiar, J. T. Yeow, *Polymer-composite materials for radiation protection*, *ACS applied materials & interfaces* 4 (11) (2012) 5717–5726.
- [183] S. Laurenzi, G. de Zanet, M. G. Santonicola, *Numerical investigation of radiation shielding properties of polyethylene-based nanocomposite materials in different space environments*, *Acta Astronautica* 170 (2020) 530–538.
- [184] L. Narici, M. Casolino, L. Di Fino, M. Larosa, P. Picozza, V. Zaconte, *Radiation survey in the international space station* (2015).
- [185] V. Zaconte, F. Belli, V. Bidoli, M. Casolino, L. Di Fino, L. Narici, P. Picozza, A. Rinaldi, W. Sannita, N. Finetti, et al., *Altea: the instrument calibration*, *Nuclear Instruments and Methods in Physics Research Section B: Beam Interactions with Materials and Atoms* 266 (9) (2008) 2070–2078.
- [186] J. Guo, T. C. Slaba, C. Zeitlin, R. F. Wimmer-Schweingruber, F. F. Badavi, E. Böhm, S. Böttcher, D. E. Brinza, B. Ehresmann, D. M. Hassler, et al., *Dependence of the martian radiation environment on atmospheric depth: Modeling and measurement*, *Journal of Geophysical Research: Planets* 122 (2) (2017) 329–341.
- [187] F. A. Cucinotta, M.-H. Y. Kim, L. Ren, *Evaluating shielding effectiveness for reducing space radiation cancer risks*, *Radiation Measurements* 41 (9-10) (2006) 1173–1185.
- [188] J. Guo, C. Zeitlin, R. F. Wimmer-Schweingruber, S. Rafkin, D. M. Hassler, A. Posner, B. Heber, J. Köhler, B. Ehresmann, J. K. Appel, et al., *Modeling the variations of dose rate measured by rad during the first msl martian year: 2012–2014*, *The Astrophysical Journal* 810 (1) (2015) 24.

- [189] D. E. Smith, M. T. Zuber, S. C. Solomon, R. J. Phillips, J. W. Head, J. B. Garvin, W. B. Banerdt, D. O. Muhleman, G. H. Pettengill, G. A. Neumann, et al., The global topography of mars and implications for surface evolution, *science* 284 (5419) (1999) 1495–1503.
- [190] L. Röstel, J. Guo, S. Banjac, R. F. Wimmer-Schweingruber, B. Heber, Subsurface radiation environment of mars and its implication for shielding protection of future habitats, *Journal of Geophysical Research: Planets* 125 (3) (2020) e2019JE006246.
- [191] R. Tripathi, J. Wilson, R. Joshi, Risk assessment and shielding design for long-term exposure to ionizing space radiation, *SAE Transactions* (2006) 254–262.
- [192] R. J. L veill , S. Datta, Lava tubes and basaltic caves as astrobiological targets on earth and mars: a review, *Planetary and Space Science* 58 (4) (2010) 592–598.
- [193] B. E. Walden, T. L. Billings, C. L. York, S. L. Gillett, M. V. Herbert, Utility of lava tubes on other worlds, in: *Using in situ Resources for Construction of Planetary Outposts*, 1998, p. 16.
- [194] D. Gakis, D. Atri, Modeling the effectiveness of radiation shielding materials for astronaut protection on mars, *arXiv preprint arXiv:2205.13786*.
- [195] N. L. Falck, Radiation exposure during space travel: Using radioisotopes for a comparative study of human feces and urine as integrated shield components, in: *Symposium*, Vol. 4, 2017, p. 4.
- [196] G. K. Shunk, X. R. Gomez, N. J. Aversch, A self-replicating radiation-shield for human deep-space exploration: Radiotrophic fungi can attenuate ionizing radiation aboard the international space station, *BioRxiv* (2021) 2020–07.
- [197] G. Baiocco, M. Giraud, L. Bocchini, S. Barbieri, I. Locantore, E. Brussolo, D. Giacosa, L. Meucci, S. Steffenino, A. Ballario, et al., A water-filled garment to protect astronauts during interplanetary missions tested on board the iss, *Life sciences in space research* 18 (2018) 1–11.
- [198] R. Musenich, V. Calvelli, S. Farinon, R. Battiston, W. J. Burger, P. Spillantini, A magnesium diboride superconducting toroid for astroparticle shielding, *IEEE transactions on applied superconductivity* 24 (3) (2013) 1–4.
- [199] L. Sargent, V. L. Coverstone, Magnetic shielding for a mars habitat, in: *AIAA Scitech 2020 Forum*, 2020, p. 0798.

- [200] F.A.Cucinotta, Radiation risk acceptability and limitations.
URL <https://three.jsc.nasa.gov/articles/AstronautRadLimitsFC.pdf>
- [201] N. T. Standard, Nasa space flight human-system standard: volume 1, Crew Health.
URL <https://standards.nasa.gov/standard/nasa/nasa-std-3001-vol-1>
- [202] K. T. Nead, N. Mitra, B. Weathers, K. L. Nathanson, P. A. Kanetsky, Diagnostic radiation and testicular germ cell tumor risk, *Journal of Clinical Oncology* 36 (2018) 556–556. doi:10.1200/jco.2018.36.6_suppl.556.
- [203] M. Utada, A. V. Brenner, D. L. Preston, J. B. Cologne, R. Sakata, H. Sugiyama, N. Kato, Radiation risk of ovarian cancer in atomic bomb survivors: 1958–2009, *Radiation Research* 195. doi:10.1667/rade-20-00170.1.
- [204] M. Utada, A. V. Brenner, D. L. Preston, J. B. Cologne, R. Sakata, H. Sugiyama, e. a. Sadakane, Radiation risks of uterine cancer in atomic bomb survivors: 1958–2009, *JNCI Cancer Spectrum* 2. doi:10.1093/jncics/pky081.
- [205] A. V. Brenner, D. L. Preston, R. Sakata, H. Sugiyama, A. Berrington de Gonzalez, B. French, e. a. Utada, Incidence of breast cancer in the life span study of atomic bomb survivors: 1958–2009, *Radiation Research* 190 433. doi:10.1667/rr15015.1.
- [206] D. B. Thomas, K. Rosenblatt, L. M. Jimenez, A. McTiernan, H. Stalsberg, A. Stemhagen, e. a. Thompson, Ionizing radiation and breast cancer in men (united states), *Cancer Causes & Control* 5 (1994) 9–14. doi:10.1007/bf01830721.

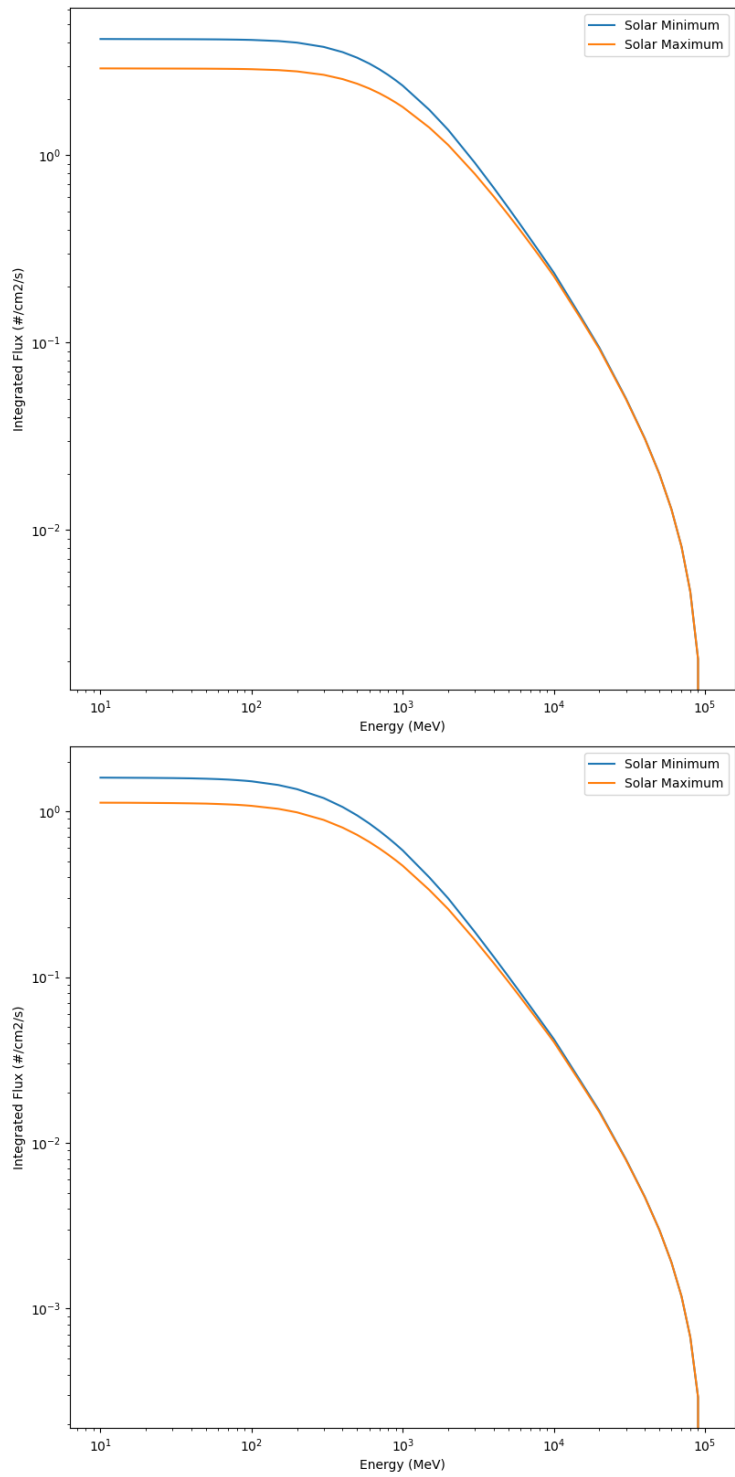


Figure 1: The spectra of GCR Hydrogen (top) and Helium (bottom) during solar min and max conditions

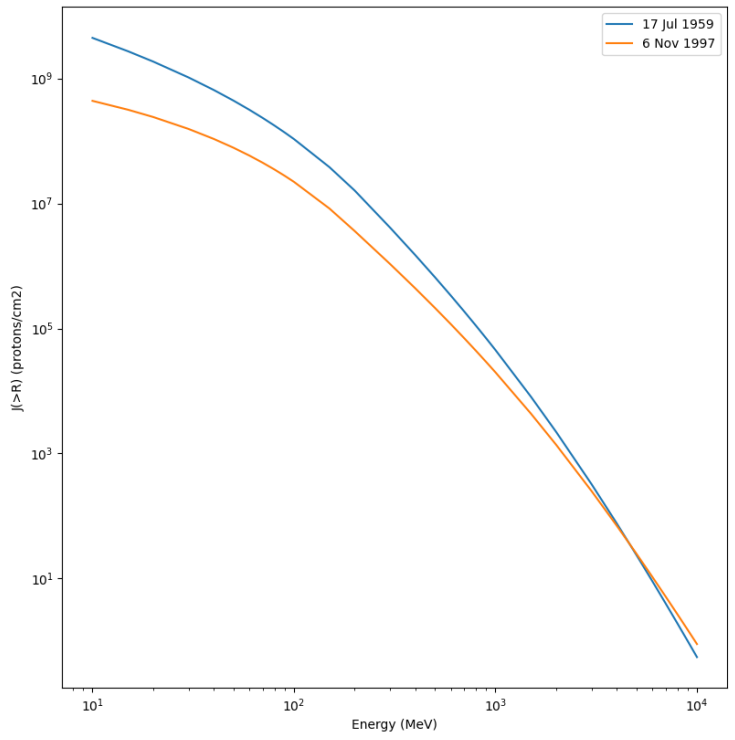


Figure 2: The spectra of SEP events of 17 July 1959 and Nov 1997